Joana Lisboa da Silva Gonçalves

Degree in Biochemisty

Molecular and Cellular Investigation of Malate:quinone oxidoreductases from *Staphylococcus aureus*

Dissertation to obtain the Master degree in Biochemistry for Health

Supervisor: Dr Manuela M. Pereira

Jury:

President: Dr Pedro Matias
Opponent: Dr Lígia O. Martins
Members of the jury: Dr Margarida Archer

Instituto de Tecnologia Química e Biológica, António Xavier

November, 2017

Molecular and Cellular Investigation of Malate:quinone oxidoreductases from *Staphylococcus aureus*

Agradecimentos

O condicionado espaço destinado a esta secção, não me permite agradecer como devia a todas as pessoas que, direta ou indiretamente, me ajudaram a caminhar e a concretizar esta etapa na minha vida. Assim, desde já deixo um profundo sentimento de agradecimento perante todos vós.

Primeiro que tudo à minha orientadora Dra. Manuela Pereira, a quem expresso o meu profundo agradecimento pela orientação e apoio incondicionais durante todo este caminho, que muito elevaram os meus conhecimentos, e que acima de tudo estimularam a minha vontade e o meu desejo de querer sempre mais, de lutar e de acreditar nas minhas capacidades. Obrigada pela responsabilidade e pela confiança que depositou em mim, desde o início. É para mim, um enorme privilégio ter tido a oportunidade de integrar o seu Grupo de Investigação, e com enorme gratidão que reconheço que tive a possibilidade de começar esta minha caminhada com um excelente acompanhamento, que não só me enriqueceu a nível profissional, como também a nível pessoal.

Esta experiência permitiu-me também conhecer pessoas fantásticas. Quero desde já agradecer a todo o Grupo de Investigação, *Biological Energy Transduction*, com quem tive a oportunidade de aprender e conviver durante este ano. Essencialmente à Patrícia Refojo e ao Filipe Sousa que sempre se prontificaram para me ajudar, em tudo o que precisasse. Obrigada Patrícia, pela motivação e por cada conselho que sempre me deste. Obrigada Filipe por todo o teu espírito crítico que tanto me ajudou, e esclareceu tantas vezes. Em especial, o meu agradecimento é dirigido à Filipa Sena, que foi uma pessoa fundamental no meu percurso. A Filipa foi um pilar imprescindível, foi acima de tudo uma amiga, uma irmã, que vou levar comigo desta experiência. A sua preocupação constante e o seu apoio incondicional em todos os passos deste projeto, foram essenciais. Obrigada por todas as vezes que exigiste o máximo de mim, pela oportunidade de aprender contigo e por todos os conhecimentos que partilhaste comigo. És um exemplo de persistência, de força e de dedicação, que são exatamente os valores pelos quais eu me rejo na minha vida. Um obrigado profundo por cada gargalhada, por todos os momentos partilhados, e principalmente, por ter tido a brilhante oportunidade de partilhar contigo um dos momentos mais bonitos da tua vida.

Quero também agradecer ao Professor Miguel Teixeira, como responsável da *Metalloproteins and Bioenergetics Unit*.

Ao ITQB, por me ter proporcionado todas as condições necessárias para a elaboração do meu projeto, e por permitir a minha integração num centro de investigação tão conceituado e de tão elevado prestígio. Um especial obrigada a todos os colaboradores, que de uma forma ou outra, contribuíram para a concretização deste projeto, desde as funcionárias da sala de lavagens, até ao admirável João Carita, que apesar de tanto trabalho, conseguiu sempre atender aos meus pedidos. À extraordinária Isabel Pacheco, que foi sempre incansável comigo e por quem eu tenho uma grande estima, um grande obrigado por todo o apoio e preocupação. À

CERMAX, e ao Dr. Pedro Lamosa, pela disponibilidade e ajuda prestada no âmbito das experiências de RMN.

Às minhas colegas de Mestrado, e amigas, que viveram comigo esta aventura e que diariamente realizaram esta caminhada comigo, em especial à Bárbara, à Diana e à Lucie, e claro, à minha melhor amiga, a Catarina, que já me acompanha há 5 anos neste percurso de vida académica, sempre a meu lado, ultrapassando todos os obstáculos juntas. Obrigada por aturares todos os meus dias menos bons, e obrigada por mais uma etapa concluída a teu lado, estou muito orgulhosa de nós. Aos meus grandes amigos Gigi e João Paredes, que mesmo à distância estiveram sempre presentes.

Não posso deixar de agradecer ao meu namorado, ao Francisco, por todo o apoio, por todas as palavras de confiança e por ter acreditado em mim em todos os momentos, sem nunca duvidar das minhas capacidades. Obrigada por teres estado comigo desde o início e por toda a paciência e compreensão, mesmo nos meus dias mais difíceis, obrigada por tudo.

E por último, mas claramente o mais importante, à minha família. Obrigada Mãe e Pai por tudo o que me proporcionaram até hoje, tudo. Não há palavras para agradecer todo o vosso esforço. Obrigada por terem feito de mim a pessoa que sou hoje, por me terem transmitido todos os valores e princípios pelos quais eu me guio diariamente. Obrigada por me terem ensinado a lutar, sem nunca desistir dos meus sonhos. Obrigada por acreditarem em mim todos os dias. Ao meu irmão, Tiago, que é, e sempre será, o meu maior orgulho. Obrigada pela vossa paciência nos meus momentos mais complicados.

A todos os que perdi durante o meu percurso académico, aos meus quatro Avós, que são o verdadeiro motivo da minha força, e que eu sei que me acompanham lá de cima. Espero que estejam orgulhosos, hoje é para vocês.

"A vida deve ser enfrentada como os cavalos, saltando e derrubando cada obstáculo."

Obrigada Avô

Resumo

Staphylococcus aureus são agentes patogénicos oportunistas e representam uma das causas mais frequentes de infeções adquiridas na comunidade e nosocomiais. *S. aureus* tem desenvolvido vários mecanismos que conduziram à seleção de estirpes mais resistentes. Estas bactérias potencialmente letais constituem uma grande ameaça para a saúde pública, sendo que o desenvolvimento de novos fármacos para combater este problema mundial é prioritário. No entanto, diversos aspetos referentes a esta bactéria têm escapado à atenção, tais como o seu **metabolismo energético** e os seus **enzimas respiratórios**. Assim, visando alargar este conhecimento, as proteínas **malato:quinona oxidoreductases** foram exploradas a níveis moleculares e celulares.

As malato:quinona oxidoreductases são proteínas membranares, envolvidas no ciclo do ácido cítrico e na **cadeia respiratória**. Estas proteínas catalisam a oxidação de malato a oxaloacetato e a concomitante redução da quinona a quinol, fornecendo eletrões à cadeia respiratória. *S. aureus* possui dois genes anotados que codificam duas malato:quinona oxidoreductases, MQO I e MQO II, no entanto as diferenças entre ambas são desconhecidas. Uma caracterização bioquímica preliminar foi realizada bem como uma extensa investigação celular. Pela primeira vez, estas duas proteínas de *S. aureus* foram purificadas. A MQO I apresentou atividade malato:quinona oxidoreductase, contrariamente à MQO II que revelou atividade com lactato. O impacto da MQO I no metabolismo de *S. aureus* foi avaliado, através de crescimentos bacterianos com diferentes fontes de carbono, da estirpe selvagem e de um mutante. Os metabolitos extracelulares, recolhidos ao longo dos diversos crescimentos, foram analisados por **espectroscopia RMN**, que revelou a incapacidade da estirpe mqoI::Tn em catabolizar acetato. Esta abordagem possibilitou também pela primeira vez, uma profunda caracterização do comportamento de *S. aureus* sob diferentes fontes de carbono. Em suma, os nossos resultados sugerem que a MQO II, é uma lactato:quinona oxidoreductase, e revelaram a importância da MQO I neste patogénico, indicando-a como possível alvo terapêutico.

Palavras-chave: Metabolismo energético; enzimas respiratórios; malato:quinona oxidoreductases; cadeia respiratória; espectroscopia RMN.

Abstract

Staphylococcus aureus are opportunistic pathogens and represent one of the most frequent causes for community acquired and nosocomial infections. Over time, *S. aureus* has developed several mechanisms which led to the selection of increasingly resistant strains. These potentially lethal bacterial pathogens have become a major public health threat, being urgent the development of new drugs against this worldwide problem. However, and intriguingly many fundamental aspects of *S. aureus* have escaped attention, such as its **energy metabolism** and **respiratory enzymes**. We aim to contribute to this knowledge by exploring **malate:quinone oxidoreductases** at molecular and cellular levels.

Malate:quinone oxidoreductases are membrane-bound proteins, involved in both the citric acid cycle and in the **respiratory chain**. These proteins catalyse the oxidation of malate to oxaloacetate and the reduction of quinone to quinol, providing electrons to the respiratory chain. *S. aureus* has two annotated genes encoding for two malate:quinone oxidoreductases, MQO I and MQO II, although the differences between these proteins are not known. Preliminary biochemical characterization and a thorough cellular investigation were performed in this work. For the first time, both proteins from *S. aureus* were purified. MQO I presented malate:quinone oxidoreductase activity, contrarily to MQO II which showed activity with lactate. The impact of the role of MQO I in *S. aureus* metabolism was evaluated by growths of a wild-type strain and of one mutant strain under different carbon sources. An **NMR metabolomics** approach was used to analyse the excreted metabolites along the growths, suggesting the inability of mqoI::Tn to catabolize acetate. This approach also provided, for the first time, a deep characterization of the wild-type strain, under different carbon sources. Our results suggest a misassignment of MQO II, being probably a lactate:quinone oxidoreductase and highlight the relevance of MQO I in this pathogen, making it an attractive candidate for targeted therapeutics.

Keywords: Energy metabolism; respiratory enzymes; malate:quinone oxidoreductases; respiratory chain; NMR metabolomics.

Table of Contents

Table of contents of figures

Index of tables

List of abbreviations

Δψ – transmembrane difference in electrical potential

ε - extinction coefficient

ATP - adenosine triphosphate

ADP – adenosine diphosphate

BCA – bicinchoninic acid assay

BSA – bovine serum albumine

CcpA – catabolite control protein A

CCR – carbon catabolite repression

CDM – chemically defined medium

CpI – complex I

CpII – complex II

CpIII – complex III

CpIV – complex IV

cyt *c* – cytochrome *c*

DDM - n-Dodecyl-β-D-maltoside

DHODH – dihydroorotate:quinone oxidoreductase

DLD – dihydrolipoyl dehydrogenase

DMN - 2,3-dimethyl-1,4-naphthoquinone

DCPIP - 2,6-dichloroindophenol

E. coli - *Escherichia coli*

EDTA - ethylenediaminetetraacetic acid

ETC – electron transfer chain

FAD - flavin adenine dinucleotide

$FADH_2$ – reduced state of FAD

G3PDH – glycerol-3-phosphate:quinone oxidoreductase

HQNO - 2-n-Heptyl-4-hydroxyquinoline N-oxide

IMAC - immobilized metal ion affinity chromatography

IPTG - isopropyl-β-D-1-thiogalactopyranoside

LMW - low molecular weight

Ldh – lactate dehydrogenase

LQO – lactate:quinone oxidoreductase

MDH – malate:NAD^+ oxidoreductase; malate dehydrogenase

MES - 2-(*N*-morpholino) ethanesulfonic acid

MRSA - methicillin-resistant *Staphylococcus aureus*

MS – mass spectrometry

MSSA – methicillin-susceptible *Staphylococcus aureus*

MQO – malate:quinone oxidoreductase(s)

MQO I – malate:quinone oxidoreductase I

mqoI::Tn – strain with a transposon in the gene coding for malate:quinone oxidoreductase I

MQO II – malate:quinone oxidoreductase II

MPS – membrane potential-generating system

MT - melting temperature

NAD^+ - oxidized nicotinamide adenine dinucleotide

NADH - nicotinamide adenine dinucleotide

NDH-2 – type II NADH:quinone oxidoreductase

NMR – nuclear magnetic resonance

OD_{600} – optic density at 600 nm

OR - oxidoreductase

PCR – polymerase chain reaction

ppm - parts per million

PQO – pyruvate:quinone oxidoreductase

PVL - Panton–Valentine leukocidin

Q - quinone

QH_2 - quinol

S. aureus - *Staphylococcus aureus*

S200 - Superdex 200

SDH – succinate:quinone oxidoreductase

SDS-PAGE - sodium dodecyl sulphate – polyacrylamide gel electrophoresis

SQR – sulphide:quinone oxidoreductase

TCA – tricarboxylic acid

Tn – transposon

TSA – tryptic soy agar

TSB – tryptic soy broth

TSP - 3-trimethylsilyl-[2,2,3,3-D_4]-1-propionic acid

UQ – ubiquinone

UQH_2 – ubiquinol

1. Introduction

1.1. Energetic Metabolism

1.1.1. Energy at the basis of Life

The study of Life Sciences requires the knowledge of Bioenergetics. Life is nothing less than a result of energy changes. Energy is the main requirement for survival, and the evidence is that all biochemical processes involve energy transfer.

Living cells exchange matter and energy with their surroundings, obtaining and conserving energy in order to survive, grow, reproduce and preserve their structures, maintaining the dynamic equilibrium.

Bioenergetics is an extensive scientific domain, which concerns the study of energy transformations in living systems.

In vertebrates, energy is obtained by oxidative phosphorylation in the mitochondria. The Chemiosmotic theory, postulated by Sir Peter Mitchel in 1961[1] (Nobel Prize for Chemistry, 1978), enabled the understanding of many biological energy transduction reactions and processes, such as the oxidative phosphorylation, in which the energy of electron flow is conserved by the translocation of protons across the membrane, leading to the establishment of a transmembrane electrochemical potential – the proton-motive force[1,2,3].

The proton-motive force comprises two different components: the different chemical concentrations between both sides of the membrane, and the charge distribution ($\Delta\psi$) across the inner mitochondrial membrane. Thus, the inherent electrochemical potential is further used by ATP synthase for the synthesis of ATP[2,4].

Science is the poetry of reality in which Energy plays the central role. As Albert Einstein once said: "*Everything is energy and that's all there is to it*".

1.1.2. Metabolic pathways

Energy is required for the maintenance of life, reproduction and for the synthesis of cell components. This energy is provided by carbohydrates, fatty acids, proteins and vitamins, among others. Metabolism is the sum of all the chemical transformations, taking place in a cell or organism, through successive enzymatic reactions via specific metabolic pathways. Cellular metabolism can be divided into catabolic and anabolic reactions. In the first one (catabolism) complex molecules with high energetic value, such as proteins, carbon hydrates and fatty acids, are degraded into structurally simpler molecules in a thermodynamically favourable process. In anabolic reactions the same molecules are combined and transformed, with energy consumption, in higher components[2,5]. Following the origin of cells, microbial life experienced a long period of metabolic diversification, exploiting the various resources available on Earth.

In the course of evolution, organisms have acquired a remarkable collection of regulatory mechanisms to maintain the homeostasis at the molecular, cellular and organism level. Cells and organisms do not live in a static environment; in fact, they exist in a dynamic equilibrium, meaning that for each metabolic reaction in a pathway, the substrate produced by the preceding reaction is then converted to product[2,5,6]. However, cells do not live in equilibrium with their surroundings, but tend to keep a steady state. Thus, when this is disrupted due to external factors, regulatory mechanisms are triggered in order to compensate this disruption. Metabolic pathways are regulated at several levels, from within the cell and from outside. This regulation occurs essentially at two levels: the control of enzyme synthesis and the variation of enzyme activity. The control of enzyme synthesis is due to the availability of substrate, while the second one is relative to the allosteric regulation, by metabolic intermediates or coenzymes that signal the cell's internal metabolic state. These signals allow the allosteric inhibition of one or more enzymes involved in the respective metabolic pathway, when its consumption is not needed[2,5,3].

Glucose has a central role in the metabolism of animals, plants and many organisms. Besides being an excellent source of energy used to produce ATP, glucose is also an important precursor, able to supply an extensive array of metabolic intermediates for biosynthetic reactions. A molecule of glucose is converted into two molecules of pyruvate by a series of enzyme-catalysed reactions, in a metabolic process denominated as glycolysis. Glycolysis is the central pathway of glucose catabolism, presenting the largest flux of carbon in most cells. In this process, some of the free energy released from glucose degradation is conserved in the form of ATP and NADH[2,5,6,7].

$$Glucose + 2NAD^+ + 2ADP + 2P_i \rightarrow 2\ pyruvate + 2NADH + 2H^+ + 2ATP + 2H_2O$$

Equation 1 – Overall equation for glycolysis. For each molecule of glucose degraded to pyruvate, are generated two molecules of ATP.

The conversion into pyruvate represents a fundamental step in the intermediary metabolism, because it corresponds to the branch point for synthetic and catabolic reactions[2,7]. Pyruvate produced from glycolysis can be further metabolized by different catabolic routes. It can be reduced to lactate, accepting electrons from NADH and thus regenerating NAD^+, in a process named lactic acid fermentation. This process occurs under anaerobic conditions but it can be even observed under aerobiosis, depending on the microorganisms and cell types[2,5]. Ethanol and CO_2 can also be generated from pyruvate under hypoxic or anaerobic conditions, via alcohol fermentation. Under aerobic conditions, pyruvate is oxidized to produce the acetyl group of acetyl-coenzyme A which is further oxidized to CO_2 by the enzymes of the citric acid cycle, where the energy released is temporarily conserved in the electron carriers – nicotinamide adenine dinucleotide (NADH) or quinones. These are oxidized, and their respective electrons pass through a chain of electron-carrying molecules in the mitochondria (respiratory chain) to the final electron acceptor, oxygen (Figure 1.1).

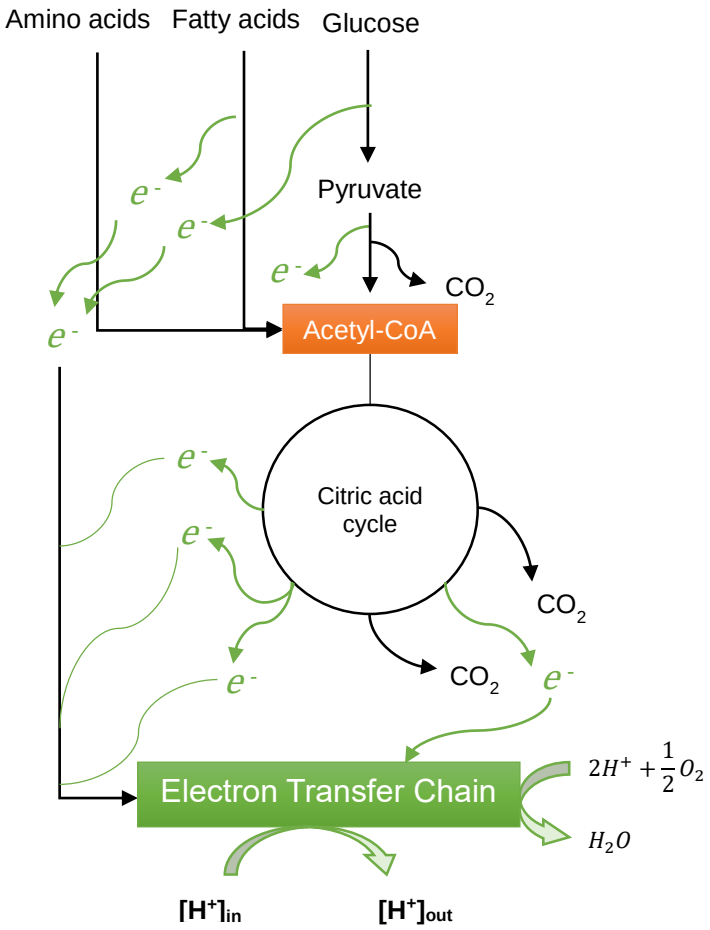

Figure 1. 1 - Schematic representation of catabolism of proteins, fatty acids and carbohydrates of cellular respiration adapted from *Nelson MC. Lehninger Principles of Biochemistry*.

The citric acid cycle (Figure 1.2) is a key metabolic pathway that takes place in the matrix of the mitochondria in eukaryotic organisms or in the cytosol of prokaryotes. Acetyl-CoA enters in this cyclic pathway through its condensation with oxaloacetate, by citrate synthase, producing citrate. This process represents the first of eight sequential reactions that characterize the citric acid cycle. For each molecule of Acetyl-CoA oxidized, the pathway produces three molecules of NADH, one molecule of quinol and one of ATP[2,5,6]. The citric acid cycle also provides precursors for many biosynthetic pathways, playing an important role in the metabolism. For example, α-Ketoglutarate and oxaloacetate are able to serve as precursors of aspartate and glutamate[2,6].

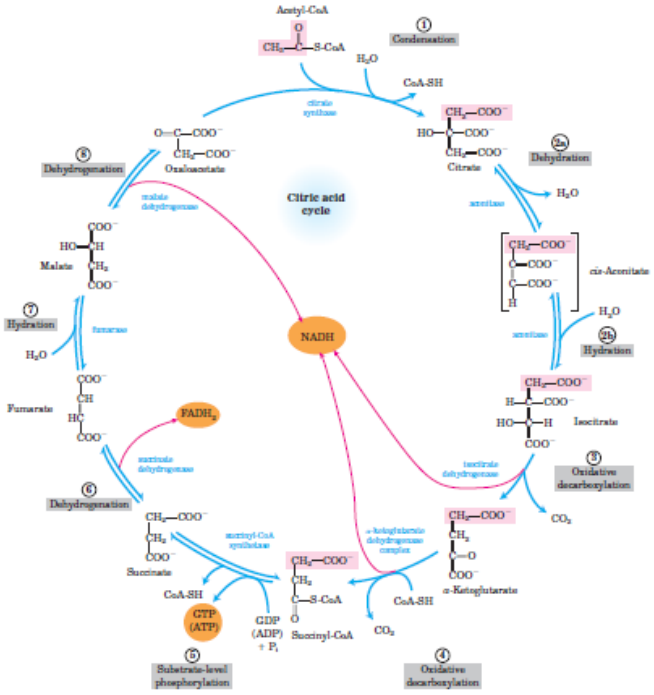

Figure 1. 2 – Schematic representation of the citric acid cycle reactions, adapted from *Nelson MC. Lehninger Principles of Biochemistry*.

1.1.3. Respiratory chains

As the diversity of Life, respiratory chains also present a large diversification depending on the organism and on its respective metabolic needs. Thus, evolution has witnessed changes in the respiratory chains[8].

The respiratory chain is composed of a number of protein complexes capable of transport electrons. In addition, some complexes also translocate protons across the membrane against the electrochemical gradient (Figure 1.3). These respiratory chain proteins differ according to the organism. In prokaryotic organisms the expression occurs in the cellular membrane, while in the eukaryotes the proteins are expressed in the inner mitochondrial membrane. In the first case, the proteins translocate protons from cytoplasm to periplasmic space, and in the second the protons are translocated from the mitochondrial matrix to the inter-membrane space[8].

The best characterized Electron Transfer Chain (ETC) is the mammalian one. The respiratory chain of mammalian mitochondria is an assembly of several electron carriers that are mainly grouped into multi-polypeptide complexes. It is described as comprising four complexes (Complex I, II, III and IV) and the mobile electron carriers, ubiquinone and cytochrome *c* (cyt *c*), that guarantee the electron transfer between the complexes[3,4].

NADH:ubiquinone oxidoreductase (Complex I, CpI) is one of the enzymes that provides electrons to the respiratory chain of mitochondria and several bacteria. This complex (EC:1.6.5.3) is also the largest one, with approximately 1 MDa and constituted by 44 subunits. CpI catalyses the transfer of two electrons between NADH and ubiquinone (UQ), which is reduced to ubiquinol

(UQH_2). The complex also functions as a proton pump, thus this redox transfer is coupled to the translocation of protons across the membrane, from the mitochondrial matrix to the intermembrane space, contributing in this way to the maintenance of the transmembrane electrochemical potential[2,9,10].

Complex II (CpII), also called succinate:quinone oxidoreductase (EC 1.3.5.1) catalyses the two-electron oxidation of succinate to fumarate, and subsequently the reduction of the ubiquinone to ubiquinol, similarly to Complex I. However, unlike CpI the catalytic reaction performed by CpII is not coupled to charge translocation[4,11].

Electrons are further transferred from ubiquinol to cytochrome *c*, by Complex III (CpIII, ubiquinol:cytochrome *c* oxidoreductase), in a reaction coupled to the transport of protons from the matrix to the intermembrane space. Translocation of protons occurs through a Q-cycle mechanism, which accommodates the switch between the two-electron carrier, ubiquinone, and the one-electron carrier, cytochrome *c*. One electron is provided, per ubiquinol molecule oxidized, through an iron sulphur cluster, to reduce cytochrome *c*. The second electron is used to reduce ubiquinone. Thus, a complete Q-cycle requires the oxidation of two ubiquinol molecules, resulting in the translocation of four protons to the positive side of the membrane, contributing to the generation of the membrane potential: 2 protons per each reduced cytochrome. This dimeric transmembrane protein complex III (EC:1.10.2.2), also called cytochrome bc_1 complex, presents 11 subunits per monomers and is composed of a cytochrome c_1, a cytochrome *b* and a Rieske iron-sulfur subunit[2,12]. After accepting an electron from the CpIII, the reduced cytochrome *c* donates electrons to Complex IV (cytochrome *c* oxidase).

Complex IV (EC:1.9.3.1) performs the oxidation of four cytochrome *c* molecules, reducing oxygen and leading to the production of H_2O. During the reduction of O_2 to H_2O, this large complex with 13 subunits pumps four protons across the membrane, to the intermembrane space[3,13].

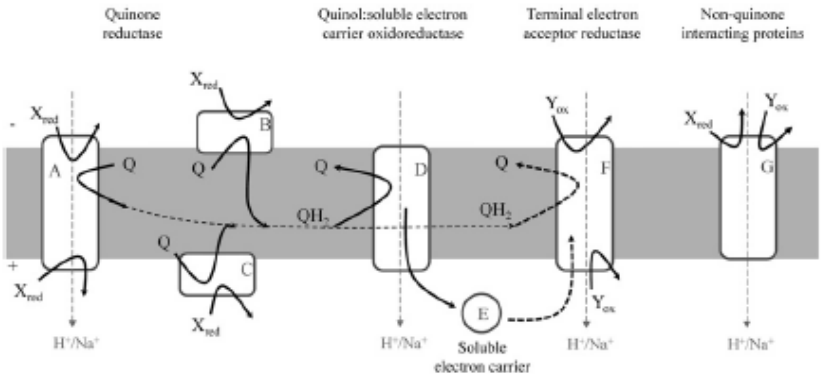

Figure 1. 3 – Schematic representation of proteins and electron carriers involved in respiratory chains, adapted from *Marreiros et al, 2016*. A - Transmembrane proteins with X:quinone oxidoreductase activity, B - Cytoplasmic facing monotopic proteins with X:quinone oxidoreductase activity. C - Periplasmic facing monotopic proteins with X:quinone oxidoreductase activity. D - Transmembrane proteins with quinol:soluble electron carrier oxidoreductase activity. E - Soluble electron carrier that is reduced by D and is oxidized by F. F - Transmembrane proteins with quinol:terminal electron acceptor or soluble electron carrier:terminal acceptor (Y) oxidoreductase activity. G - Transmembrane proteins with oxidoreductase activity with no interaction with quinones. (+ and – indicate the positive and negative sides of the transmembrane difference in electrochemical potential, respectively).

Prokaryotic organisms have the ability to survive under different conditions, due to the diversity of their energetic metabolism that allows the capability of living even in primitive environments. The respiratory chains of prokaryotes may include similar complexes to the mammalian ones but different in several points, for example in the respiratory proteins, presenting fewer polypeptide chains. However, prokaryotes are able to use oxygen, iron, sulphur, nitrogen compounds or even organic metabolites as final electron acceptors. Respiratory chains of prokaryotes show thus remarkable diversity, flexibility and robustness, containing several electron entry branch points and comprising enzymes with apparently the same functions, such as malate:quinone oxidoreductases (MQO), the focus of this thesis[4,8].

1.1.4. Malate:quinone oxidoreductase

Several bacteria possess membrane-bound dehydrogenases other than cytosolic dehydrogenases in their respiratory chains, such as the membrane-bound malate:quinone oxidoreductase (MQO) which has a fundamental role for bacterial growth. According to the literature, this protein is described in the three domains of life, Eukarya (5%), Bacteria (27%) and Archaea (9%)[4].

Malate:quinone oxidoreductase (EC 1.1.5.4), like CpII, is part of both citric acid cycle and of the respiratory chain[4]. Malate:NAD^+ oxidoredutase (EC 1.1.1.37), MDH catalyses the same reaction as MQO in the TCA cycle[14].

MQO was first described by David Cohn in *Micrococcus lysodeikticus*, in 1958[15] and, since then, it has been described in several other prokaryotic organisms, namely in *Bacillus sp.* PS3[16], *Helicobacter pylori* [17], *Corynebacterium glutamicum*[18,19] and *E. coli*[14].

MQO is a membrane bound protein, encoded by the gene *mqo*, and contains a Flavin adenine dinucleotide (FAD) as prosthetic group (Figure 1.4). As MDH, this protein catalyses the oxidation of malate to oxaloacetate, but in contrast to MDH, it donates electrons from malate oxidation to quinones, reducing quinone to quinol, providing directly electrons to the Electron Transfer Chain[3,4,16,17,14].

MQO has been overlooked, although it has been described as a monotopic enzyme localized at the surface of the lipid bilayer through electrostatic or hydrophobic interactions[17]. Presenting a FAD as a prosthetic group, the oxidized flavin accepts two electrons from the substrate (malate) yielding the reduced state, $FADH_2$. The presence of FAD gives the characteristic yellow color to the protein, corresponding to a maximum absorption at 450 nm in the absorption UV Visible spectrum (Figure 7.1 in Supplemental Material) with an extinction coefficient (ε) of 11.3 mM^{-1} cm^{-1} [20].

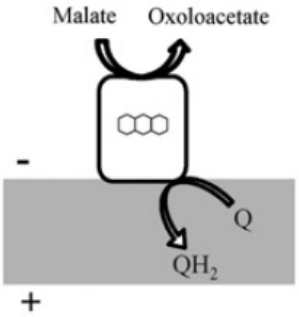

Figure 1. 4 – Schematic representation of malate:quinone oxidoreductase, a monotopic protein facing the periplasm, that catalyses the oxidation of malate into oxaloacetate and reducing the quinone to quinol. FAD is represented by the three rings. (+ and – indicate the positive and negative sides of the transmembrane difference in electrochemical potential, respectively). Adapted from *Marreiros et al, 2016*.

The absence of MQO in mammalian cells makes this protein a potential drug target for the production of pharmaceutical agents against some pathogenic microorganisms, in which MQO is the only malate oxidase present[16]. For that reason, it is also important to understand the mechanism of this protein, its interaction with the substrates and its impact on microorganisms' metabolism.

MQOs from *Staphylococcus aureus* (*S. aureus*) were the systems under study in this thesis.

1.2. *Staphylococcus aureus*

1.2.1. General characteristics

Staphylococcus aureus (*S. aureus*) strains are potentially lethal bacterial pathogens that have been considered a serious worldwide threat to public health due to its multiple drug resistance to the antibiotics, capable to cause several infections[21,22,23]. For this reason, *S. aureus* strains have been extensively studied.

This organism belongs to the Firmicutes phylum and is a facultative anaerobic Gram-positive bacterium. Staphylococci are nonsporulating cocci with a diameter of approximately 0.5-1.5 µm, that divide in multiple planes in order to produce irregular clumps of cells[6].

S. aureus are opportunistic pathogens that can be frequently found in the human respiratory tract and in the skin, representing one of the most frequent causes for community acquired and nosocomial infections[6,21]. The most common features caused by this pathogen are skin infections, but it also frequently to causes pneumonia, sepsis episodes, endocarditis and osteomyelitis[24].

In the US more than 50 % of all *S. aureus* isolates causing clinical diseases are Methicillin-Resistant *Staphylococcus aureus* (MRSA) strains. These strains present resistance to β-lactam

antibiotics, including methicillin, a penicillin. Resistance to methicillin occurs through the acquisition of the *mecA* gene, located in the staphylococcal cassette chromosome *mec* (SCC*mec*)[21]. MRSA is one of the major hospital-associated pathogens (HA-MRSA). Initially, these strains affected people with chronic diseases and hospitalized patients, but nowadays healthy individuals began to be affected as well in all the community (CA-MRSA) around the world[22]. Thus, over time these strains quickly led to epidemic CA-MRSA infections with serious consequences and high mortality rates. Currently, the existence of more than 20 distinct genetic lineages of CA-MRSA is known, but the outbreaks associated with each one varies according to the different clones. USA 300 is one of the most epidemic strains and it has already been reported in 50 different countries[21,24,22]. In addition, there are other types of *S. aureus* strains causing lower levels of mortality comparing to the MRSA ones, the methicillin-susceptible *Staphylococcus aureus* (MSSA).

Portugal represents the country in Europe with the highest rate of MRSA in nosocomial infections[22]. This high frequency of MRSA seems to result mainly from dissemination from the hospitals. Data from 2013 showed that the highest prevalence was found in the northern region (Oporto and Braga) followed by the Lisbon district[22].

Due to the increased incidence of *S. aureus*' drug resistance, the treatment for these opportunistic pathogen infections is urgent and has become a therapeutic challenge.

1.2.2. Virulence mechanism

The pathogenicity of *S. aureus* is mainly determined by the secretion of several virulence factors, such as enzymes, toxins, adhesions and immunomodulators that allow the pathogen to colonize and interact with the host cells, causing cell destruction[21,25].

Almost all CA-MRSA strains carry Panton-Valentine leukocidin (PVL) genes, as well as MSSA strains, but with small expression levels. PVL is a cytotoxin that forms pores in the membranes of leukocytes, specifically in neutrophils, causing cell lysis leading to a leukocyte destruction and tissue necrosis[26].

Another virulence factor in *S. aureus* is α-toxin. This cytotoxic agent lysis immune system cells, such as macrophages and lymphocytes, and is able to modify the platelet morphology, leading to thrombotic problems[21].

These are the most studied *S. aureus'* virulence factors. Nonetheless, the pathogen possesses several others which are responsible for its high pathogenicity[21].

1.2.3. Metabolic pathways of *S. aureus*

The major metabolic pathways are almost identical in all living organisms, but there are a few groups of bacteria in which some systems are modified[2,5,6].

S. aureus is a facultative anaerobic bacteria able to perform both aerobic and anaerobic respiration. Under aerobic conditions the pathogen uses oxygen as final electron acceptor, otherwise under anaerobic environments *S. aureus* can grow by fermentation or nitrate respiration[27]. This ability to adapt to different conditions allows the colonization of the pathogen, from the skin or nasal cavity to the internal host niches, where the availability of free oxygen diminishes[27,28,29]. *S. aureus* uses the pentose phosphate and glycolytic pathways to catabolize glucose. It also uses the citric acid cycle and the amino acids catabolism to obtain energy but it is not able to metabolize fatty acids, since according to the annotated genome sequence, *S. aureus* lacks the enzymes necessary for β-oxidation[30,31].

S. aureus must rapidly adapt to a diversity of carbon sources during host invasion. The fast metabolic adaptation of this opportunistic pathogen provides it with greater pathogenicity when compared to other innocuous staphylococci in humans[32]. This versatile capability to adapt to different conditions is associated with its bioenergetic metabolism. Nevertheless, even though it is a prominent human pathogen, its respiratory enzymes have been escaping attention. *S. aureus* expresses several quinone reductases that feed electrons to the respiratory chain at different metabolic points, whether using O_2 or nitrate as electron acceptors.

1.2.4. Respiratory chain of *S. aureus*

The knowledge of the *S. aureus* respiratory chain is very limited. *S. aureus* is able to perform both aerobic and anaerobic respiration[27,28,29].

The genome of this pathogen does not reveal any gene cluster encoding Complex I (http://www.sanger.ac.uk/resources/downloads/bacteria/staphylococcus-aureus.html). This means that NADH oxidation has to be performed by an alternative respiratory enzyme. Type 2 NADH:quinone oxidoreductase (NDH-2) plays this role[33]. Also, instead of reducing NADH, electrons may be fed directly to the respiratory chain, via quinones.

Besides two NDH-2, *S. aureus* has more genes coding for quinone reductases present in its genome, such as Malate:quinone oxidoreductase (OR), MQO; Lactate:quinone OR, LQO; Pyruvate:quinone OR, PQO; Succinate:quinone OR, SDH; Glycerol-3-phosphate:quinone OR, G3PDH; Sulfide:quinone OR, SQR; Dihidroorotate:quinone OR, DHODH and the so-called MPS (membrane potential-generating system)[4]. These allow a direct link between different metabolic pathways and the respiratory chain. Figure 1.5 shows a schematic representation of *S. aureus* cell highlighting the central carbon metabolism and the quinone reductases present in *S. aureus*' respiratory chain.

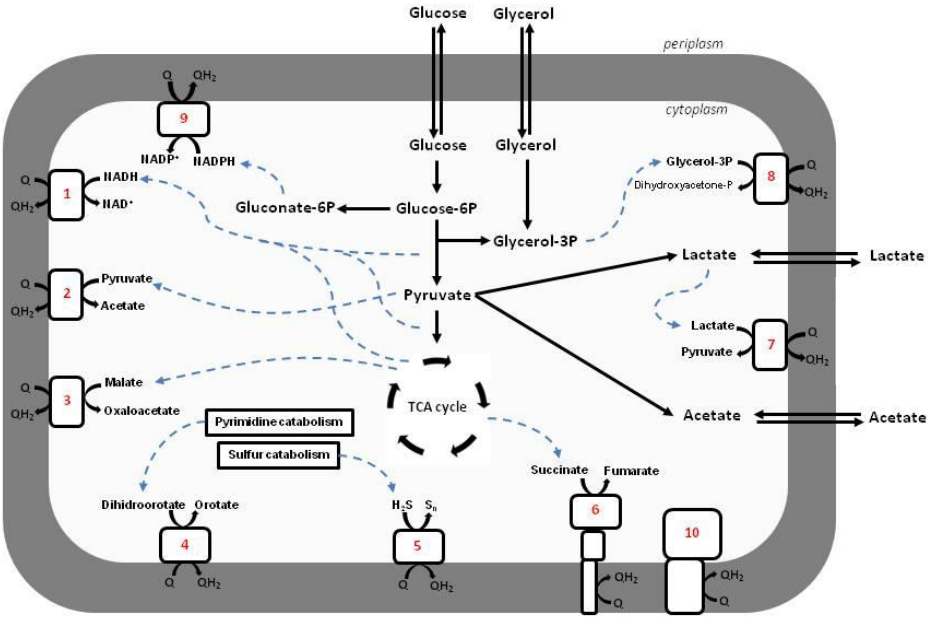

Figure 1. 5 - Brief schematic representation of quinone reductases present in *S. aureus*' respiratory chain and metabolic pathways, adapted from *Marreiros et al*, 2016. In the grey box is represented the membrane, with the monotopic quinone reductases. 1 – NDH-2-A; 2 – PQO; 3 – MQO; 4 – DHODH; 5 – SQR; 6 – SDH; 7 – LQO; 8 – G3PDH; 9 – NDH-2-B; 10 – MPS.

1.2.5. Malate:quinone oxidoreductases

Several bacteria possess membrane-bound dehydrogenases instead of cytosolic dehydrogenases in their respiratory chains, such as the membrane-bound malate:quinone oxidoreductases (MQOs).

The malate:quinone oxidoreductase (EC 1.1.5.4) from *S. aureus* is a respiratory enzyme that catalyses the transfer of two electrons from malate to menaquinone. This pathogen presents two genes encoding two different MQOs, *mqoI* and *mqoII*, which are referred as MQO I and MQO II, respectively [34]. Despite not being yet understood the differences between the two copies, the first one is described as a malate:quinone oxidoreductase, originally annotated as a MQO I, with a molecular mass equivalent to 57 kDa. Preliminary studies indicate that this *S. aureus*' enzyme has a flavin adenine dinucleotide (FAD) and lipid-dependent peripheral membrane protein[34,35]. However, further biochemical studies are needed.

The second copy of MQO from *S. aureus* was originally annotated as malate:quinone oxidoreductase II with approximately 56 kDa, although its function remains unknown. Recent studies revealed that MQO II has affinity to the substrate lactate, instead to malate, suggesting a new function to the second copy[34].

Despite the differences, published studies also revealed that both copies have an important role in *S. aureus'* respiratory chain and survival[34,35,36]. Another important fact is the

absence of the gene coding for the soluble MDH in this microorganism[34], which is also capable of oxidizing malate into oxaloacetate; Thus, without this enzyme the oxidation of malate is only dependent on the activity of MQO. Therefore, the study of these proteins (MQO I and II) is promising and challenging since they are poorly biochemically characterized; For example no crystallographic structure is available. Also, since *S. aureus* presents two copies of MQO, it is important to know the cellular role of these enzymes.

2. Aims

This project aimed to contribute to the knowledge of *S. aureus*' energetic metabolism by exploring respiratory enzymes, namely malate:quinone oxidoreductases, at molecular and cellular levels. Specifically, our objectives were:

- Expression, purification and biochemical characterization of the two malate:quinone oxidoreductases, MQO I and MQO II, from *S. aureus*;
- Investigation of the function of both MQO I and MQO II;
- Explore the impact of MQO I in the metabolism of *S. aureus*;
- Characterization of *S. aureus* behaviour under different carbon sources.

3. Materials and Methods

3.1. Molecular Studies

3.1.1. Cloning and Protein Expression

The genes SAI6T6_1017480 and SAI6T6_1019420 encoding *S. aureus* ST228/18341 (MRSA) MQO I and MQO II, respectively, were individually cloned into plasmid pET-28a(+) (GenScript). The gene product MQO I corresponds to a protein of 511 amino acid residues, while MQO II presents 498 residues, with theoretical molecular masses of approximately 57 kDa and 56 kDa, respectively. The plasmid DNA was extracted using the Wizard® Plus SV Minipreps DNA Purification System (Promega) and competent cells, *Escherichia coli* (*E. coli*) C43(DE3) cells (Lucigen) and *E. coli* Rosetta 2 (DE3) pLysS cells (Novagen), were prepared. Transformation was achieved using a heat shock protocol[37]. *E. coli* C43 and Rosetta 2 cells, were transformed with the vector *mqoI-S. aureus* and grown, respectively, in Luria Bernati (LB) medium supplemented with 50 µg mL^{-1} kanamycin (Roth), or in 2×YT-rich medium supplemented with 100 µg mL^{-1} kanamycin (Roth) and 34 µg mL^{-1} chloramphenicol (Roth), at 37 ºC and 180 rpm. Several expression conditions were tested, some of which prior to the beginning of the project. Most promising gene expressions were induced with 0.5 mM or 1 mM IPTG (isopropyl β-D-1-thiogalactopyranoside) (Apollo Scientific) when the cells reached an optic density at 600 nm (OD_{600}) of 0.6. The cells were harvested 4 h after induction or after an overnight growth, by centrifugation at 8,000 rpm for 10 min, and stored at -20 ºC.

For MQO II, expression tests were performed in the host lab and optimized before the beginning of the project. *E. coli* C43 cells were transformed with the vector *mqoII-S. aureus* and grown in Terrific Broth (TB) medium supplemented with 50 µg mL^{-1} kanamycin (Roth), at 37 ºC and 180 rpm. Gene expression was induced with 0.1 mM IPTG (Apollo Scientific) when the cells reached an optic density at 600 nm (OD_{600}) of 0.6. The temperature was changed to 18 ºC after the induction[35]. Cells were harvested after an overnight growth, by centrifugation at 8,000 rpm for 10 min, and stored at -20 ºC.

3.1.2. Protein Purification

Cells were resuspended in 20 mM Tris-HCl buffer pH 7.8, 10 % glycerol, 250 mM NaCl, or 100 mM K_2HPO_4/KH_2PO_4 pH 7.0, 250 mM NaCl, both containing one complete protease-inhibitor cocktail tablet (Roche). Cells were disrupted in a French press at 41.4 MPa and cellular debris and undisrupted cells were separated out by centrifugation at 10,000 rpm, 10 min. The membrane fraction was ultracentrifuged at 42,000 rpm, and different times were tested: for 2 h, 4 h and overnight. Several experiments were also performed in order to remove the protein from the membrane; these included tests with sodium chloride (NaCl) and with detergent DDM (n-Dodecyl β-maltoside) (Glycon), varying the concentrations of each. In some trials, the membrane pellet was resuspended using a Potter homogenizer in 100 mM K_2HPO_4/KH_2PO_4 buffer pH 7.0, 2

M NaCl, and incubated overnight at 4 ºC, under agitation. In another approach the membrane pellet was resuspended with a Potter homogenizer in 20 mM Tris-HCl buffer pH 7.8, 10 % glycerol, 500 mM NaCl, 0.1 % ethylenediaminetetraacetic acid (EDTA). DDM was gradually added (3 g of detergent per 1 g of protein) and incubated overnight at 4 ºC, under agitation. The membrane fraction was further ultracentrifuged at 42,000 rpm for 1 h or 3 h, depending on the different approaches. NaCl concentration in the supernatant containing the protein of interest was decreased to approximately 50 mM NaCl at 4 ºC by successive additions of the same buffers used in the steps before according to the different trials, but no NaCl. The sample was concentrated in an Amicon system (30 000 MWCO).

The obtained washed membrane fraction was injected in an ion-exchange Q-Sepharose High Performance 74 mL column (GE Healthcare) and eluted with a concentration gradient from 0 to 1 M NaCl in 20 mM Tris-HCl buffer pH 7.8, 10 % glycerol, or in 100 mM K_2HPO_4/KH_2PO_4 buffer pH 7.0. The fraction containing the protein of interest was then injected into a size exclusion chromatography column, Gel-filtration Superdex 200 XK 26/60 300 mL column (GE Healthcare) and eluted with 20 mM Tris-HCl buffer pH 7.8, 10 % glycerol, 150 mM NaCl or with 100 mM K_2HPO_4/KH_2PO_4 pH 7.0, 250 mM NaCl. The buffers used contained one complete protease-inhibitor cocktail tablet (Roche). These two columns were chosen as initial steps of the purifications and were common to most of the different experiments, although there were cases where more than one injection was needed, depending on the trials. Fractions containing the protein of interest, selected by absorption spectroscopy and enzymatic assays, were further injected in different columns and different procedures were tested: His-Trap HP 5 mL column (GE Healthcare) was used, since it presents affinity for histidines, using as eluent a concentration gradient from 20 mM to 300 mM imidazole (Sigma Aldrich). An affinity chromatography Hi Trap IMAC HP 5 mL column (GE Healthcare) was also tested, charged with zinc ($ZnCl_2$; MERCK) or with cobalt ($CoCl_2$; MERCK), and eluted with a concentration gradient from 5 mM to 250 mM of L-Histidine (Roth). An anion exchanger Mono Q 5/50 GL column (GE Healthcare) was used in some purification trials, and the elution step was performed with a concentration gradient from 0 to 1 M NaCl in 100 mM K_2HPO_4/KH_2PO_4 buffer pH 7.0. Chromatography columns were operated by an AKTA Prime Plus system (GE Healthcare) and detection was monitored by the change in absorbance at 280 nm. All the protein fractions were stored at -20 ºC.

The described procedures were applied to both MQO I and MQO II.

3.1.3. Biochemical and Biophysical Characterization

3.1.3.1. Protein purity assessment

Protein purity of the different samples was analysed by sodium dodecyl sulphate – polyacrylamide gel electrophoresis (SDS-PAGE) using a Mini-PROTEAN® Electrophoresis System from BIORAD. Samples were diluted in 5 µL of loading buffer (Tris-HCl 50 mM, pH 8; SDS; Bromophenol Blue; Glycerol; β-mercaptoethanol and Urea) and were subsequently injected

in a 15 % acrylamide stacking and resolving gel. Precision Plus Protein™ Dual Color (BIORAD) and Low Molecular Weight (LMW) standards (GE Healthcare) were used ranging from 10 to 280 kDa and from 14 to 97 kDa, respectively. Electrophoreses were carried out at 180 V, 400 mA, 200 W for 1 h. Gels were revealed using Blue Coomassie Stainer and destaining solution in order to observe the protein bands.

3.1.3.2. Absorption spectroscopy

UV-Visible absorption spectroscopy was used to evaluate the fractions resulting from the purification steps. UV-Visible absorption spectroscopy was performed on a Shimadzu UV-1800 spectrophotometer, at room temperature, using a wavelength range from 250 to 750 nm.

Absorption spectroscopy was also used to characterize the different reduction states of the protein. Spectra were collected on a spectrometer placed inside an anaerobic chamber (Coy Laboratory Products) with an O_2 level below 1 ppm. All solutions were prepared inside the anaerobic chamber with degassed water to guarantee the absence of oxygen. Reduction of 4.6 µM MQO II was achieved by addition of sodium dithionite (Sigma Aldrich) in a proportion of 1:10. Spectra were collected from 250 to 750 nm, in 100 mM phosphate buffer pH 7.0, 250 mM NaCl.

3.1.3.3. Protein quantification

Protein concentration was determined by the BCA (bicinchoninic acid assay) Protein Assay Reagent (Pierce) using BSA (bovine serum albumin) as standard (Thermo Fisher Scientific) according to the respective kit protocol[38] or using the Biuret Protein Assay according to the protocol[39].

3.1.3.4. Enzymatic studies

Kinetic assays were performed under anaerobic conditions, in an anaerobic chamber with low O_2 levels, below 1 ppm. All the solutions were prepared inside the anaerobic chamber with degassed water. Each experiment was performed in triplicate at 30 °C and with continuous agitation. Each assay started with the addition of the electron acceptor, 150 µM 2,3-dimethyl-1,4-naphtoquinone (DMN) (synthesized from menadione[40] from Sigma Aldrich) or 100 µM 2,6-dichloroindophenol (DCPIP) (Sigma Aldrich), in 100 mM phosphate buffer pH 7.0, 250 mM NaCl, followed by the addition of 15 mM of substrate, Malate (L-malic acid; Sigma Aldrich) or Lactate (Potassium L-Lactate; FLUKA), and finally the addition of protein. In some specific cases, enzymatic activities were also tested with 150 µM DMN in the presence of 150 µM 2-n-Heptyl-4-hydroxyquinoline-N-oxide (HQNO) (Alexis Biochemicals). The reactions were monitored by the change in the absorbance at 300 nm for DMN or 600 nm for DCPIP.

Enzymatic assays were also performed in the same conditions, as a screening procedure, in order to select fractions containing the protein of interest during the purification steps.

3.1.3.5. Protein stability analyses

In order to study the thermal stability of the protein, thermal denaturation assays were performed using a Peltier temperature controller with a rate of 0.5 °C/min between 25 and 90 °C. Data was recorded in intervals of 1 ºC with an acquisition time of 0.1 min. Denaturation was monitored by fluorescence spectroscopy using two different excitation wavelengths, 450 nm (monitoring FAD) and 280 nm (monitoring tryptophan) with emission wavelengths of 530 nm and 355 nm, respectively. The assays were performed using 2 µM of protein diluted in 100 mM phosphate buffer pH 7.0, 250 mM NaCl.

The Melting Temperature was calculated using the *OriginPro8 software*, fitting a Boltzmann function (sigmoidal curve) to the data.

3.2. Functional Characterization

3.2.1. Enzymatic activity pH profile

The kinetic assays at different pH values were performed under anaerobic conditions, in an anaerobic chamber with low O_2 levels, below 1 ppm. All solutions were prepared only inside the anaerobic chamber with degassed water. Enzymatic reactions were evaluated at 600 nm. Each experiment was performed in triplicate at 30 °C and with continuous agitation. The enzymatic activity was tested at different pH values, namely pH 5.5, pH 6, pH 6.5, pH 7, pH 7.5 and pH 8, in 50 mM MES (2-(*N*-morpholino) ethanesulfonic acid) (Roth), 50 mM Bis-Tris Propane buffer (Sigma Aldrich), 250 mM NaCl. Each assay started with the addition of 0.1 mM DCPIP (Sigma Aldrich), followed by the addition of 15 mM Lactate (Potassium L-Lactate; FLUKA), and then of 0.92 µM of protein, MQO II.

3.2.2. Mass Spectrometry analysis

Proteins were identified by mass spectrometry at the ITQB/IBET MS Unit. Data were acquired in a positive reflector MS and MS/MS modes using a 4800 plus MALDI-TOF/TOF (AB Sciex) mass spectrometer, using *4000 Series Explorer software v.3.5.3* (Applied Biosystems). External calibration was performed using Pepmix1 (Laser BioLabs).

3.3. Cellular Studies

With the aim of understanding the impact of MQO I in the energetic metabolism of *Staphylococcus aureus*, bacterial growths of a wild-type strain and of a mutant with a transposon in the gene coding for MQO I, were performed.

3.3.1. Bacterial Strains

The *S. aureus* strains used were all derived from JE2 (the wild-type strain). The *bursa aurealis* transposon mutant was obtained from the Nebraska Transposon Mutant Library[41]. *S. aureus* strain JE2 is a plasmid-cured derivative of strain LAC that was isolated in 2002 from a skin and soft tissue infection of an inmate in the Los Angeles County Jail in California, USA. Strain JE2 is a methicillin-resistant *S. aureus* (MRSA) strain and is a USA300 isolate.

Staphylococcus aureus transposon mutant NE1381 (SAUSA300_2541) was created by disruption of *mqoI*, the gene coding for malate:quinone oxidoreductase I. This transposon mutant was derived from *S. aureus* strain JE2. Mutagenesis occurred through the use of the *mariner*-based transposon (Tn) *bursa aurealis* resulting in an erythromycin-resistant deletion strain of JE2[42]. This mutant strain is mentioned throughout this thesis as mqoI::Tn.

3.3.2. Confirmation of the Mutation mqoI::Tn

In order to verify the location of the transposon insertion in the gene coding for MQO I (SAUSA300_2541), we used specific primers. Therefore, the forward primer (5'-CTCGATTCTATTAACAAGGG-3') was used to hybridize with the *bursa aurealis* transposon while the reverse primer was the gene-specific primer (5'-GGCTCCAATTAAAACGATG-3') to generate a polymerase chain reaction (PCR) product. The PCR product size was confirmed by an agarose gel electrophoresis.

3.3.3. Cell Growth

Staphylococcus aureus strains obtained from the Nebraska Transposon Mutant Library were grown in Tryptic Soy Agar (TSA) (Difco) plates, containing 15 g L^{-1} agar, incubated overnight at 37 ºC. Precultures were inoculated with a single colony, from the correspondent TSA plate, grown for 14 hours under aerobic conditions in Tryptic Soy Broth (TSB) (Difco) medium at 37 ºC and 180 rpm. Erythromycin 25 µg μL^{-1} (Roth) was used as the selective antibiotic in the mutant strain (mqoI::Tn).

S. aureus growths were performed in a complex and rich medium, TSB, containing 14 mM glucose (Table 7.1 in Supplemental Material), and also in a chemically defined medium (CDM) (Table 7.2 in Supplemental Material) prepared according to Nicholas P. Vitko and Anthony R. Richardson[43].

Since CDM is a controlled medium, it is possible to vary the growth conditions, thus the carbon sources were varied according to the different experiments: 5 mM glucose (D-Glucose anhydrous, extra pure; Scharlau); 5 mM acetate (sodium acetate anhydrous; Panreac); or 5 mM lactate (Potassium L-Lactate; FLUKA). In all the different conditions, two variables were monitored during the growth, the optical density at 600 nm (OD_{600}) (Shimadzu UV-3100

spectrophotometer) and the pH (pH meter GLP 22; Crison Instruments, SA), measured at 1-hour intervals.

Cultures were grown aerobically in 250 mL Erlenmeyer flasks (VWR) (volume 1:5 of the flasks total capacity) in an orbital shaker (INFORS HT) at 220 rpm under 37 ºC, to guarantee aerobic conditions. Cultures were initiated by addition of the correspondent pre-culture, to an initial optical density at 600 nm (OD_{600}) of about 0.13-0.15, in TSB medium, or about 0.04-0.05 for CDM medium.

For metabolite NMR (nuclear magnetic resonance) analyses, *S. aureus* growths (triplicates) were used. Samples were collected at different time-points during the growth. Culture cells were grown in the same conditions (volume 1:5 of the flasks total capacity) in 500 mL Erlenmeyer flasks (VWR). OD_{600} and pH values were measured every 2 h for TSB medium, and at 1.5 h for CDM medium. Samples (1.5 mL) were collected by centrifugation (13,000 rpm, 5 min, 4 ºC) (Micro Star 17R; VWR) and the supernatant solutions were stored at -20 ºC.

The handling of *S. aureus* was always performed inside a laminar flow chamber (Class II Type A/B3 Laminar Flow Biological Safety Cabinet; NUAIRE).

3.3.4. NMR-based Metabolomics

3.3.4.1. Sample preparation

Extracellular metabolome ^{1}H-NMR analysis performed in 5 mm glass tubes (7 inch in length; NORELL 508-UP). For each collected sample, 400 µL were used and buffered to pH 7.0 by adding 200 µL 200 mM sodium hydrogen phosphate buffer (Panreac) solution, prepared with 100 % D_2O (deuterium oxide) (CortecNet), to provide a nuclear magnetic resonance (NMR)-lock signal. Additionally, the buffer solution contained a final concentration of 1 mM of TSP (3-trimethylsilyl-[2,2,3,3-D_4]-1-propionic acid) (Uvasol®) as an internal standard for subsequent quantification, used for chemical shift referencing and normalization of NMR peak intensities.

3.3.4.2. NMR data collection

All ^{1}H-NMR spectra were obtained at 25 ºC on a Bruker AVANCE III 500 NMR spectrometer, operating at a central frequency of 500.13 MHz (Bruker Biospin, Rheinstetten, Germany), equipped with a 5 mm TCI C/N Prodigy Cryo probe. The equipment was controlled via *Topspin version 3.2 software* (Bruker Biospin, Rheinstetten, Germany). Spectra were acquired with water presaturation during a delay of 2 s and using a total recycling time of 35 s to allow full relaxation of the signals. Two hundred forty-three spectra were collected. 16 transients were collected into 64k data points using a spectral width of 16 ppm. Fourier transform was performed with no exponential multiplication. The NMR data was acquired at CERMAX, ITQB-NOVA, Oeiras, Portugal.

3.3.4.3. NMR data analyses and quantification

^{1}H-NMR spectra analyses were performed using *Topspin version 3.2 software* (Bruker Biospin, Rheinstetten, Germany). Spectra were automatically phased and baseline-corrected, and the chemical shift scale was set by assigning the value of δ=0.00 ppm to the signal from the added TSP. Compound identification was done by matching the obtained spectra with a ^{1}H-NMR spectra databank using *Chenomx Nmr Suite Version 8.12 software* (Chenomx Inc.) and comparing with spectra of standard compounds.

Quantification was done by integration of designated peaks, considering the number of protons responsible for each signal in the defined frequencies (Table 7.3 in Supplemental Material), and comparing with the added standard TSP (integral calibrated as 9 protons, considering the number of protons and the concentration in which it was present, 1 mM). The molar concentration of each compound was estimated also considering the sample dilution (3:2). For each triplicate assay, the median was calculated and the standard deviations were determined, for all the metabolic peaks studied.

4. Results and Discussion

4.1. Malate:quinone oxidoreductase I

4.1.1. Protein expression and purification

Malate:quinone oxidoreductases from *S. aureus* have been overlooked and were never purified. In order to study and biochemically characterize these proteins, purification experiments were initiated.

Ten purification trials were performed to obtain MQO I, changing different conditions, including type of expression cells, growth medium, IPTG concentration for gene expression, centrifugation times for harvesting cells, buffer solutions, extraction methods for protein removal from the membranes, chromatographic procedures (different columns and/or gradients), among others. Taking into account all attempts and optimization steps, the two most promising purification processes of MQO I will be described below.

4.1.1.1. First purification trial

Expression tests had been already performed at the beginning of this thesis project, thus we started with the best achieved methodology. In the first purification trial, *E. coli* C43 cells were used, because these cells usually provide high growth levels and are recommended for membrane protein expression[44]. Transformed *E. coli* cells with the plasmid containing the gene coding for MQO I, grew overnight in LB medium with 50 µg mL^{-1} kanamycin at 25 ºC and 180 rpm. Gene expression was induced with 0.5 mM IPTG at cell density correspondent to OD_{600} of 0.6. A SDS-PAGE confirming the expression of the enzyme is shown below in Figure 4.1.

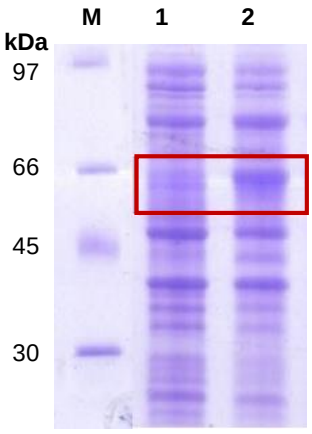

Figure 4. 1 - SDS-PAGE of cells expressing MQO I. SDS-PAGE: Stacking Gel – 4 % acrylamide; Resolving Gel – 15 % acrylamide; Lane 1 – *E. coli* C43 cell extract before IPTG addition (OD_{600} = 0.6); Lane 2 – *E. coli* C43 cell extract after overnight (16 h) induction. Theoretical molecular mass of MQO I: ~ 57 kDa. Low molecular weight (LMW) protein marker was used (M).

The gel shows in lane 2 (cells after induction) the presence of a band between the 45 and 66 kDa markers that is not observed in lane 1 (cells before induction), indicating the expression of the protein. Based on the obtained results, large cell growths were performed in the same conditions, in order to obtain sufficient cell mass as starting material to purify the protein of interest. The growth yield was approximately 5 g L^{-1}. Cells were harvested after overnight growth and stored at -20 ºC until further use.

Approximately 100 g of thawed cells were suspended in 20 mM Tris-HCl buffer pH 7.8, 10 % glycerol, 250 mM NaCl, before being disrupted using a French Press at 41.4 MPa. Disrupted cells were separated from non-disrupted ones by centrifugation at 10,000 rpm for 10 min, and the membrane fraction (containing the protein) was separated from the soluble fraction by ultracentrifugation at 42,000 rpm, 4 h. This duration was not sufficient to separate both fractions, and a new ultracentrifugation was performed for 14 h (overnight). The obtained membrane pellet was resuspended in 20 mM Tris-HCl buffer pH 7.8, 10 % glycerol, 500 mM NaCl, 0.1 % EDTA, with a Potter homogenizer. EDTA was added to the buffer to increase protein stability.

Removal of protein from the membrane was achieved by solubilizing the membranes with the detergent n-dodecyl-β-D-maltoside (DDM). The process of solubilisation of membrane proteins depends on the amount of detergent relative to membrane protein. Thus, the amount of detergent added was proportional to the amount of protein, which was measured by the Biuret Protein Assay.

In this protein quantification method, samples are combined with Biuret Reagent which contains copper ions in a basic solution. When an amino group and a carboxyl group join to form a peptide bond, the amino group ($-NH_2$) becomes an amide group (-NH). In a basic pH, copper ions will complex with the amide groups of the proteins, providing a characteristic blue colour that is measured using absorbance spectroscopy. The quantity of protein is directly proportional to the intensity of the blue colour[45].

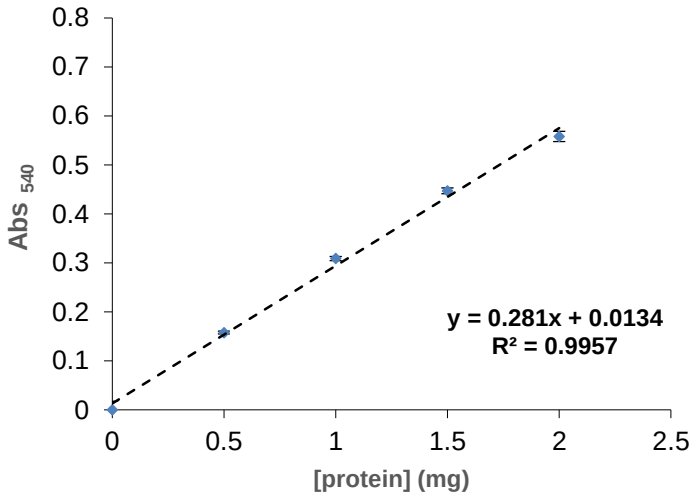

Figure 4. 2 - Calibration curve (dotted line) was calculated by a linear regression equation. The absorbance was measured at 540 nm. The error bars are relative to triplicate assays.

A calibration curve was constructed according to the protocol[39] (Figure 4.2), varying the standard protein concentration. The absorbance of the sample of interest was also measured and

the amount of protein determined was about 2.82 g L^{-1}, calculated based on the regression equation. Three grams of detergent were used per gram of protein, thus 8.4 g of DDM were gradually added to the membrane fraction and incubated overnight at 4 ºC, under agitation.

Detergents play an essential role in the solubilisation, purification, and manipulation of membrane proteins; their amphiphilic structure (both hydrophobic and hydrophilic) allows the interaction with hydrophobic membrane proteins to keep them water-soluble outside of their native bilayer environment. Detergent binds to the membrane, and solubilisation occurs in the form of a detergent-lipid-protein complex. Furthermore, the solubilisation of this complex provides detergent-protein complexes and detergent-lipid complexes[46]. MQO I has been described as a monotopic enzyme, like other quinone reductases, but since these proteins have not been yet properly characterized, their interactions with the membranes are not known[4,17,47].

The solubilized membrane fraction gained a “yellowish” hue, suggesting a successful solubilisation of MQO I. Soluble and membrane fractions were separated again by ultracentrifugation at 42,000 rpm, 3 h. The ionic strength of the resulting supernatant (solubilized fraction) containing MQO I, was decreased stepwise in an Amicon concentrator/Diaflo from 500 mM to 50 mM NaCl in order to allow an ionic exchange chromatography step.

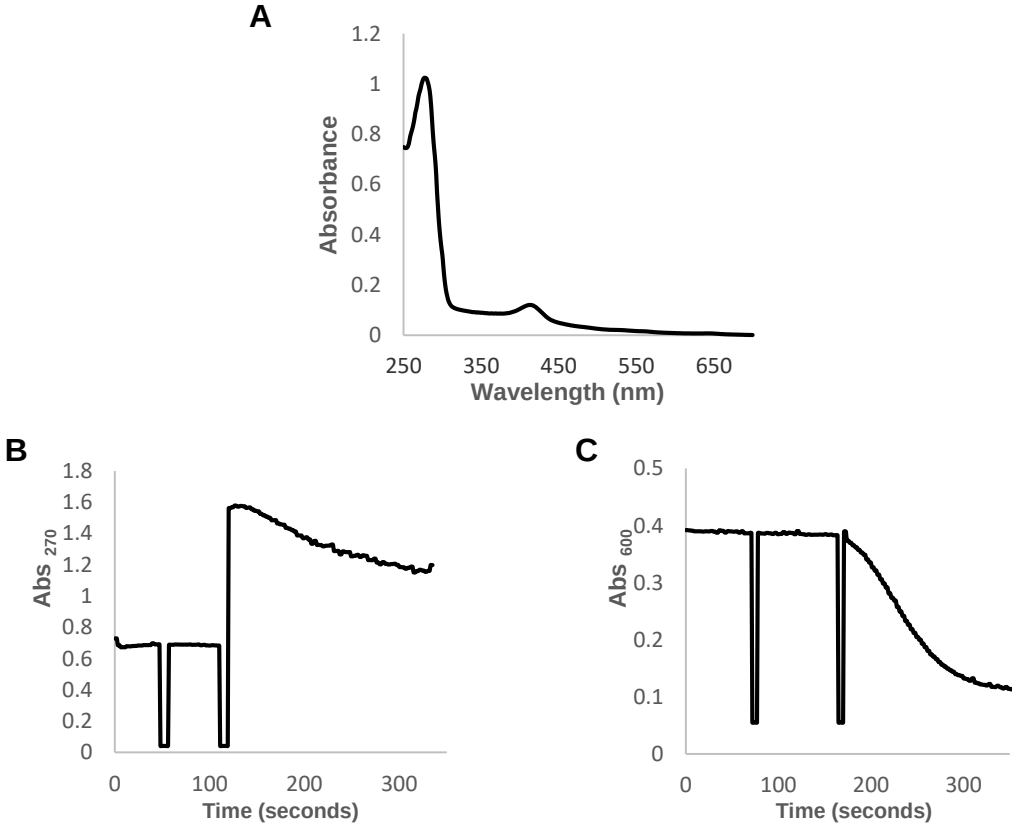

Figure 4. 3 - A) UV-Visible absorption spectrum of the solubilized membrane fraction. B) Malate:quinone oxidoreductase activity of the solubilized membrane fraction, using 15 mM L-malic acid and 150 µM DMN. The wavelength was monitored at 270 nm, 30 ºC. C) Enzyme activity of the solubilized membrane fraction, using 15 mM L-malic acid and 100 µM DCPIP, as electron acceptor. This activity was monitored at 600 nm, 30 ºC.

The solubilized fraction was evaluated by UV-Visible absorption spectroscopy and enzymatic activity, with both DMN or DCPIP as electron acceptors, in order to confirm the presence of malate:quinone oxidoreductase I (Figure 4.3).

Figure 4.3 (A) shows a band with absorbance at 450 nm characteristic of a flavoprotein[20], although absorbance attributed to some contaminants is also observable, especially at 410 nm, probably due to the presence of a cytochrome contamination. Cytochromes are proteins with characteristic strong absorption of visible light. Absorption spectrum of cytochrome *c* reveal a typical absorption peak at 410 nm in the oxidized state, while in the reduced form it presents three characteristic *α*, *β* and *γ* absorption bands, approximately absorbing at 550, 520 and 420 nm, respectively[2,48,49] – Figure 7.2 in Supplemental Material. Despite being a soluble protein, cytochrome *c*, associates with the membrane through electrostatic interactions[2].

Malate:quinone oxidoreductase activity was followed by absorption spectroscopy, at 270 nm evaluating the redox state of the quinone (DMN). Malate (L-malic acid) was used as electron donor and DMN as electron acceptor. The enzymatic activity was also tested using the DCPIP as electron acceptor (600 nm). DCPIP is an artificial electron acceptor, often used to detect MQO activity in membranes and it has the advantage of absorbing at 600 nm with a high extinction coefficient[14,17]. In the respective monitored wavelengths, the absorbance should decrease for the two electron acceptors. These are being reduced and their respective reduced state does not present change at the chosen wavelengths. These enzymatic assays were performed to confirm the success of the protein solubilisation and by consequence to confirm the presence of MQO I in our sample.

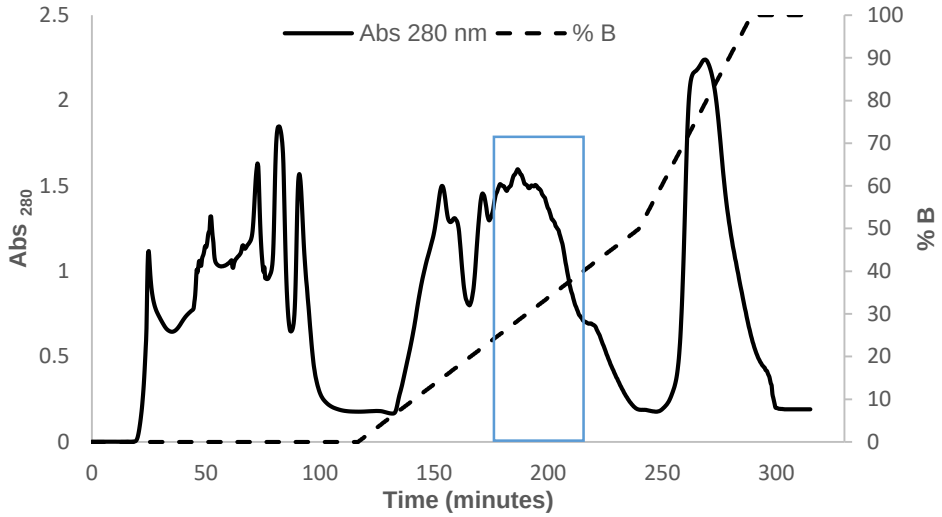

Figure 4. 4 - Chromatogram obtained in the purification of MQO I from *S. aureus*, by a Q-Sepharose HP column 74 mL. Flux = 3 mL/min. In black filled line is represented the absorbance at 280 nm, in dashed line is represented the % of 1 M NaCl, 20 mM Tris-HCl buffer pH 7.8, 10 % glycerol (buffer B). The protein eluted approximately at 30 % of B (blue).

The solubilized fraction was injected in a Q-Sepharose HP column 74 mL and eluted with a NaCl gradient ranging from 0 to 1 M. This strong anion exchange chromatography column promotes the binding of the proteins of interest to the separation medium at low ionic strength,

which are then eluted with a salt gradient. The resulting chromatogram is shown in Figure 4.4. Fractions containing MQO I were identified by UV-Visible spectroscopy and by enzymatic assays. The protein eluted at around 30 % buffer B, corresponding to 300 mM NaCl, as shown in Figure 4.4.

Since the fraction of interest still presented some contaminants, observed in the UV-Visible absorption spectrum, another injection in Q-Sepharose HP column was performed in the same conditions. The chromatogram revealed a similar pattern, with the protein eluting equally at 300 mM NaCl. Fractions containing MQO I were concentrated and further injected in a size-exclusion chromatography column (S200 300 mL). This type of chromatography separates the different compounds according to their molecular size. Separation occurs depending on the inclusion or exclusion of the molecules from the pores within the matrix. Small molecules diffuse into the pores and their flow through in the column is retarded according to their size, while large molecules do not enter into the pores and are consequently eluted in the column's void volume. Thus, molecules are separated based on their size and are eluted in order of decreasing molecular mass.

The resulting chromatogram is shown in Figure 4.5. Fractions were selected according to the corresponding absorption spectra, to the ratio between the absorbance intensities at 280 nm and 450 nm (Abs_{280}/Abs_{450}), and also based on a positive result for enzymatic activities with malate:DCPIP oxidoreductase. DCPIP was used, instead of the quinone, due to its advantages namely having a higher ε, which allows higher sensitivity. The fraction containing MQO I eluted at about 300 min (~ 150 mL). Three injections were done in this size exclusion column, considering the injection volume limit. All presented the same elution pattern.

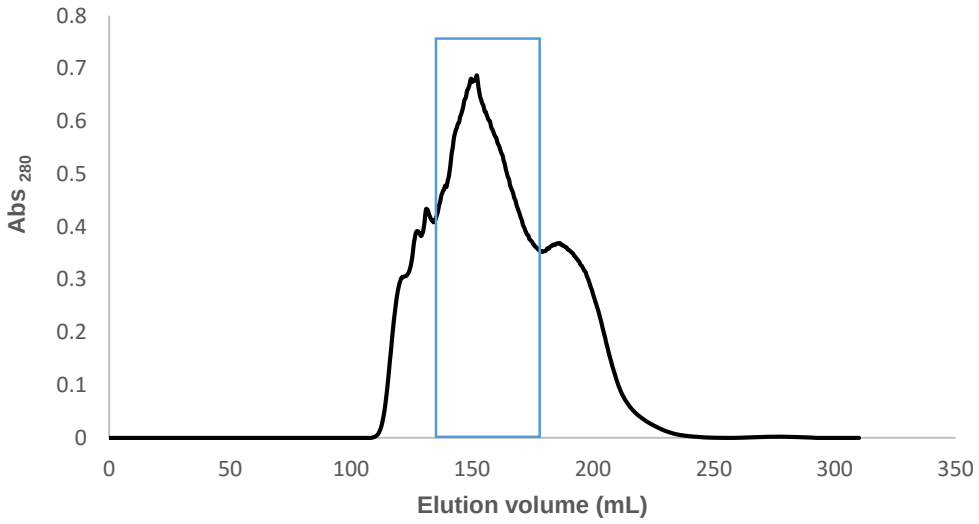

Figure 4. 5 - Chromatogram obtained in the purification of MQO I from *S. aureus* in a S200 column 300 mL, with 20 mM Tris-HCl buffer pH 7.8, 10 % glycerol, 150 mM NaCl. Flux = 0.5 mL/min. In black filled line is represented the absorbance at 280 nm. The protein eluted around 150 mL (blue).

Since the fraction of interest was still not pure, another injection was performed, this time in an affinity chromatography Hi Trap IMAC HP 5 mL column charged with zinc (Zn^{2+}) and using a concentration gradient of L-histidine as eluent. This chromatographic method is used for the purification of histidine-tagged proteins and provides high binding capacity. MQO is expressed with a tail of six histidines inserted and so we decided to try this procedure. The use of zinc as the ion chosen for Immobilized Metal ion Affinity Chromatography (IMAC) was based on several factors. Cobalt had already been tried and the purification was not successful, and copper, manganese and nickel were described as inhibitors of MQO activity at very low concentrations, for *Bacillus* sp. PS3[16]. The resulting chromatogram is presented in Figure 4.6.

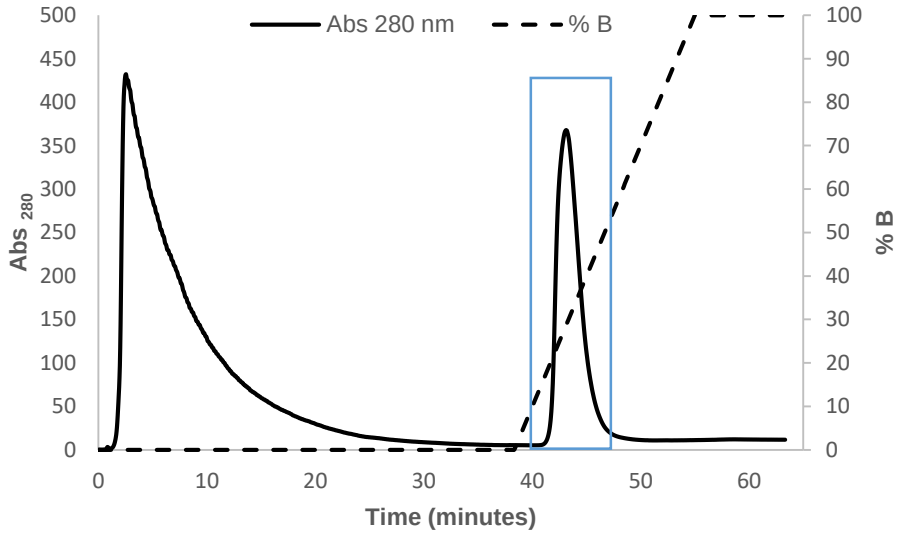

Figure 4. 6 - Chromatogram obtained in the purification of MQO I from *S. aureus*, by Hi Trap IMAC HP column 5 mL charged with Zn^{2+}. Flux = 3 mL/min. In black filled line is represented the absorbance at 280 nm and in dashed line the % of 250 mM L-Histidines, 20 mM Tris-HCl buffer pH 7.8, 250 mM NaCl, 10 % glycerol (buffer B). The protein eluted approximately at 28 % of B (blue).

Again, fractions were selected according to the corresponding absorption spectra, to the ratio between the absorbance intensities at 280 nm and 450 nm (Abs_{280}/Abs_{450}), and also based on enzymatic activities with malate:DCPIP oxidoreductase. The protein eluted at around 28 % B, corresponding to 70 mM L-histidine.

The resulting absorption spectrum of the MQO I from *S. aureus* is presented in Figure 4.7 (A), where contaminants are still noticed. However, it is possible to observe the protein expression in the SDS-PAGE gel, represented by an intense band in the 50-75 kDa region. During the different purification steps throughout the process, enzymatic activities were measured spectroscopically at 600 nm, using 15 mM Malate (L-malic acid) as electron donor and 0.1 mM DCPIP as electron acceptor. Total enzyme activity and specific activity were calculated based on the Beer-Lambert law and according to the molar extinction coefficient of DCPIP at 600 nm (ε_{600}) equivalent to 20.7 mM^{-1} cm^{-1} – Table 4.1 [50]. No enzymatic activities were detected using 15 mM Lactate (L-lactate) as substrate.

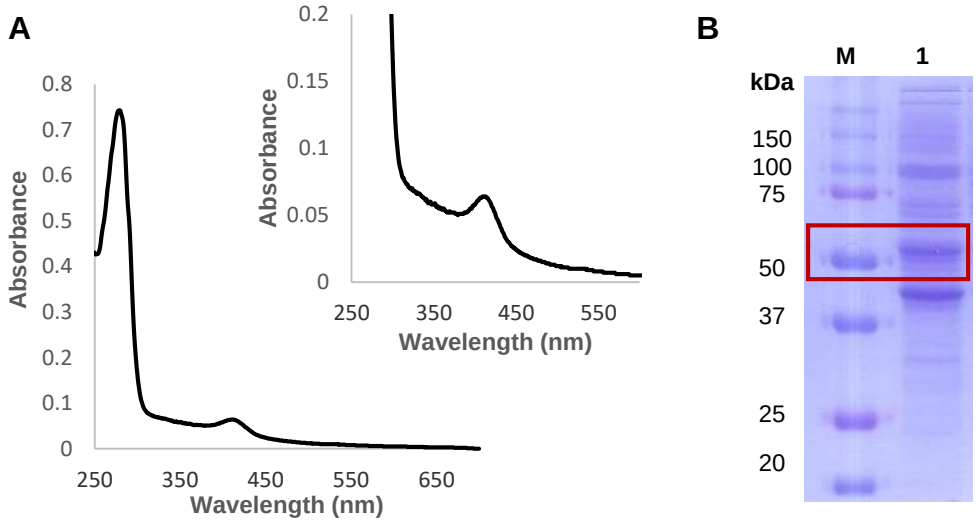

Figure 4. 7 - A) UV-Visible absorption spectrum of MQO I from *S. aureus* partially purified. The inset expands the absorption spectrum in the 250–550 nm region. B) The respective SDS-PAGE with MQO I expression (highlighted in red) – lane 1. SDS-PAGE: Stacking Gel – 4 % acrylamide; Resolving Gel – 15 % acrylamide; Theoretical molecular mass of MQO I: ~ 57 kDa. Precision plus protein dual colour standard was used as marker (M).

Table 4. 1 - Purification of MQO I from *S. aureus*. Enzymatic activities were measured at 30 ºC and 600 nm, following the change of absorbance of DCPIP by absorbance spectroscopy, using 15 mM Malate (L-malic acid) as electron donor and 0.1 mM DCPIP as electron acceptor. Total and specific enzymatic activities were calculated based on the Beer-Lambert law, following DCPIP at 600 nm using ε = 20.7 mM^{-1} cm^{-1} [50]. Kinetic assays were performed under anaerobic conditions, in an anaerobic chamber with O_2 levels below 1 ppm.
.

Steps	Volume (mL)	Protein (mg/mL)	MQO I Activity	
			Total (U)	Specific (U/mg)
1st Q-Sepharose	0.04	1.54	3.10	2.02
2nd Q-Sepharose	0.02	2.98	7.86	2.64
Size Exclusion	0.02	1.48	22.11	14.89
Hi Trap IMAC (Zn^{2+})	0.02	0.84	5.67	6.75

Table 4.1 shows an increase in the specific activities along the purification steps, excepting in the last one, in which the MQO I activity was decreased. An increase in the specific enzymatic activity is observed till the size exclusion step. However, the last tentative to obtain a higher purified protein was not succeed, as reflected by a lower specific activity in relation to the previous step.

An intense band between the 50-75 kDa region (highlighted in red on Figure 4.7 (B)) is observed in the SDS-PAGE gel, which probably corresponds to the protein of interest. This band was analysed by ITQB/IBET UniMS for protein identification by mass spectrometry analysis. The protein was identified by MALDI-TOF/TOF and the search was performed against a SwissProt protein database with taxonomic restriction to *Bacteria*. A positive protein identification was obtained. The report from the UniMS identified that protein as malate:quinone oxidoreductase I from *S. aureus* (Report number 1 in Supplemental Material).

Thus, the MQO I purification from *S. aureus* was achieved. Despite not being completely pure, considering the absorption spectrum which was not entirely characteristic of a flavoprotein and considering the SDS-PAGE gel, which still presented some contaminants, the purification process was further optimized. We verified that this procedure was too extensive, passing through several chromatography columns, leading to a low yield of protein. Thus, several trials were again performed to optimize the process. Taking into account all the different optimization trials, the most promising will be described below.

4.1.1.2. Second purification trial

E. coli Rosetta 2 (DE3) pLysS cells were now used as expression cells. Many possible *E. coli* strains are candidates to use as a host, all presenting advantages and disadvantages. Besides improving the levels of protein production, *E. coli* Rosetta_(DE3) strains were chosen considering they were already successfully used for the expression of other monotopic quinone reductases from *S. aureus*[44,51,52]. Expression tests were performed using these competent cells, which were transformed with the plasmid containing the gene coding for MQO I. The cells were grown in 2×YT-rich medium with 34 µg mL^{-1} chloramphenicol and 100 µg mL^{-1} kanamycin at 37 ºC and 180 rpm. The gene expression was induced with 1 mM IPTG at cell density corresponding to OD_{600} of 0.6 and cells were harvested after 4 h of induction. Figure 4.8 shows a SDS-PAGE gel with the expression test.

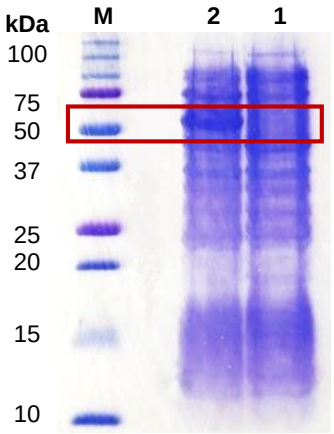

Figure 4. 8 - SDS-PAGE showing MQO I expression (highlighted in red). SDS-PAGE: Stacking Gel – 4 % acrylamide; Resolving Gel – 15 % acrylamide; Lane 1 – *E. coli* Rosetta cell extract before IPTG addition (OD_{600} = 0.6); Lane 2 – *E. coli* Rosetta cell extract after 4 h of induction. Theoretical molecular mass of MQO I: ~ 57 kDa. Precision plus protein dual colour standard was used as marker (M).

The gel shows in lane 2 (cells after induction) the presence of a band between the 50-75 kDa markers that is not observed in lane 1 (cells before induction), indicating the expression of the protein. Thus, large cell growths were performed in the same conditions. The growth yield was approximately 5 g L^{-1}.

In this second trial the buffer solutions were also changed: the phosphate buffer, 100 mM K_2HPO_4/KH_2PO_4 pH 7.0, 250 mM NaCl was used. The cells were disrupted using a French Press at 41.4 MPa. The posterior separation of the disrupted cells from the non-disrupted ones was achieved in the same way, through a centrifugation at 10,000 rpm, 10 min. The resulting suspension was ultracentrifuged at 42,000 rpm for 2 h, and not overnight as in the first trial. The membrane solubilized fraction containing the protein of interest was obtained by washing the membranes with high ionic strength, instead of using detergent, as in the previous described procedure. Thus, the membrane pellet was resuspended with a Potter homogenizer in 100 mM K_2HPO_4/KH_2PO_4 pH 7.0, 2 M NaCl and incubated overnight at 4 ºC under agitation. Then, the membrane fraction was again ultracentrifuged at 42,000 rpm for 1 h and the ionic strength of the resulting supernatant containing MQO I, was equally decreased stepwise in an Amicon concentrator/Diaflo from 2 M to 50 mM NaCl in order to further inject into an ionic exchange chromatography column.

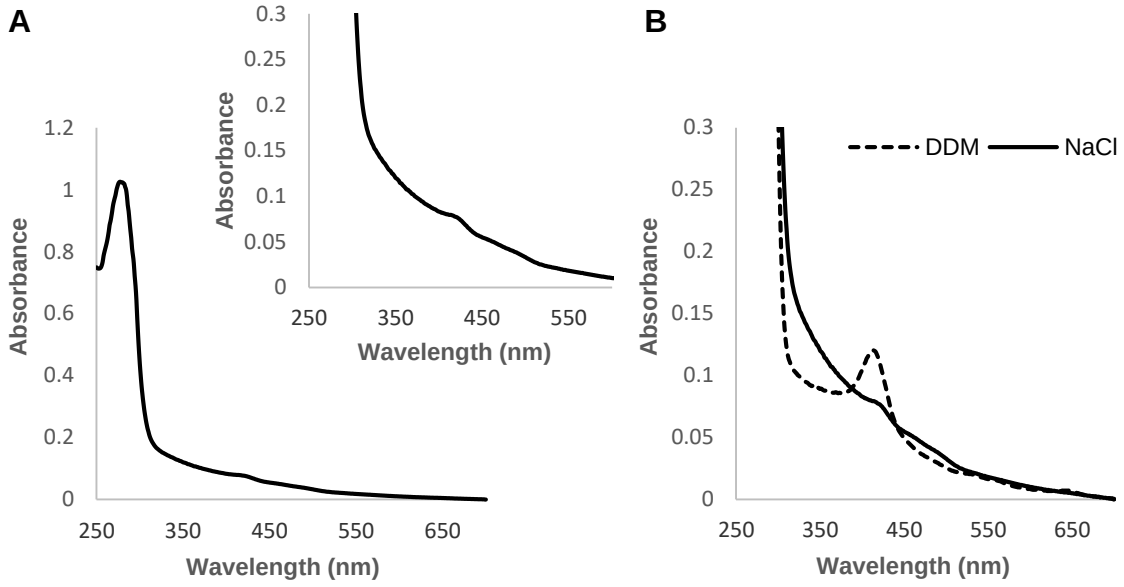

Figure 4. 9 - A) UV-Visible absorption spectrum of the membrane fraction washed with 100 mM K_2HPO_4/KH_2PO_4 pH 7.0, 2 M NaCl. The inset expands the absorption spectrum in the 250–550 nm region. B) Comparison of the absorption spectra of the membrane fractions solubilized with detergent (dashed line) and washed with 2 M NaCl (filled line).

Figure 4.9 (A) represents the absorption spectrum of the washed membrane fraction, and Figure 4.9 (B) shows the comparison between the spectra of the membrane fraction solubilized with detergent (black dashed line) and the membrane fraction obtained by washing with high ionic strength (black filled line), respectively described in the first and in the second trials.

In this second trial, the cytochrome contamination is less intense when cells were harvested 4 h after induction of gene expression and when the protein is removed from the membranes with 2 M NaCl (Figure 4.9). Host laboratory experience suggests that the cytochrome's expression increases during an *E. coli* overnight growth, which is also supported by

these data. This method is advantageous when compared to the methodology described in the previous trial (using detergent), not only due to the elimination of contaminants, but also because it has no detergent related interferences for further studies, and it is important to bear in mind that the use of NaCl instead of detergent is more economical and environmentally friendly. These changes contributed positively to the optimization of the purification process.

The fraction washed with high ionic strength, containing MQO I, was injected in a Q-Sepharose HP column 74 mL and eluted with a NaCl gradient ranging from 0 to 1 M, similarly to the first described procedure. The resulting chromatogram is shown in Figure 4.10.

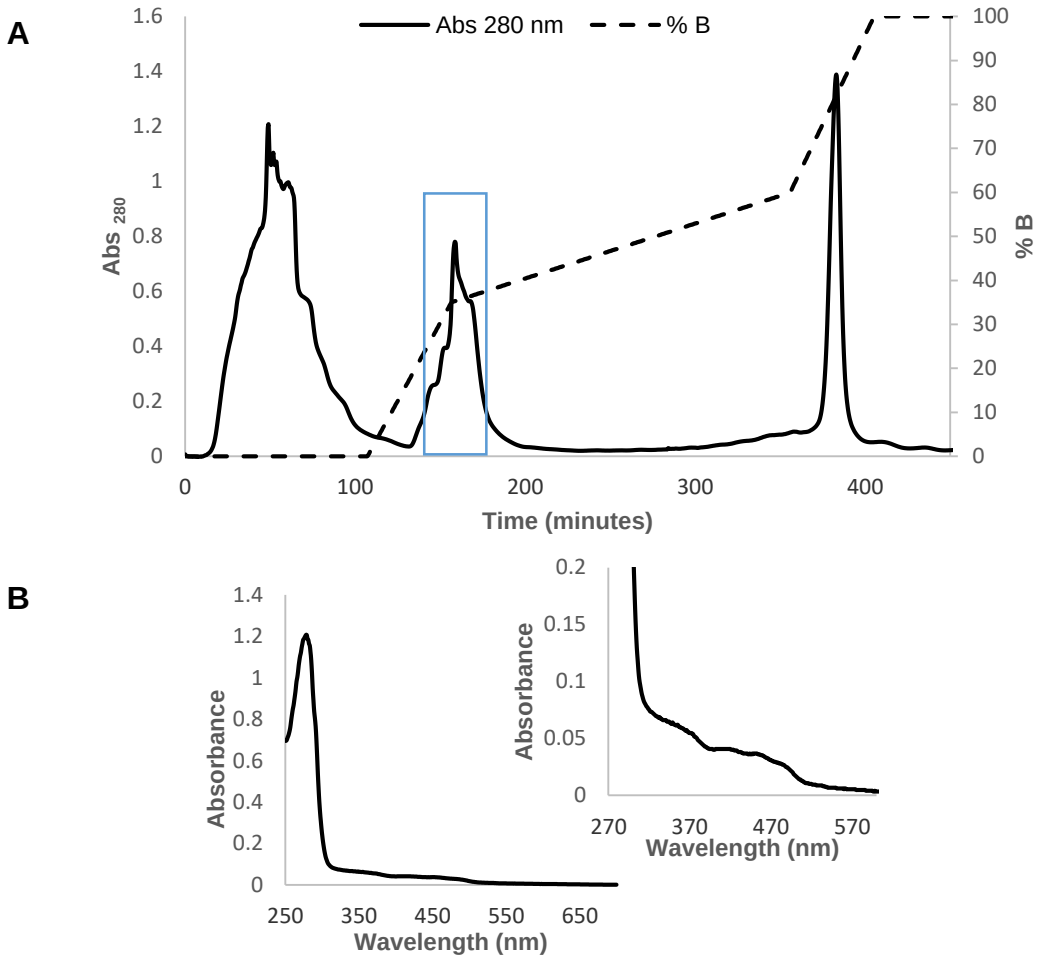

Figure 4. 10 - A) Chromatogram obtained in the purification of MQO I from *S. aureus*, by a Q-Sepharose HP column 74 mL. Flux = 3 mL/min. In black filled line is represented the absorbance at 280 nm, in black dashed line is represented the % of 1 M NaCl, 100 mM K_2HPO_4/KH_2PO_4 pH 7.0 (buffer B). The protein eluted approximately at 35 % of B (blue). B) UV-Visible absorption spectrum of the selected fraction from the Q-Sepharose HP column (blue box in (A)) containing MQO I. The inset expands the absorption spectrum in the 270–570 nm region.

Fractions containing MQO I were identified by UV-Visible absorption spectroscopy, based on the ratio between the absorbance intensities at 280 nm and 450 nm (Abs_{280}/Abs_{450}). Figure 4.10 (B) presents the absorption spectrum of the selected fraction resultant from the Q-Sepharose HP column. Several contaminants were eliminated with this chromatography step. Similarly to the

first described procedure, MQO I eluted with approximately 350 mM NaCl. These fractions were concentrated and further injected in a size exclusion chromatography column, using a phosphate buffer, 100 mM K_2HPO_4/KH_2PO_4 pH 7.0, 250 mM NaCl. The fraction containing MQO I eluted at about 125 min (~ 250 mL) – Figure 4.11.

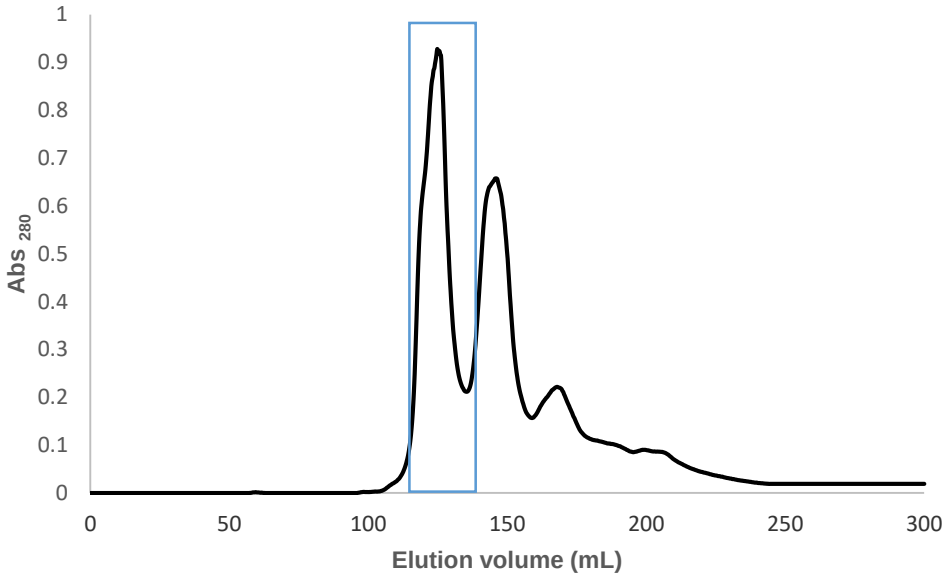

Figure 4. 11 - Chromatogram obtained in the purification of MQO I from *S. aureus* by a S200 column 300 mL, with 100 mM K_2HPO_4/KH_2PO_4 pH 7.0, 250 mM NaCl. Flux = 0.5 mL/min. In black filled line is represented the absorbance at 280 nm. The protein eluted around 125 mL (blue).

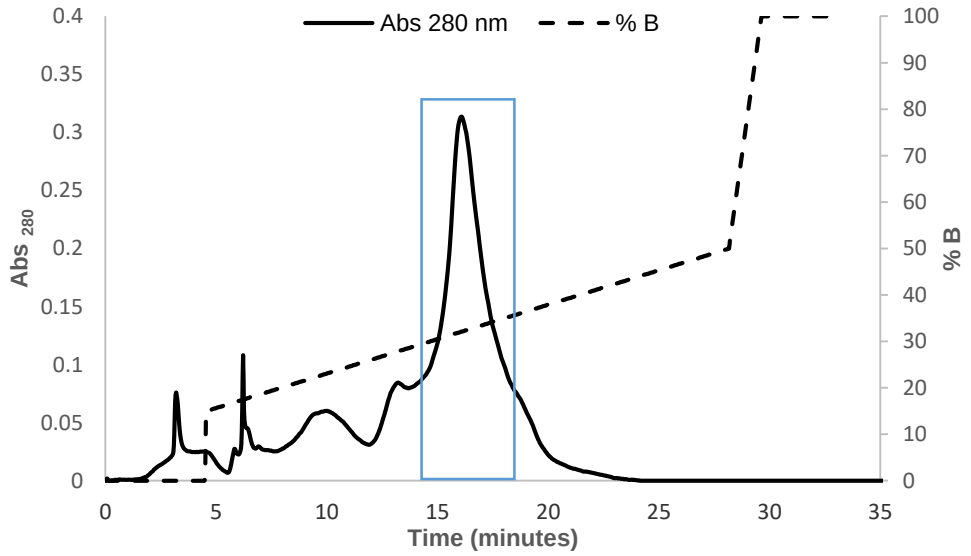

Figure 4. 12 - Chromatogram obtained in the purification of MQO I from *S. aureus*, by a Mono Q 5/50 GL column. Flux = 1 mL/min. In black filled line is represented the absorbance at 280 nm, in black dashed line is represented the % of 1 M NaCl, 100 mM K_2HPO_4/KH_2PO_4 pH 7.0 (buffer B). The protein eluted approximately at 35 % of B (blue).

Finally, fractions containing the protein of interest were injected in an anion exchange Mono Q 5/50 GL column, which is a chromatography column that presents maximum resolution leading to high purity levels. The chromatographic principle is the same applied for the Q-

Sepharose HP column, providing the binding of the proteins of interest to the separation medium which are further eluted with a gradient of salt, ranging from 0 to 1 M NaCl. Fractions containing MQO I were selected in the same way as in the previous steps. The chromatogram is represented in the Figure 4.12. The protein eluted around 35 % buffer B, corresponding to 350 mM NaCl.

The resulting absorption spectrum of the MQO I from *S. aureus* is presented in Figure 4.13. In this case, the spectrum seems only to present characteristics of a flavoprotein, with its absorption band at 450 nm, in contrast with the final spectrum of the first described trial (Figure 4.7 (A)), in which the cytochrome contamination was considerable.

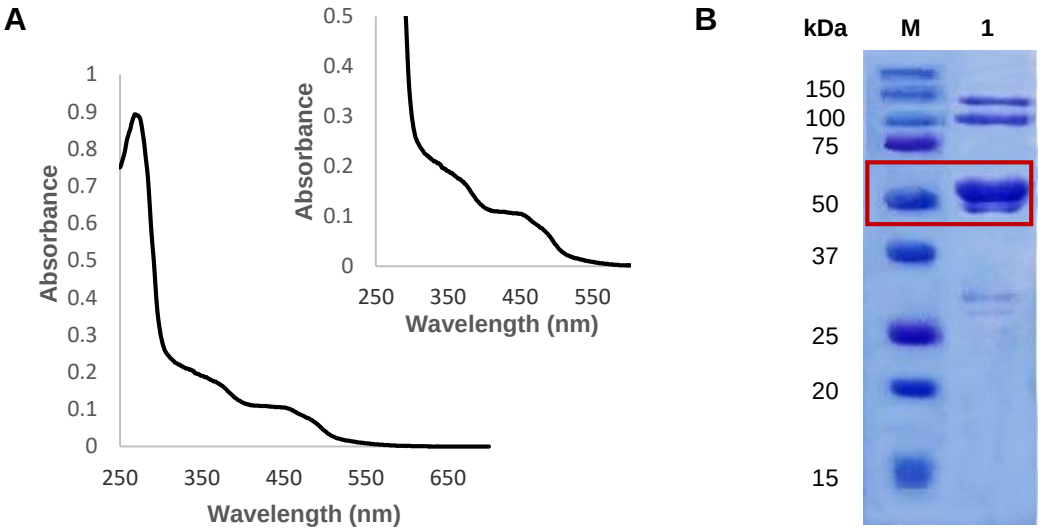

Figure 4. 13 - A) UV-Visible absorption spectrum of MQO I from *S. aureus* purified. The inset expands the absorption spectrum in the 250–550 nm region. B) The respective SDS-PAGE with MQO I protein (highlighted in red) – lane 1. SDS-PAGE: Stacking Gel – 4 % acrylamide; Resolving Gel – 15 % acrylamide; Theoretical molecular mass of MQO I: ~ 57 kDa. Precision plus protein dual colour standard was used as marker (M).

The SDS-PAGE gel (Figure 4.13 (B)) shows an intense band at around 50 kDa which probably corresponds to the protein of interest (theoretical molecular mass ~ 57 kDa). When compared to the final gel of the first described trial (Figure 4.7 (B)), we can observe that this gel presents less contaminants. However, there are still a set of thinner and less intense bands, which indicate that the protein is not completely pure. Enzymatic assays were performed to confirm the presence of malate:quinone oxidoreductase, following the quinone reduction 150 µM DMN, at 300 nm, and using 15 mM Malate (L-malic acid) as electron donor, at 30 ºC. These enzymatic activities were also tested in the presence of an inhibitor, the 2-n-heptyl-4-hydroxyquinoline-N-oxide (HQNO), which is a known inhibitor of many proteins of the respiratory chain that interacts with quinones[52,53]. HQNO functions as a potent quinone-site inhibitor. In order to confirm that the enzymatic activity measured was specific, experiments were also performed using 150 µM HQNO (the same proportion as the quinone). We observed that in the presence of HQNO the MQO I

activity was approximately 47 % decreased (Figure 4.14). No enzymatic activity was detected using Lactate as substrate.

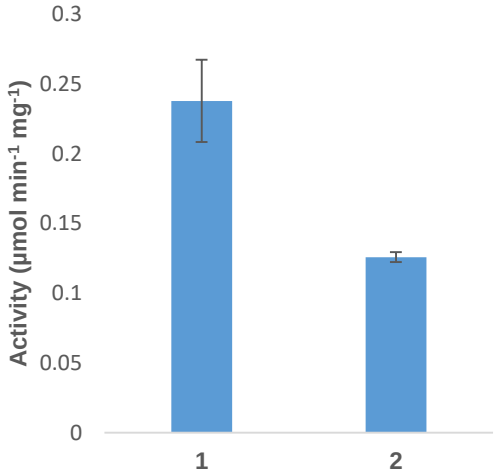

Figure 4. 14 - Specific MQO I Activity. 1: Malate:quinone oxidoreductase activity; 2: MQO I activity in the presence of 0.15 mM HQNO. Enzymatic activities were performed under anaerobic conditions, in an anaerobic chamber with O_2 levels below 1 ppm. Each assay was performed in triplicate at 30 ºC and following the quinone reduction (DMN) by absorption spectroscopy at 300 nm, using 15 mM Malate (L-malic acid) as electron donor and 0.15 mM DMN as electron acceptor, in 100 mM phosphate buffer pH 7.0, 250 mM NaCl. HQNO was used in a proportion 1:1 to the quinone. Total enzyme activity and specific activity were both calculated based on the Beer-Lambert law and according to a molar extinction coefficient of DMN of 15.2 mM^{-1} cm^{-1} [64].

In summary, after ten attempts, the purification of malate:quinone oxidoreductase I from *S. aureus* was achieved. Nonetheless, this process still needs further optimization in order to proceed with the biochemical characterization of this promising protein.

4.2. Malate:quinone oxidoreductase II

4.2.1. Protein expression and purification

The purification of the so assigned second copy of malate:quinone oxidoreductases (MQO II) from *S. aureus* was achieved on the first attempt. The expression conditions of MQO II had already been tested when this thesis project started. Under the stipulated conditions, transformed *E. coli* C43 cells with the plasmid containing the gene coding for MQO II, were grown in TB medium supplemented with 50 µg mL^{-1} kanamycin, at 37 ºC and 180 rpm. Gene expression was induced with the addition of 0.1 mM IPTG at an optical density of 0.6, at 600 nm. The temperature was changed to 18 ºC after the induction. Cells were harvested after overnight growth, and stored at -20 ºC.

Cell growths were performed under the described conditions, in large scale, to obtain sufficient cell mass as starting material to purify the protein of interest. The growth yield was approximately 5 g L^{-1}. Approximately 100 g of thawed cells were suspended in 100 mM K_2HPO_4/KH_2PO_4 buffer pH 7.0, 250 mM NaCl and disrupted in a French press at 41.4 MPa.

Cellular debris and undisrupted cells were separated out by centrifugation at 10,000 rpm for 10 min. The resulting suspension was ultracentrifuged at 42,000 rpm, 2 h. Partial membrane protein solubilization was achieved by washing the membranes with high ionic strength (2M NaCl). This was the chosen procedure since it was shown to be the most suitable for MQO I. Thus, the membrane pellet was resuspended with a Potter homogenizer in 100 mM K_2HPO_4/KH_2PO_4 buffer pH 7.0, 2 M NaCl and incubated overnight at 4 ºC, under agitation. No detergents were used during the solubilisation and purification of the enzyme. The transfer of the protein to the soluble fraction was confirmed by the observed colour change, to the characteristic yellowish hue of a flavoprotein. The membrane fraction was again ultracentrifuged at 42,000 rpm, 1 h, to isolate the soluble fraction containing the protein of interest. The ionic strength of the resulting soluble fraction (supernatant) was decreased to approximately 50 mM NaCl at 4 ºC by successive additions of 100 mM phosphate buffer pH 7.0 in order to inject it in an ionic exchange chromatography column, Q-Sepharose HP 74 mL.

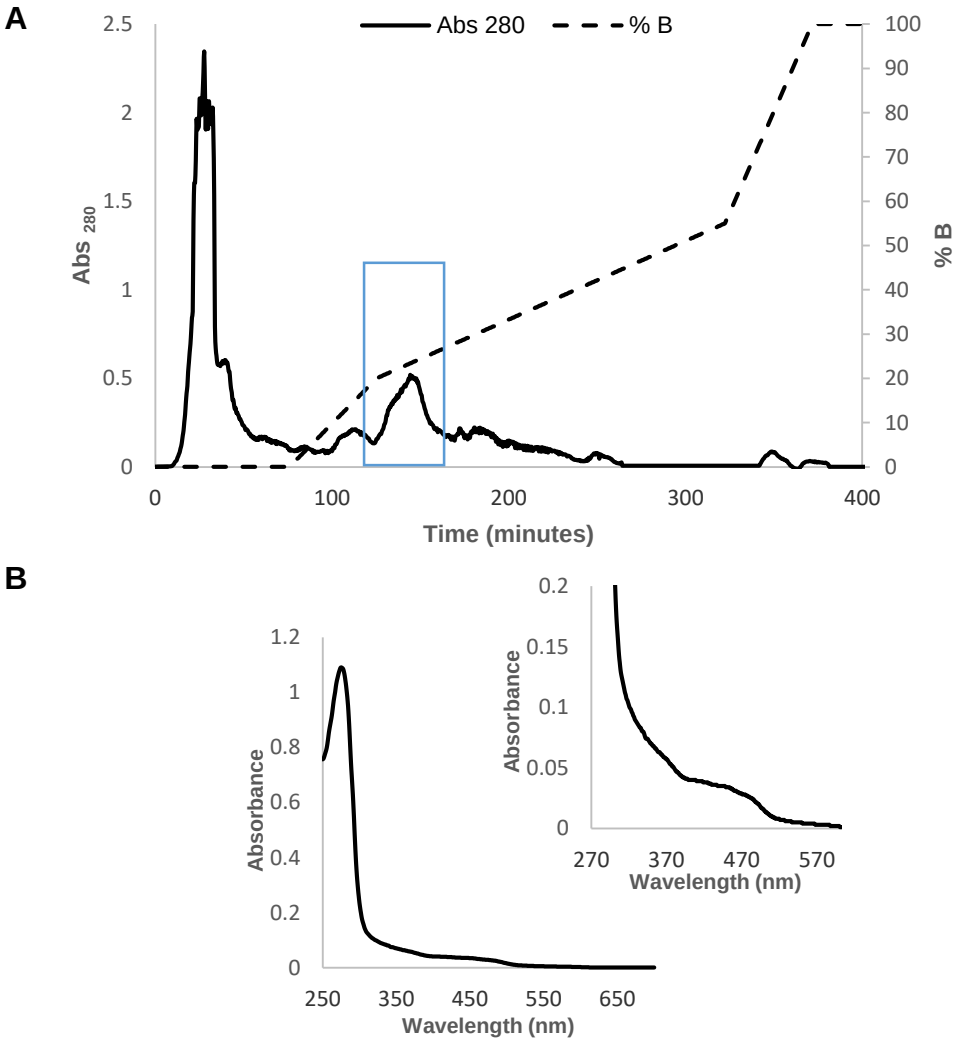

Figure 4. 15 - A) Chromatogram obtained in the purification of MQO II from *S. aureus*, by a Q-Sepharose HP column 74 mL. Flux = 3 mL/min. In black filled line is represented the absorbance at 280 nm, in dashed line is represented the % of 1 M NaCl, 20 mM Tris-HCl buffer pH 7.8, 10 % glycerol (buffer B). The protein eluted approximately at 30 % of B (blue). B) UV-Visible absorption spectrum of the selected fraction from the Q-Sepharose HP column (blue box in (A)) containing MQO II. The inset expands the absorption spectrum in the 270–570 nm region.

The chromatogram is shown in Figure 4.15 (A). Fractions containing MQO II were selected according to their UV-Visible absorption spectra, considering the ratio between the amount of flavin per amount of protein (Abs_{280}/Abs_{450}). Figure 4.15 (B) shows the absorption spectrum of the resulting fraction, containing MQO II, from this chromatography column. Similarly, to MQO I, MQO II eluted with approximately 300 mM NaCl (30 % buffer B).

Fractions were concentrated and applied to a size exclusion chromatography column, using a phosphate buffer, 100 mM K_2HPO_4/KH_2PO_4 pH 7.0, 250 mM NaCl, which separated the different compounds according to their size. The resulting chromatogram is presented in Figure 4.15. Again, fractions containing MQO II were identified by the respective absorption spectra, and selected according to their Abs_{280}/Abs_{450} ratio. The protein eluted at around 260 min, corresponding to 130 mL elution volume and the respective spectrum is shown in Figure 4.17 (A).

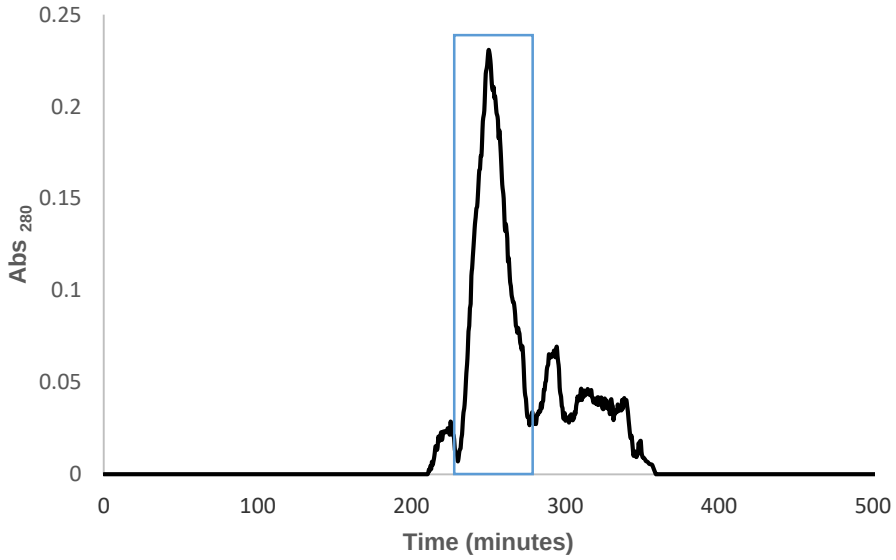

Figure 4. 16 - Chromatogram obtained in the purification of MQO II from *S. aureus* by a S200 column 300 mL, with 100 mM K_2HPO_4/KH_2PO_4 pH 7.0, 250 mM NaCl. Flux = 0.5 mL/min. In black filled line is represented the absorbance at 280 nm. The protein eluted around 260 minutes (130 mL) (blue).

Two chromatography columns were sufficient to purify malate:quinone oxidoreductase II from *S. aureus*. The final UV-Visible absorption spectrum of MQO II is presented in Figure 4.17 (A), and the corresponding protein band is shown in the SDS-PAGE gel in Figure 4.17 (B). The spectrum is characteristic of a flavoprotein, presenting a relevant absorption band with maximum at 450 nm [20]. The SDS-PAGE gel reveals an intense band between the 45-66 kDa markers, which probably corresponds to MQO II (theoretical molecular mass of 56 kDa). We can also observe a set of less intense bands, indicating that there are vestigial amounts of contaminant proteins present. However, they do not seem to interfere in the studies further performed.

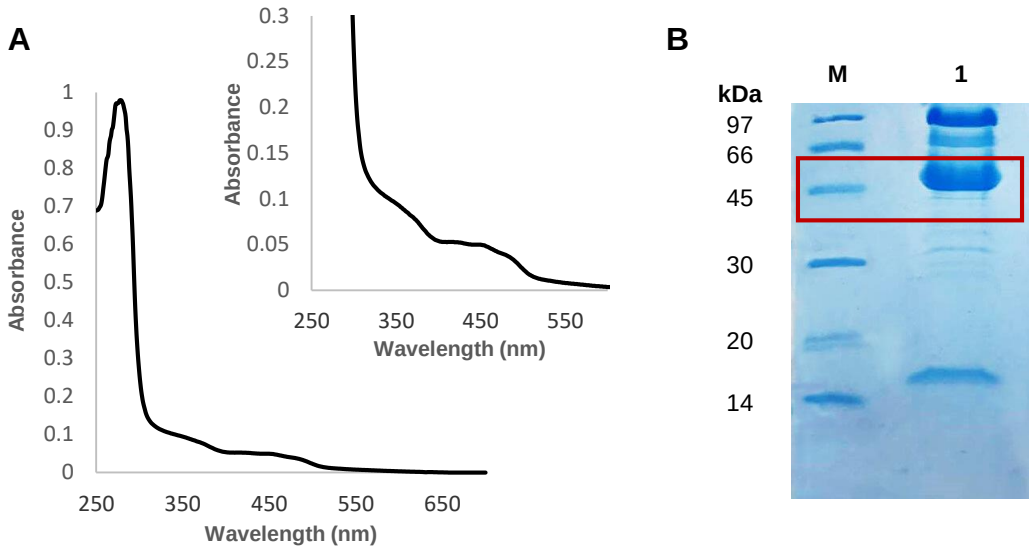

Figure 4. 17 - A) UV-Visible absorption spectrum of MQO II from *S. aureus* purified. The inset expands the absorption spectrum in the 250–550 nm region. B) The respective SDS-PAGE with the MQO II protein (highlighted in red) – lane 1. SDS-PAGE: Stacking Gel – 4 % acrylamide; Resolving Gel – 15 % acrylamide. Theoretical molecular mass of MQO II: ~ 56 kDa. Low molecular weight (LMW) protein marker was used (M).

At the end, we obtained 13.26 mg of protein for further characterization. Protein concentration was determined using the BCA protein assay reagent, according to the respective kit protocol[38].

4.2.2. Protein identification

The intense band present in the gel (Figure 4.17 (B)) (highlighted in red) was analysed by the ITQB/IBET UniMS, for protein identification. Similarly to MQO I, the protein was identified by MALDI-TOF/TOF and the search was performed against a SwissProt protein database with taxonomic restriction to *Bacteria*. A positive protein identification was obtained. The report from the Mass Spectrometry Unit determined that the protein was a Dihydrolipoyl dehydrogenase (DLD) from *Escherichia coli* (Report number 2 in Supplemental Material). This protein (EC 1.8.1.4) is a soluble enzyme that oxidizes dihydrolipoamide to lipoamid, and also presents a FAD cofactor, with a molecular mass of approximately 51 kDa [54]. Thus, this band should be very close to the protein band relative to MQO II from *S. aureus*, which has a theoretical molecular mass of ~ 56 kDa. With this small difference between their molecular weights, it is difficult to separate both proteins in the SDS-PAGE gel, which also has an error associated. It is possible to conclude that MQO II is not completely pure. Bands are overlapping or other possibilities are an inefficient removal of the protein from the gel and/or the DLD protein ionized and MQO II did not. Data was acquired using a 4800plus MALDI-TOF/TOF mass spectrometer, and the twenty-five most intense precursor ions from the MS spectra were selected for MS/MS analysis.

4.2.3. Absorption spectroscopy

Absorption spectroscopy was used to characterize the reduction state of the protein. Under anaerobic conditions, in an anaerobe chamber with O_2 levels below 1 ppm, reduction of 4.6 μM MQO II was achieved using a universal reducing agent, sodium dithionite ($Na_2S_2O_4$) (Figure 4.18). Oxidized flavin presents maximum absorption at 450 nm [55]. When the reduced protein was exposed to air, the spectrum immediately reassumed an oxidized pattern. These data show the protein is redox active.

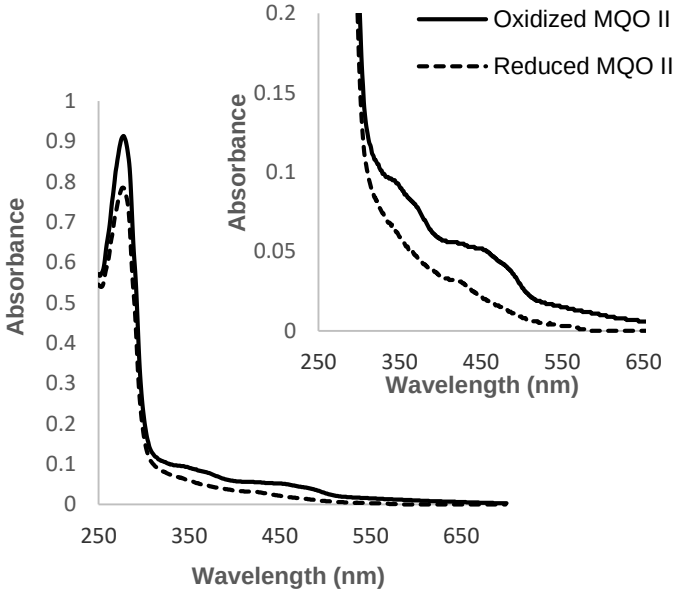

Figure 4. 18 - Absorption spectrum of MQO II from *S. aureus* oxidized (black filled line) and reduced (black dashed line) with sodium dithionite, in 100 mM phosphate buffer pH 7.0, 250 mM NaCl. Spectra were acquired under anaerobic conditions, on a spectrophotometer placed inside an anaerobe chamber with O_2 levels below 1 ppm. The inset expands the absorption spectrum in the 250–650 nm region.

4.2.4. Enzymatic studies and substrate affinity

A fraction containing 1.18 mg mL^{-1} was used for enzymatic activity tests in order to confirm the presence of the MQO II, using both Malate (L-malic acid) and Lactate (L-lactate) as electron donors, also to study the substrate specificity. Triplicate assays were performed under anaerobic conditions at 30 ºC, following DCPIP, the acceptor, at 600 nm. In Figure 4.19 are represented the obtained results. Total enzyme activity and specific activity were both calculated based on the Beer-Lambert law and according to a molar extinction coefficient of DCPIP at 600 nm (ε_{600}) of 20.7 mM^{-1} cm^{-1} [50]. It is clear that MQO II presented affinity for L-lactate and did not react readily with Malate, contrary to what is observed for MQO I. These results are in agreement with some publications which suggest to rename of this protein to lactate:quinone oxidoreductase (LQO)[34,35]. These results demonstrate that MQO I and MQO II catalyse different reactions.

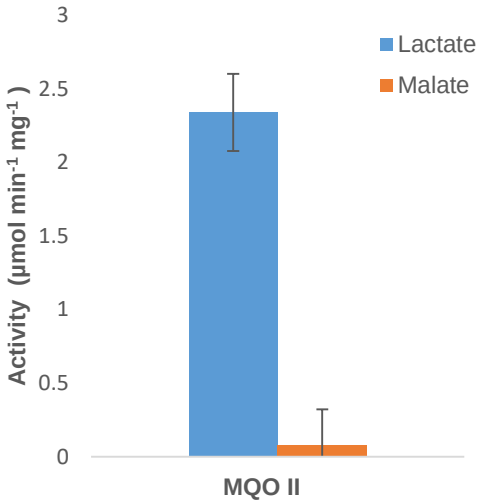

Figure 4. 19 - Specific MQO II activity. Enzymatic activities were performed under anaerobic conditions, in an anaerobic chamber with O_2 levels below 1 ppm. Each assay was performed in triplicates at 30 ºC and following the DCPIP spectroscopically at 600 nm, using 15 mM Malate (L-malic acid) or 15 mM Lactate (L-lactate) as electron donors and 0.1 mM DCPIP as electron acceptor, in 100 mM phosphate buffer pH 7.0, 250 mM NaCl. Total enzyme activity and specific activity were both calculated based on the Beer-Lambert law and according to a molar extinction coefficient of DCPIP at 600 nm (ε600) equivalent to 20.7 $mM^{-1}cm^{-1}$ [50].

4.2.5. Enzymatic activity pH profile

Enzymatic activities were tested at different pH values, with the aim of determining the pH at which MQO II presents the highest activity. Experiments were performed in triplicate, under anaerobic conditions, at 30 ºC and following the change in absorbance of DCPIP at 600 nm. 0.1 mM DCPIP was used as electron acceptor and 15 mM Lactate (L-lactate) used as electron donor. pH values between pH 5.5 and pH 8, were provided by 50 mM MES, 50 mM Bis-Tris Propane, 250 mM NaCl buffer, by changing the buffer pH. The protein concentration used was approximately 0.92 µM. The results are shown in Figure 4.20.

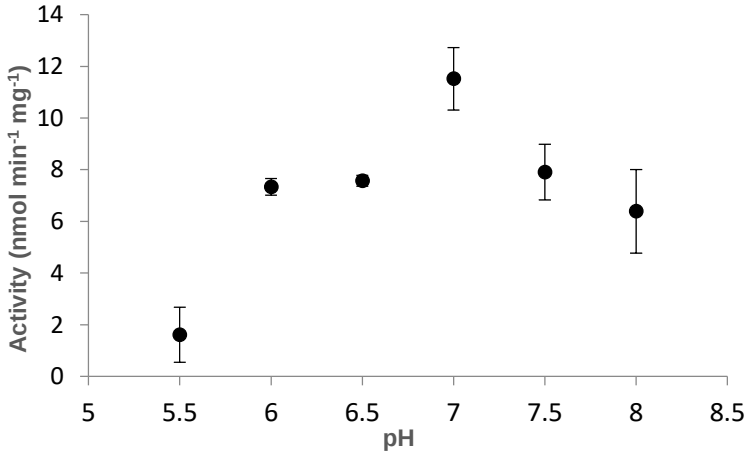

Figure 4. 20 - pH-dependent enzyme activity of MQO II from *S. aureus*. Each point is representative of three experiments (respective error bars), using 0.1 mM DCPIP as electron acceptor and 15 mM L-lactate as electron donor, and with a protein concentration of 0.92 µM MQO II. Assays were measured in an anaerobe chamber with O_2 levels below 1 ppm, at 30 ºC and 600 nm, with different pH buffer solutions 50 mM MES, 50 mM Bis Tris Propane, 250 mM NaCl buffer. Specific enzyme activity was calculated based on the Beer-Lambert law and according to a molar extinction coefficient of DCPIP at 600 nm (ε600) equivalent to 20.7 mM^{-1} cm^{-1} [50].

In the stipulated conditions, the results shown in Figure 4.20 indicated that the maximal activity for MQO II occurs at pH 7.0, with a specific activity of approximately 12 nmol min^{-1} mg^{-1}. At pH 5.5, the protein presents a minimal activity (~ 1.5 nmol min^{-1} mg^{-1}), which consequently increases with the pH increase until pH 7.0.

4.2.6. Protein stability analysis

Thermal denaturation experiments were performed, aiming to study protein stability and contributing in this way to the biochemical and functional characterization of MQO II. Temperature stability was analysed by measuring the fluorescence emission intensity at two different wavelengths, 355 nm (excitation at 280 nm) and 530 nm (excitation at 450 nm), respectively corresponding to the tryptophan and to the flavin emission peaks. The protein denaturation profile was followed in the range 25 to 90 ºC, and the obtained results are presented in Figure 4.21.

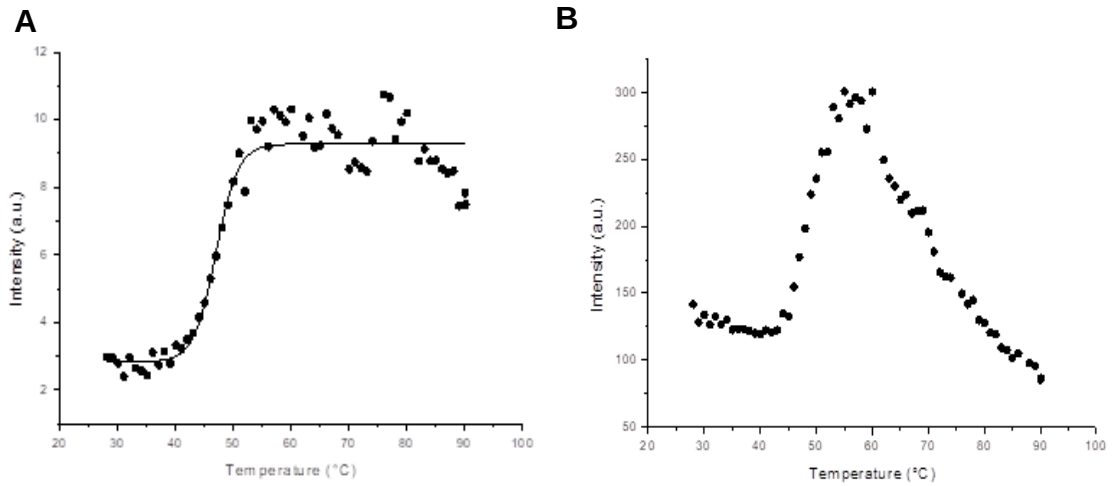

Figure 4. 21 - Thermal denaturation curve of the purified MQO II from *S. aureus*. In black dots are represented: (A) the fluorescence emission intensity at 530 nm (excitation at 450 nm). In filled lines is represented the corresponding sigmoid fit; (B) the fluorescence emission intensity at 355 nm (excitation 280 nm), both in function of the temperature, between 25 and 90 ºC, to 2 μM MQO II.

Figure 4.21 panel (A) shows that the denaturation pattern of MQO II has an approximate sigmoid behaviour, starting at lower emission intensities and increasing as the temperature increases. The observed increase in the fluorescence emission is assumed as an increase of the exposure of the cofactor (FAD), upon protein denaturation. The temperature at which 50 % of the protein's population is considered denatured is mathematically represented by the inflexion point in the sigmoid fit, named as the Melting Temperature (MT). The MT was determined using *OriginPro 8 software*, fitting a Boltzmann function (sigmoidal curve) to the data, and it was defined as 46.9 ºC for MQO II. In Figure 4.21 panel (B) is observed the exposure of tryptophan, by the increased intensity at ~ 50 ºC, and the following protein aggregation, observed from ~ 60 ºC.

4.3. *Staphylococcus aureus* behaviour with Different Carbon Sources

Nowadays, *S. aureus* has a large contribution to the high morbidity and mortality levels, due to the increased incidence of its drug resistance. Therefore it is important to increase the knowledge on this opportunistic pathogen, including the understanding of its energetic metabolism. The present work contributes to this knowledge, by exploring a membrane enzyme involved in the catabolism of *S. aureus*, namely malate:quinone oxidoreductase I. We aimed at understand the impact of MQO I in its metabolism.

S. aureus growths were performed for the wild-type strain (JE2 strain was used) and for the mutant stain, mqoI::Tn (JE2 background), presenting a transposon in the gene coding for MQO I. These strains were provided by the Nebraska Transposon Mutant Library[41]. The insertion of the transposon in the gene coding for MQO I was confirmed by PCR having the PCR product the expected size of 1,106 bp (Figure 7.3 in Supplemental Material).

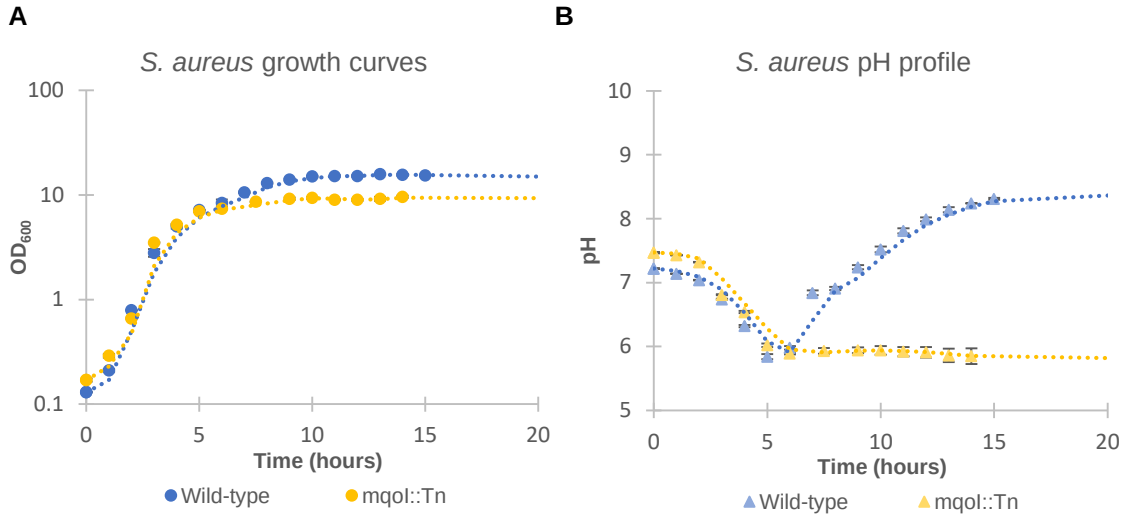

Figure 4. 22 - Logarithmic representation of *S. aureus* JE2 growth in TSB medium (initial OD 0.15, in aerobic conditions). The absorbance at 600 nm and the pH values were measured at 1 h intervals. The results presented are representative of three independent experiments (respective error bars). Comparison of the growths of *S. aureus* wild-type (blue) and mqoI::Tn (yellow) strains by optical density (A) and pH (B).

The growths under different conditions were evaluated by monitoring optical density, acquired using absorption spectroscopy at 600 nm (OD_{600}) and pH changes, measured using a pH electrode. *S. aureus* growth was first studied in a nutrient-rich medium, Tryptic Soy Broth (TSB) containing 14 mM glucose and an ill-defined concentration of peptides and free amino acids (Table 7.2 in Supplemental Material), for 15 hours (Figure 4.22).

Figure 4.22 shows that *S. aureus* wild-type growth presented an exponential phase of ~ 6 h (blue points). This strain reached a maximal OD of approximately 16. In Figure 4.22 it is also observed that the pH profile is characterized by a continuous decrease since the beginning of growth until ~ 6 h, which corresponded to an inflection point, since this decrease was

subsequently followed by a pH rise. The minimum pH value was observed to be around 5.8, and in the end of the growth the pH value was higher than that observed in the beginning.

On the contrary, our data show that *S. aureus* mqoI::Tn strain reached a maximal OD of approximately 9 after 5 h of growth, when the stationary phase was reached (Figure 4.22; yellow points). Similarly to the observed for the wild-type, the pH value decreased since the beginning of the growth until ~ 5 h, but then it remained constant, at approximately 5.9.

A significant difference between the growths of the wild-type strain and the strain with a transposon in the gene coding for MQO I was observed. *S. aureus* mqoI::Tn growth reached the stationary phase earlier than the wild-type strain, revealing a different phenotype. A significant difference was also observed in the pH profile, since our data show that the initial value was not recovered (Figure 4.22).

Because TSB is a very rich medium and difficult to control, additional *S. aureus* growths were performed, in a chemically defined medium (CDM) prepared as described in Table 7.2 – Supplemental Material. CDM is a minimal medium, easy to control. In a first approach, *S. aureus* growths of the wild-type and mqoI::Tn strains were performed in this medium supplemented with 5 mM glucose. The variation in absorbance at 600 nm and pH values were both followed during the 11 hours of growth (Figure 4.23).

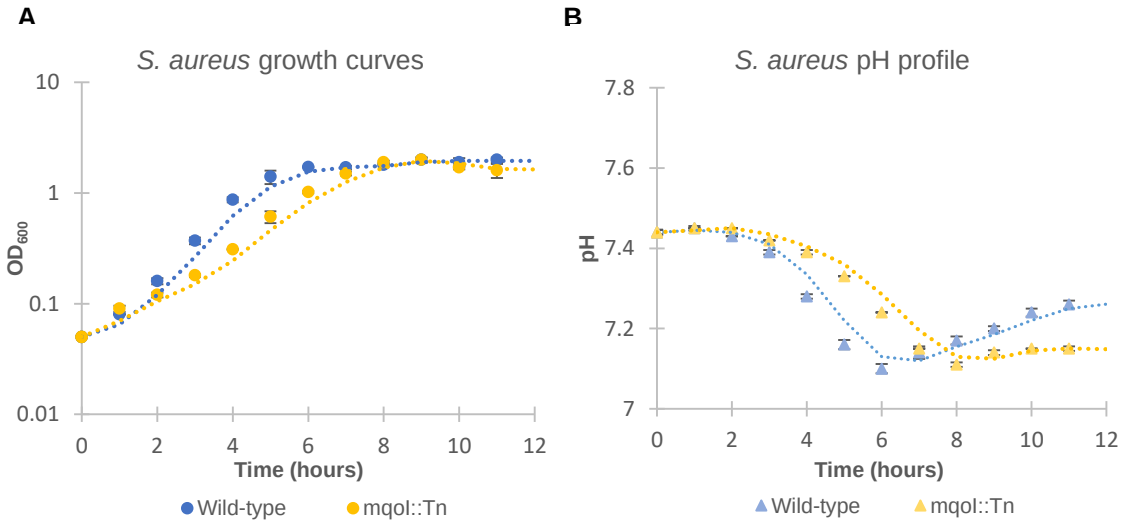

Figure 4. 23 – Logarithmic representation of *S. aureus* JE2 growth in CDM supplemented with 5 mM glucose (initial OD 0.05, in aerobic conditions). The absorbance at 600 nm and the pH values were measured at 1 h intervals. The results presented are representative of three independent experiments (respective error bars). Comparison of the growths of *S. aureus* wild-type (blue) and mqoI::Tn (yellow) strains by optical density (A) and pH (B).

In CDM conditions (Figure 4.23) both *S. aureus* strains were observed to grow less when compared with the respective growths in TSB medium (Figure 4.22). In CDM supplemented with 5 mM glucose, the wild-type strain reached a maximal OD around 2, after 9 h of growth (Figure 4.23; blue points). As observed in TSB medium, the pH profile is characterized by a decrease

since the beginning of the growth, until a minimal pH value equivalent to 7.1 after 6 h of growth, and subsequent increase. However, the pH value registered in the end of the growth was lower than that initially measured, contrarily to the observed for the wild-type growth in TSB medium.

In CDM supplemented with glucose, the *S. aureus* mqoI::Tn strain reached the stationary phase after around 8 h of growth with a maximal OD value of around 2 (Figure 4.23; yellow points). As observed in TSB medium (Figure 4.22), the pH values decreased since the beginning of the growth, presenting a minimal pH value around 7.1 after 8 h of growth. A subsequent pH increase was not observed for *S. aureus* strain with a transposon in the gene coding for MQO I, in TSB either or in CDM with glucose.

The mutant strain presented a delay in the growth, compared with the wild-type strain, as observed in Figure 4.23 panels (A) and (B), although both reached the same final OD, contrarily to what was observed in TSB medium (Figure 4.22).

It is described in the literature that under aerobic conditions, *S. aureus* first metabolizes glucose, generating pyruvate, using the pentose phosphate and glycolytic pathways[28]. Under nutrient-rich conditions (TSB medium), in the presence of a rapidly catabolizable carbon source such as glucose, several bacteria repress the TCA cycle. This inhibition takes place by a sophisticated and complex regulatory mechanism denominated as carbon catabolite repression (CCR). CCR is described to allow bacteria to control their energy sources and to avoid an energetic overflow. In this case the genes coding for proteins that enable the use of less energetic carbon sources, so-called secondary carbon sources, are not expressed when glucose is available. The catabolite control protein A (CcpA) is the major global transcription regulator of CCR in Firmicutes, and thus responsible for the repression of the genes and proteins of the TCA cycle and also the genes involved in the consumption of amino acids, when glucose is present in the culture growth medium[56,57,58,59].

It this situation, even under reported aerobic conditions for other microorganisms, such as *E. coli*, glucose is oxidized to Acetyl-CoA, but this does not enter the TCA cycle. Instead, Acetyl-CoA is converted into acetyl-phosphate and then into acetate which is subsequently excreted. When needed, i.e. after the complete consumption of glucose, cells consume the excreted acetate as carbon and energy sources to support their growth[60,61]. This procedure could also be performed by *S. aureus* strains, possibly explaining the pH profile during the growths.

The pH drops observed since the beginning of the growths (TSB and CDM) of both strains (wild-type and mqoI::Tn) could presumably be related with the production and excretion of acidic metabolites, possibly acetate, during the consumption of glucose. The subsequent pH rise, only observed for the wild-type growths, is in agreement with a possible uptake of acetate and normal operation of the TCA cycle, after glucose depletion, also allowing the use of other metabolites, such as amino acids present in the culture growth medium. In the case of *S. aureus* mqoI::Tn growth, the pH drop was not followed by a subsequent increase (Figures 4.22 and 4.23, yellow points). The minimal pH value was coincident with the reach of the stationary phase in CDM

supplemented with glucose (Figure 4.23), possibly corresponding to the total glucose consumption and thus inability of this strain to catabolize acetate. This could be justified with the absence of the MQO I enzyme; the presence of a transposon in the gene coding for MQO I leading to the impairment of the TCA cycle. As described before, *S. aureus* does not have MDH, the soluble malate dehydrogenase, which is also capable to perform the oxidation of malate to oxaloacetate in the TCA cycle.

In short, the differences observed between *S. aureus* wild-type and mqoI::Tn strains were more pronounced in TSB medium. This probably occurred because TSB is a nutrient rich medium, containing other carbohydrates besides glucose, like sucrose, and thus influencing the results. Despite growing less in CDM, the minimal pH values were also higher than the minimal pH values registered in TSB, which can be justified considering the concentration of glucose and assuming the CCR model.

Other *S. aureus* wild-type and mqoI::Tn growths were performed in CDM, changing the available carbon sources. The CDM was supplemented with 5 mM acetate and the absorbance (600 nm) and the pH profile were both measured during the 14 hours of growth. The results are shown in Figure 4.24.

Figure 4.24 panel (A) shows that both *S. aureus* strains presented a long lag phase. *S. aureus* wild-type strain had a maximal OD of ~ 1.3, and reached the stationary phase after approximately 9 h of growth (Figure 4.24; blue points). The pH values remained constant during the observed lag phase, and increased after ~ 7 h of growth. Contrarily to what was observed when cells grew in a growth medium containing glucose, the pH did not decrease. This was an expected situation, since no acids are being expected to be excreted in these conditions. Acetate was used as sole carbon source and is presumably oxidized by the TCA cycle producing CO_2.

On the opposite, *S. aureus* mqoI::Tn strain did not reveal a significant growth in CDM supplemented with acetate, as sole carbon source (Figure 4.24; yellow points). This strain presented a maximal OD value of 0.4 in 14 h of growth. The measured pH remained constant along the growth, also revealing a significant difference when compared with the pH profile registered for the wild-type growth. A considerable discrepancy was observed in these conditions for *S. aureus* strains lacking MQO I. One possible explanation to the observed phenotype could be the need for the cells, to have a functional TCA cycle in order to metabolize acetate, which is not the case for *S. aureus* mqoI::Tn.

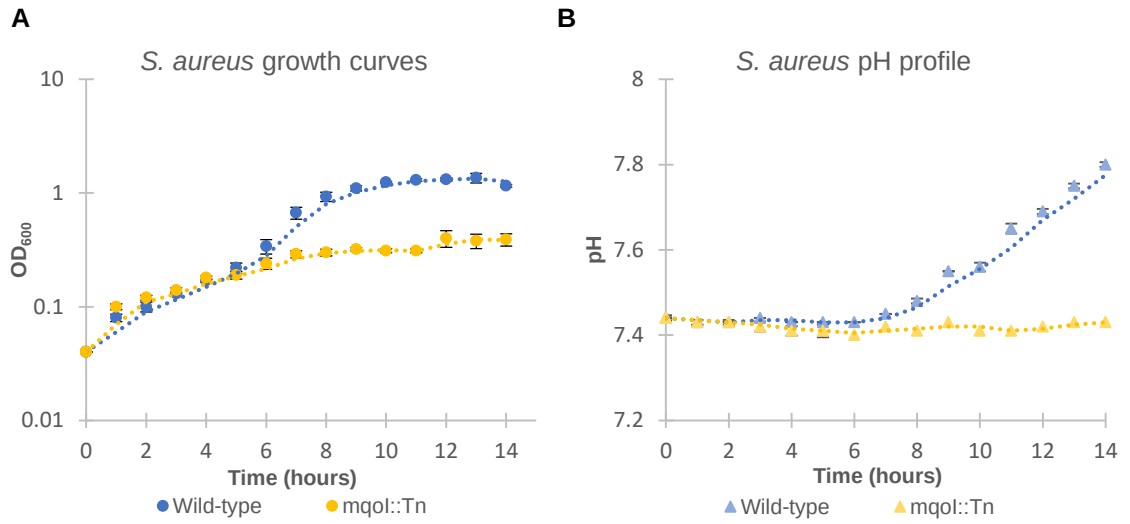

Figure 4. 24 – Logarithmic representation of *S. aureus* JE2 growth in CDM supplemented with 5 mM acetate (initial OD 0.05, in aerobic conditions). The absorbance at 600 nm and the pH values were measured at 1 h intervals. The results presented are representative of three independent experiments (respective error bars). Comparison of the growths of *S. aureus* wild-type (blue) and mqoI::Tn (yellow) strains by optical density (A) and pH (B).

S. aureus wild-type and mqoI::Tn strains were also grown in CDM supplemented with 5 mM lactate. The absorbance (600 nm) and the pH profile were both measured during the 11 hours of growth. The results are shown in Figure 4.25.

Figure 4.25 shows that *S. aureus* wild-type strain presented a maximal OD value corresponding to ~ 2.1 and reached the stationary phase after 5 h of growth, when grown in CDM supplemented with lactate, as sole carbon source (blue points). The pH profile remained constant at 7.3 until ~ 6 h, and then increased to a final value around 7.5.

S. aureus mqoI::Tn cells reached a maximal OD value around 1.5 after ~ 6 h of growth. A small increase was observed in the pH profile after ~ 7 h of growth, as observed in Figure 4.25 (yellow points).

In CDM supplemented with lactate both wild-type and mutant strains presented a similar growth curve behaviour, although reaching different maximum OD values (Figure 4.25 panel (A)). Nevertheless, *S. aureus* mqoI::Tn strain revealed a delayed growth when compared with the wild-type growth. Similarly to the growths performed in CDM with acetate, the pH values were constant from the beginning and increased after ~ 6/7 h, probably due to the consumption of metabolites present in the growth medium. Once more our results show that the absence of MQO I affects *S. aureus*' fitness.

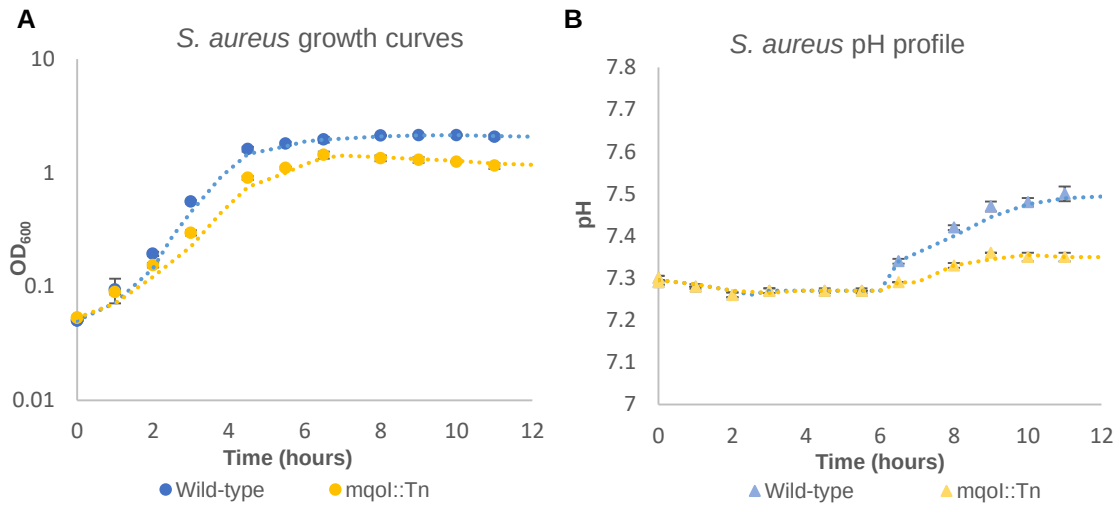

Figure 4. 25 - Logarithmic representation of *S. aureus* JE2 growth in CDM supplemented with 5 mM lactate (initial OD 0.05, in aerobic conditions). The absorbance at 600 nm and the pH values were measured at 1 h intervals. The results presented are representative of three independent experiments (respective error bars). Comparison of the growths of *S. aureus* wild-type (blue) and mqoI::Tn (yellow) strains by optical density (A) and pH (B).

Our data allowed to perform a characterization of *S. aureus* JE2 wild-type growths under different carbon sources, illustrated in Figure 4.26. The growths differed only in the carbon sources used in CDM, making them comparable. Our results show that *S. aureus* growths are similar in CDM supplemented with glucose (red points) or with lactate (green points), presenting the same final OD values, around 2. On the opposite, when grown in CDM using acetate as sole carbon source (orange points), *S. aureus* cells grow less and more slowly, probably because the consumption of acetate is not energetically favourable. On the other hand, the consumption of glucose involves the production of NADH in glycolysis, and the consumption of lactate also comprises the production of NADH. In these cases, cells would obtain energy by oxidation of NADH by the respiratory chain, and this could be one possible explanation to justify the higher observed yield.

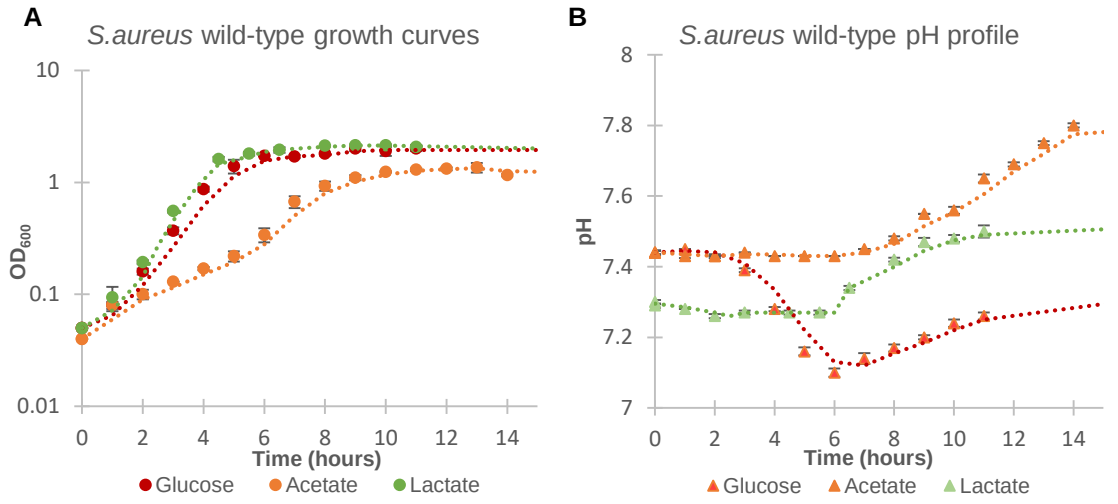

Figure 4. 26 – Logarithmic representation of *S. aureus* JE2 growth under different carbon sources (initial OD 0.05, in aerobic conditions). The results presented are representative of three independent experiments (respective error bars). Comparison of *S. aureus* wild-type growths in CDM supplemented with 5 mM glucose (red), 5 mM acetate (orange) or 5 mM lactate (green), by optical density (A) and pH (B).

A pH decrease is only observed in CDM supplemented with glucose, possibly inferring the presence of an active CCR in a growth medium containing glucose. In order to further explore these results, all *S. aureus* growths of both strains were repeated in exactly the same conditions, in TSB medium, and in CDM supplemented with 5 mM glucose, acetate or lactate, and samples were collected during the growth curves, to analyse the metabolites present in the culture growth medium, by NMR techniques.

4.4. Impact of MQO I in the Energetic Metabolism of *Staphylococcus aureus*

S. aureus has developed several resistance mechanisms which consequently led to the production of increasingly resistant strains, thus it is really important to demystify what is behind this particular resistance ability. With the aim of investigating the impact of MQO I in the energetic metabolism of *S. aureus*, a thorough NMR-based metabolomic analysis was performed for different growths of wild-type and mqoI::Tn strains with several carbon sources, as described in the previous section. New *S. aureus* growths were performed (triplicate assays), in TSB medium (14 mM glucose) and in CDM supplemented with 5 mM glucose, acetate or lactate, in order to collect the samples for NMR analyses. The respective growth curves are presented in Supplemental Material (Figures 7.4 - 7.7). Samples of 1.5 mL were collected every 2 h or 1.5 h, depending on the growths. Cells were centrifuged and discarded, the supernatant (culture growth medium) was stored for analysis.

NMR spectroscopy was selected because it is a powerful analytical technique widely used in metabolomics. It is remarkably suitable for the qualitative and quantitative analyses of low molecular weight metabolites in different complex biological samples. NMR offers several advantages for metabolomics data acquisition, since it requires minimal sample preparation.

A ^{1}H-NMR spectrum comprises a collection of several peaks originated from the molecules present in the sample which are directly proportional to their relative amounts in solution. Representative ^{1}H-NMR spectra are shown in Figure 4.27. These refer to cultures performed in TSB medium (panel (A)) and in CDM (panel (B)).

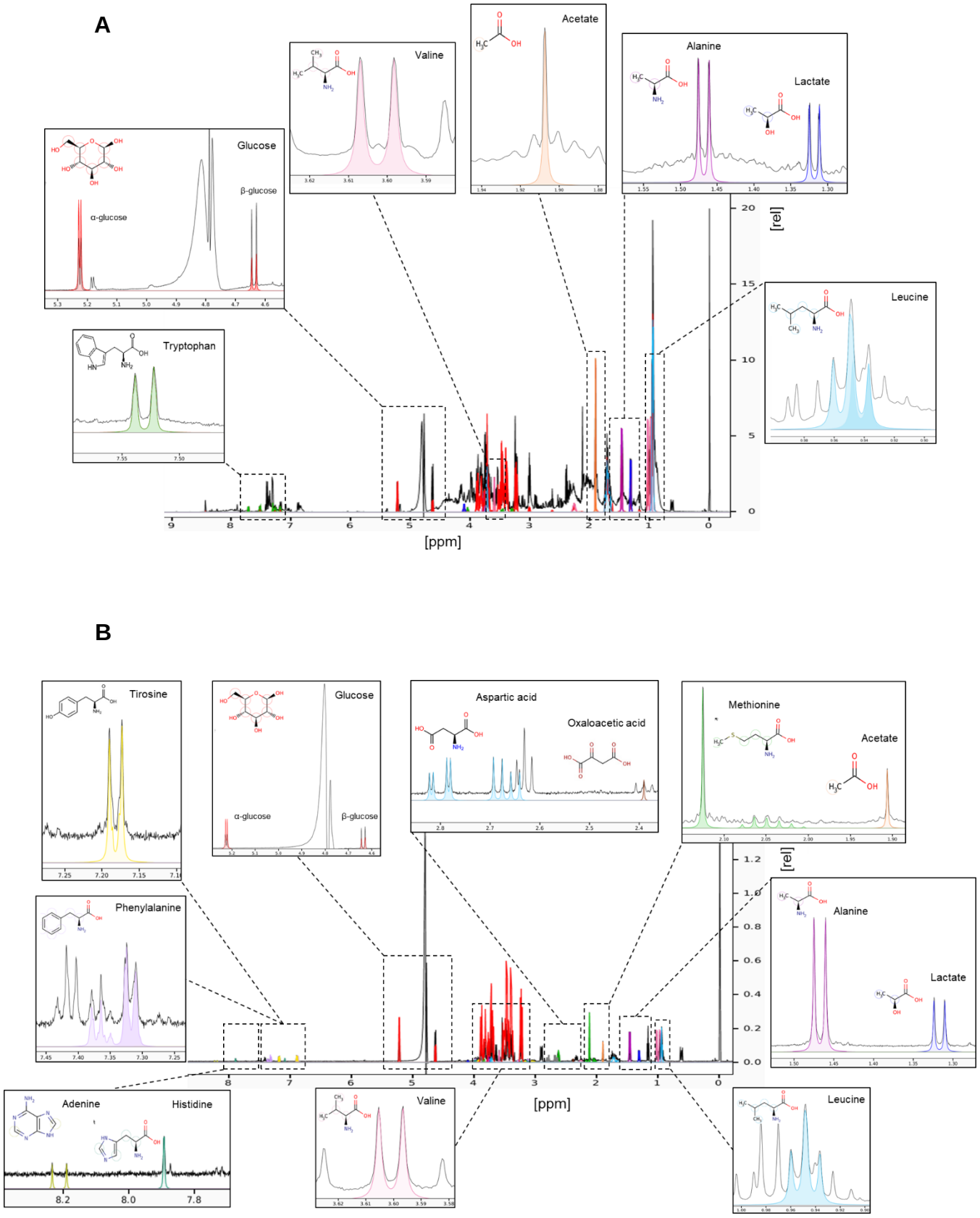

Figure 4. 27 - Representative[1]H-NMR spectra of samples collected from a *S. aureus* growth, in TSB medium (A) and in CDM supplemented with 5 mM glucose (B). Standard metabolite peaks are evidenced, in the respective frequencies. Compound identification was performed with *Chenomx Nmr Suite Version 8.12 software*.

Compound identification was done by comparison of the obtained spectra with those of standard compounds available at *Chenomx Nmr Suite software*. The peaks highlighted in Figure 4.27 were those selected to quantify the respective metabolites.

Once the assignment of the compounds was performed, all the collected spectra were analysed using *Topspin 3.2 software* for quantification. Figure 4.28 shows a representative raw data of selected compounds, such as glucose (panel (A)), acetate (panel (B)), alanine and lactate (panel (C)) in the respective chemical shifts, for different growth points collected at different times. For each analysed compound, a bar graph was created with the respective calculated concentration along the growth, considering the triplicate assays (Figure 4.28).

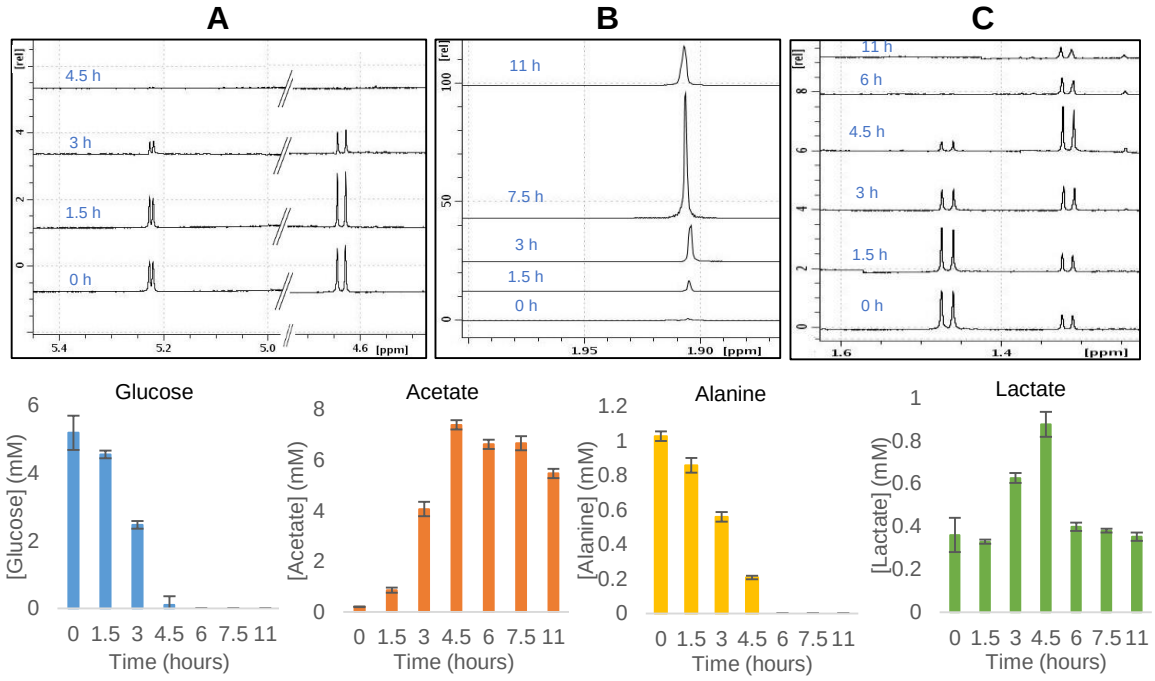

Figure 4. 28 - Example of raw data spectra showing the variation of glucose (panel (A)), acetate (panel (B)), alanine and lactate (panel (C)) at different times of the growth (top). Respective bar graph showing [glucose], [acetate], [alanine] and [lactate] for different growth points. Each bar is representative of triplicate assays (bottom).

This procedure was applied for each analysed compound, for every *S. aureus* growth. A total of two hundred forty-three spectra were collected and analysed. Figure 4.29 presents the variation of the concentration of all identified metabolites along the growth, in this case referring to the *S. aureus* wild-type growth in CMD supplemented with 5 mM glucose.

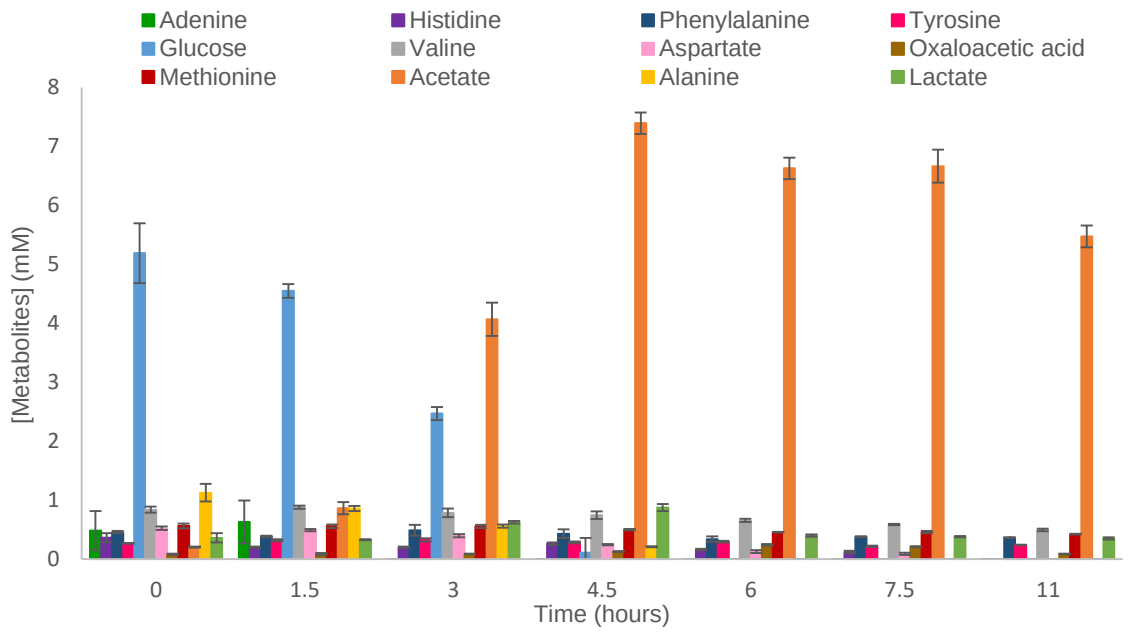

Figure 4. 29 - Bar Graph representing the concentration of the metabolites along the growth of *S. aureus* wild-type in CDM supplemented with 5 mM glucose.

The same was done for all growths of the both *S. aureus* strains, wild-type (filled bars), and mqoI::Tn (dashed bars), in triplicates. The results are schematized in Figures 4.30 to 4.33, referring to the growth of the two *S. aureus* strains in TSB medium, in CDM supplemented with glucose, in CDM supplemented with acetate, and in CDM supplemented with lactate, respectively.

Figures 4.30 and 4.31 show the variation of extracellular metabolites along *S. aureus* aerobic growth with glucose as the carbon source, in TSB medium and in CDM, respectively. Since TSB is a nutrient-rich medium, the ^{1}H-NMR spectra were difficult to analyse, due to the overlapping of several peaks associated to the presence of several nutrients, which prevented the quantification of all metabolites. On the opposite, the ^{1}H-NMR spectra obtained from cells grown in CDM were less crowded, due to the defined conditions of the growth medium, which consequently allowed the quantification a higher number of extracellular metabolites, providing also a good assess to the amino acids catabolism. It was not possible to analyse all the amino acids present in the medium since we used proton NMR method, and some amino acids require the use of other techniques, for example the carbon NMR, to be fully assessable.

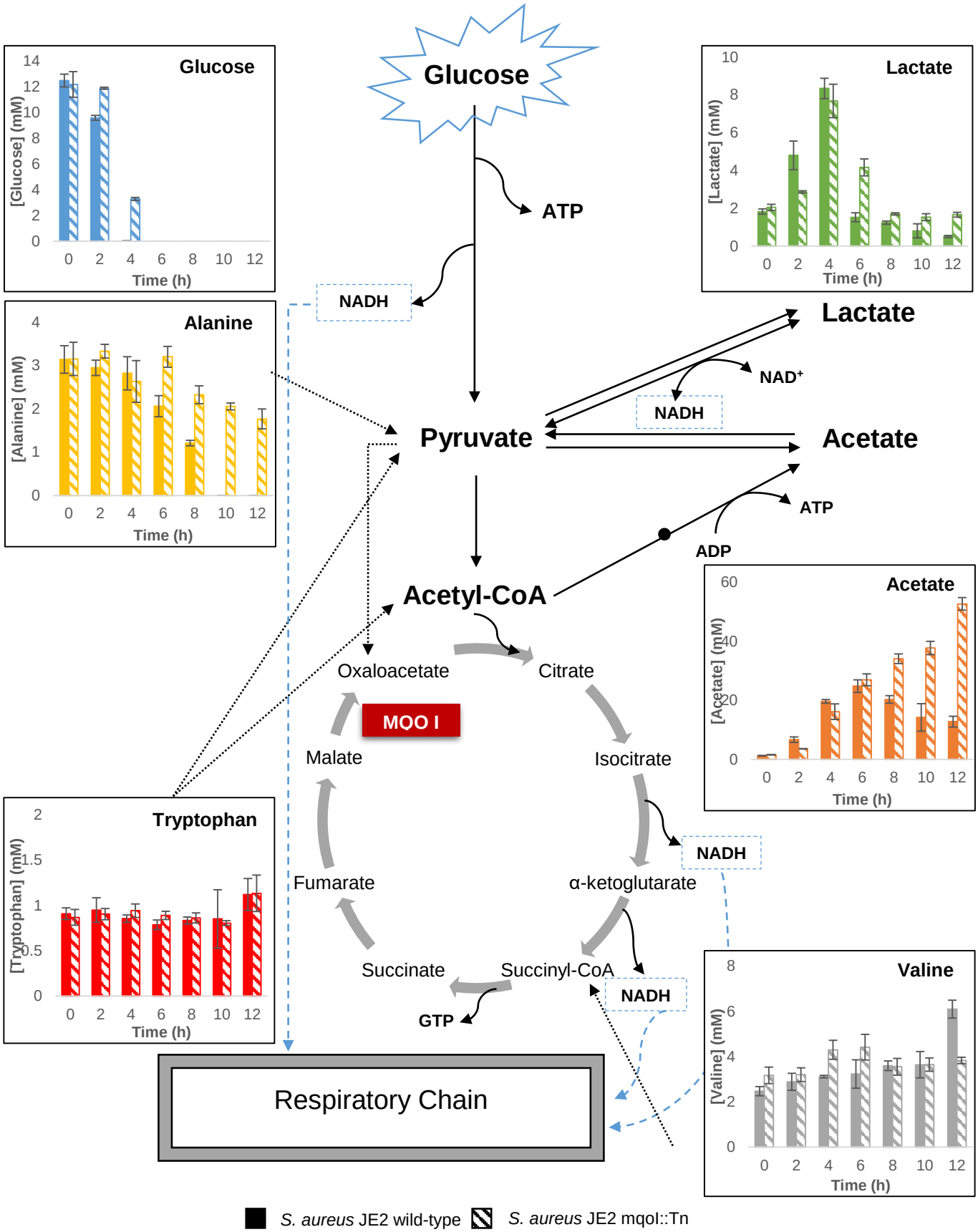

Figure 4. 30 – Metabolomic analyses of *S. aureus* JE2 wild-type (filled bars) and mqoI::Tn (dashed bars) growths under aerobic conditions, monitored by ^{1}H-NMR. In the red box is represented MQO I. *S. aureus* strains grew aerobically in TSB medium, at 37 ºC. Samples were collected every 2 h of growth, centrifuged and the supernatant was stored. Extracellular metabolite concentrations were measured (milimoles). The results are representative of three independent experiments. The respective growth curves are shown in Figure 7.4 in Supplemental Material.

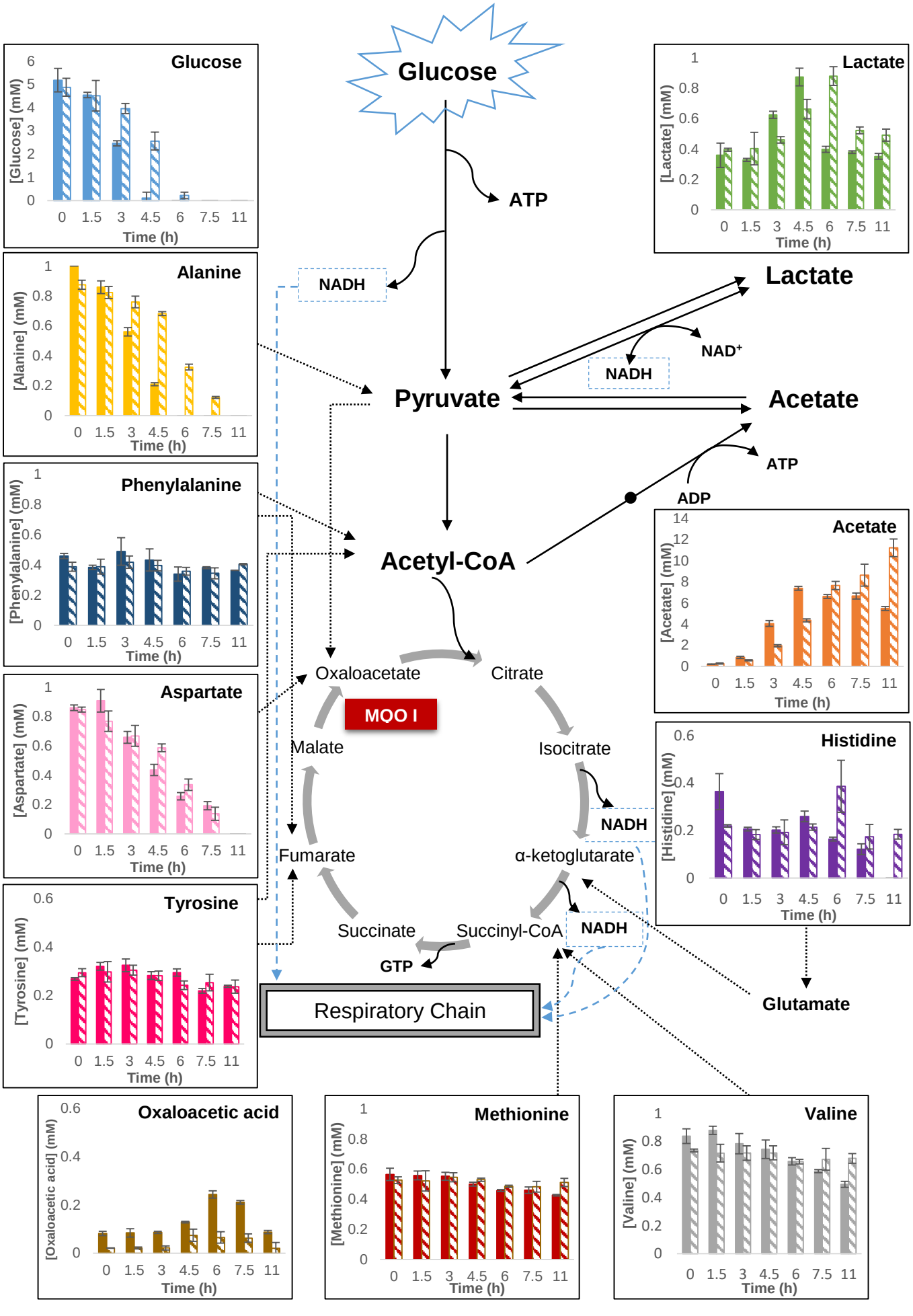
Glucose
ATP
NADH
Lactate
NAD+
NADH
Pyruvate
Acetate
ATP
ADP
Acetyl-CoA
Oxaloacetate
Citrate
MQO I
Malate
Isocitrate
NADH
Fumarate
α-ketoglutarate
Succinate
Succinyl-CoA
NADH
GTP
Respiratory Chain
Glutamate
Glucose
[Glucose] (mM)
Time (h)
Lactate
[Lactate] (mM)
Time (h)
Alanine
[Alanine] (mM)
Time (h)
Phenylalanine
[Phenylalanine] (mM)
Time (h)
Acetate
[Acetate] (mM)
Time (h)
Aspartate
[Aspartate] (mM)
Time (h)
Histidine
[Histidine] (mM)
Time (h)
Tyrosine
[Tyrosine] (mM)
Time (h)
Oxaloacetic acid
[Oxaloacetic acid] (mM)
Time (h)
Methionine
[Methionine] (mM)
Time (h)
Valine
[Valine] (mM)
Time (h)
S. aureus JE2 wild-type
S. aureus JE2 mqoI::Tn

Figure 4. 31 - Metabolomic analyses of *S. aureus* JE2 wild-type (filled bars) and mqoI::Tn (dashed bars) growths under aerobic conditions, monitored by ^{1}H-NMR. In the red box is represented MQO I. *S. aureus* strains grew aerobically in CDM supplemented with 5 mM glucose, at 37 ºC. Samples were collected every 1.5 h of growth, centrifuged and the supernatant was stored. Extracellular metabolite concentrations were measured (milimoles). The results are representative of three independent experiments. The respective growth curves are shown in Figure 7.5 in Supplemental Material.

Figure 4.30 shows that in a nutrient rich medium, as TSB, *S. aureus* wild-type catabolized all the glucose present in the culture growth medium after around 4 h of growth (blue filled bars). Data also show that during that time lactate (green filled bars) and acetate (orange filled bars) concentrations increased in the growth medium, being the increase of acetate more pronounced. In the growth medium, both lactate and acetate presented a maximum concentration of approximately 8.5 mM after 4 h and 25 mM after 6 h. In both cases, the concentration of these metabolites decreased afterwards (Figure 4.30). Our data also show that *S. aureus* wild-type catabolized alanine (yellow bars) present in the culture medium after 10 h of growth, and that neither tryptophan (red filled bars) nor valine (grey filled bars) concentrations changed significantly.

Similarly to *S. aureus* wild-type, Figure 4.30 shows that *S. aureus* mqoI::Tn totally catabolized the glucose present in TSB medium, although this strain took more time to do so (blue dashed bars). The lactate variation presented a similar profile to that of the wild-type. For the mutant strain, lactate levels presented a maximum concentration of ~ 8 mM after 4 h of growth, which subsequently decreased (green dashed bars). In the case of acetate, the profile was different from the wild-type. Acetate concentration increased significantly during *S. aureus* mqoI::Tn growth, to ~ 60 mM after 12 h of growth (orange dashed bars). Figure 4.30 also shows that alanine was not totally catabolized by *S. aureus* mutant strain after 12 h of growth (yellow dashed bars). Tryptophan (red dashed bars) and valine (grey dashed bars) did not change their respective concentrations in the culture medium during the growth.

In CDM, both *S. aureus* strains revealed similar behaviours to those observed in TSB medium, respectively. Figure 4.31 shows that in CDM supplemented with 5 mM glucose, *S. aureus* wild-type strains catabolized all glucose present in the culture growth media after ~ 4.5 h of growth, observed by a decrease in glucose concentration (blue filled bars). As previously observed in a rich media (TSB), lactate and acetate concentrations also increased in the culture growth medium, up to 4.5 h of growth, presenting a maximum concentration of approximately 1 mM for lactate (green filled bars) and 8 mM for acetate (orange filled bars). After 4.5 h a decrease in lactate and acetate concentrations was observed. Our data also demonstrate that alanine (yellow filled bars) was totally catabolized after ~ 4.5 h, and both histidine (purple filled bars) and aspartate (soft pink filled bars) after ~ 11 h of growth. Phenylalanine (dark blue filled bars), tyrosine (pink filled bars) and methionine (burgundy filled bars) concentrations remained constant in the growth medium. Valine levels decreased but not completely (grey filled bars). Oxaloacetic acid was also detected along the growth.

Like observed in TSB medium, *S. aureus* mutant strain also completely catabolized the 5 mM glucose present in CDM (Figure 4.31; blue dashed bars), after ~ 6 h of growth. Lactate levels increased in the growth medium and presented a maximum concentration around 1 mM, after ~ 6 h (green dashed bars). Figure 4.31 shows that this increase was followed by a decrease in lactate concentration. As previous observed in TSB medium, acetate concentration constantly increased during S*. aureus* mqoI::Tn growth, presenting a maximum concentration of around 12 mM after 11 h (orange dashed bars). Figure 4.31 also shows that alanine (yellow dashed bars) and aspartate (soft pink dashed bars) were totally catabolized by the mutant strain. On the contrary, our data demonstrate that histidine (purple dashed bars) phenylalanine (dark blue dashed bars), tyrosine (pink dashed bars), methionine (burgundy dashed bars) and valine (grey dashed bars) did not vary their concentrations in the culture growth medium.

Our observations are in agreement with those observed for *S. aureus* growths in TSB medium (Figure 4.30). Analysing the results presented in Figures 4.30 and 4.31 it is possible to investigate *S. aureus*' energetic metabolism when glucose is used as carbon source.

In both *S. aureus* strains, wild-type (filled bars) and mqoI::Tn (dashed bars), glucose was rapidly depleted from the culture growth media. Under aerobic conditions *S. aureus* is described to use the pentose phosphate and glycolytic pathways for the catabolism of glucose[28]. The two *S. aureus* JE2 strains are observed to accumulate lactate and acetate while consuming glucose, although the accumulation of acetate is more pronounced.

Accumulation of lactate and acetate indicates that glucose is only partially oxidized. This is in agreement with the literature that describes that *S. aureus* possesses a complex regulatory mechanism, the carbon catabolite repressor (CCR), as mentioned in the previous section. CCR is a sophisticated mechanism that prevents the loss of energy, precluding the consumption of other carbon sources or amino acids, while glucose is available. In the presence of CCR, the genes and proteins of the TCA cycle are not expressed, and consequently this cyclic pathway is inhibited until glucose depletion[56,57,58,59]. According to these reports, when *S. aureus* grows in a medium containing glucose, pyruvate produced by glucose degradation is subsequently oxidized to acetate, leading to its accumulation[28,29,33,30,62,63]. The accumulation of both products in the culture growth media until glucose depletion is probably responsible for the characteristic pH drop previously observed in both growths curves (section 4.3, Figures 4.22 and 4.23). In this case the organisms would obtain energy by oxidation of NADH by the respiratory chain, and by substrate level phosphorylation including the production of ATP from Acetyl-CoA to acetate (see the schematised metabolic pathways in Figure 4.31). In both *S. aureus* wild-type growths, the total glucose consumption is observed to be coincident with the uptake from the culture growth media of excreted lactate and acetate (Figures 4.30 and 4.31), which indicates that lactate and acetate are now being catabolized. This is in agreement with the reports observing that de-repression of the TCA cycle occurs upon glucose depletion. Then, in the form of Acetyl-CoA, acetate is oxidized by the TCA cycle.

Until glucose depletion, both *S. aureus* strains presented the same behaviour, although with different times for glucose consumption and acetate/lactate accumulation. The differences between both strains are more evident in the uptake of the excreted products from the respective growth media. As expected, the ^{1}H-NMR analyses of collected samples from *S. aureus* mqoI::Tn growth revealed several differences when compared with the ^{1}H-NMR results of the wild-type strain. *S. aureus* mqoI::Tn strains grew in the presence of glucose, although, the accumulated acetate was not imported from the growth medium after glucose depletion after ~ 6 h (Figures 4.30 and 4.31), as observed for the wild-type. MQO I protein is involved both in the TCA cycle and respiratory chain. The uptake of acetate did not occur, probably because this *S. aureus* strain has the TCA cycle compromised, indicating that a fully functioning TCA cycle is essential for acetate catabolism. These data agree with the CCR model, even though CCR is no longer inhibiting the cyclic pathway. Because the *S. aureus* mqoI::Tn strain does not perform acetate catabolism, acetate concentration constantly increased during the growth (Figures 4.30 and 4.31). On the contrary, in Figures 4.30 and 4.31, lactate was seen to be uptaken from the growth medium, after glucose depletion. Taking into account that the TCA cycle is hampered and based on the assigned metabolic pathways, the imported lactate seemed to be possibly converted into acetate, first through its conversion into pyruvate (leading to the production of NADH) which was then converted into acetate, via Acetyl-CoA since this reaction would be advantageous to the cells due to the production of ATP. The non-uptake of acetate from the culture growth medium observed trough these ^{1}H-NMR results, is probably responsible for the non-recovery of the pH values observed in *S. aureus* mqoI::Tn growth curves, in the previous section (Figures 4.22 and 4.23). On the opposite, a pH rise was observed for *S. aureus* wild-type growth presumably due to the catabolism of acetate (in both CDM and TSB) and of other carbohydrates, only present in TSB medium, which were uptake from the medium to the cells.

Analysing amino acids catabolism through *S. aureus* growths in CDM supplemented with glucose (Figure 4.31) the two *S. aureus* strains were observed to initiate the consumption of alanine and aspartate, before the uptake of both lactate or acetate. According to the literature, the catabolism of alanine and aspartate reflects the direct production of metabolic intermediates, respectively, pyruvate and oxaloacetate. Both amino acids were completely consumed by both *S. aureus* strains. This observation led us to conclude that the absence of MQO I does not interfere with the catabolism of aspartate, despite the compromised TCA cycle.

Our results are in agreement with data published in March 2017, also obtained with Nebraska Transposon mutants using the same *S. aureus* JE2 wild-type strain[36]. This recent publication suggests that amino acids which serve to fuel the synthesis of pyruvate (namely alanine), and oxaloacetate (namely aspartate) are important for initiation of growth in CDM. These data also report the total consumption of the amino acids involved in the generation of pyruvate (alanine, glycine, threonine and serine). The authors suggest the existence of a bifurcation during amino acid catabolism in which pyruvate is produced, proposing primarily their utilization to generate acetate and ATP via Acetyl-CoA, and also proposing the entry of little carbon to the TCA cycle via citrate synthase, until the consumption of acetate from the growth medium.

Furthermore, Figure 4.31 shows that histidine was only completely catabolized by *S. aureus* wild-type strain after 11 h of growth. Previously mentioned data illustrate that histidine was catabolized slower than glutamate, proline and arginine. We could not quantify the concentration of those amino acids (glutamate, proline and arginine), although we observed that the consumption of histidine was slow, when compared with the catabolism of alanine and aspartate. A direct comparison between the data obtained in this thesis and that reported on March 2017 may not be possible, because no carbon source apart from amino acids was present in the medium, in the mentioned report.

Figure 4.31 also shows a gradual consumption, but not significant, of valine, methionine, tyrosine and phenylalanine, observed for both *S. aureus* strains. The concentration of these amino acids remained practically the same during the growth, suggesting that they are not used for catabolic purposes, in these conditions. Again, our results agree with the literature[36].

Both Figures 4.30 and 4.31 illustrate the dynamics of the metabolism of *S. aureus* growth of the wild-type strain and of a mutant strain lacking MQO I enzyme, in a growth media containing glucose, respectively, in TSB (a nutrient-rich medium) and in CDM. Both *S. aureus* strains respectively presented a similar profile in TSB and in CDM.

Figure 4.32 shows the variation of extracellular metabolites along *S. aureus* aerobic growths in CDM supplemented with 5 mM acetate. Samples collected during these growths were analysed by ^{1}H-NMR, aiming to study their energetic metabolism in a growth medium containing acetate as carbon source.

S. aureus wild-type growth (Figure 4.32; filled bars), shows an increase on the acetate concentration, up to 5 h of growth (orange bars). In the beginning of the growth, acetate concentration was around 6 mM, although it presented a maximum concentration of approximately 7.5 mM in the growth medium. This concentration rise was followed by a subsequent decrease, suggesting the consumption of acetate only after ~ 6.5 h of growth. Our data also show that the concentration of lactate in the culture growth medium decreased since the beginning of the growth (green filled bars). No glucose was detected during the growth, which allowed the quantification of glycine. Glycine (salmon colour filled bars) and alanine (yellow filled bars) were totally catabolized up to ~ 6.5 h of growth. Aspartate (soft pink filled bars) was completely depleted from the growth medium up to ~ 8 h of growth, and histidine (purple filled bars) only after 11 h. Data also demonstrate that phenylalanine (dark blue filled bars), tyrosine (pink filled bars) and methionine (burgundy filled bars) concentrations remained practically constant in the growth medium. Valine levels decreased but not completely (grey filled bars).

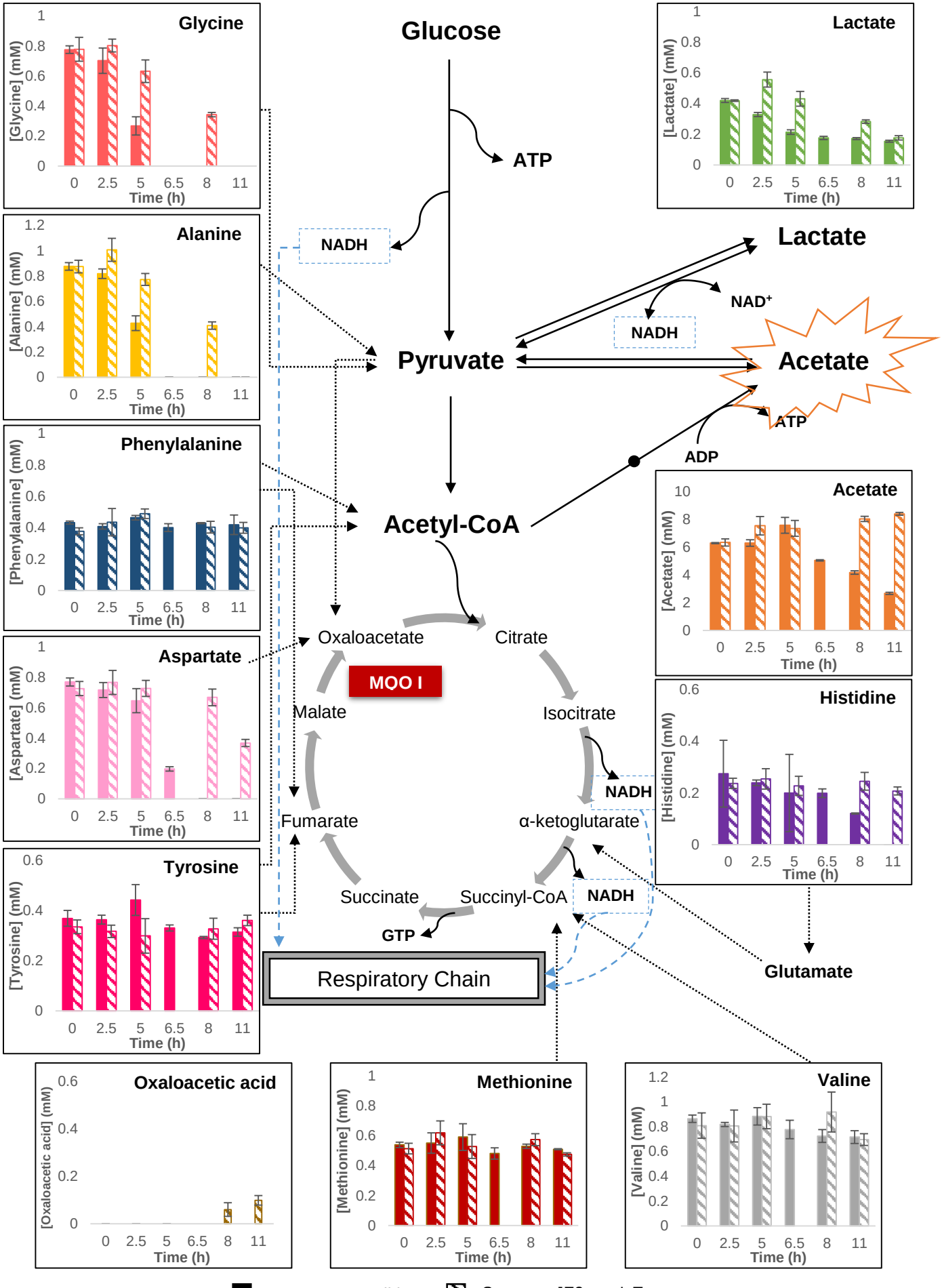

■ *S. aureus* JE2 wild-type ▨ *S. aureus* JE2 mqol::Tn

Figure 4. 32 – Metabolomic analyses of *S. aureus* JE2 wild-type (filled bars) and mqoI::Tn (dashed bars) growths under aerobic conditions, monitored by ^{1}H-NMR. In the red box is represented MQO I. *S. aureus* strains grew aerobically in CDM supplemented with 5 mM acetate, at 37 ºC. Samples were collected every 1.5 h of growth, centrifuged and the supernatant was stored. Extracellular metabolite concentrations were measured (milimoles). The results are representative of three independent experiments. Please note missing bars relative to 6.5 h of *S. aureus* mqoI::Tn growth. The respective growth curves are shown in Figure 7.6 in Supplemental Material.

In the case of the *S. aureus* mqoI::Tn growth, acetate levels were observed to be constantly increasing along the growth, presenting a maximum concentration of around 8.5 mM after 11 h (Figure 4.32; orange dashed bars). Lactate concentration decreased during the growth (green dashed bars). After ~ 11 h of growth, only alanine (yellow dashed bars) and glycine (salmon colour dashed bars) were completely catabolized by these strains, among the quantified amino acids. Our data also showed that aspartate started to be consumed after ~ 8 h of growth (soft pink dashed bars). Histidine (purple dashed bars), phenylalanine (dark blue dashed bars), tyrosine (pink dashed bars), methionine (burgundy dashed bars) and valine (grey dashed bars) concentrations remained constant in the growth medium (Figure 4.32). Oxaloacetic acid was detected, although in small amounts, after 8 h of growth (brown dashed bars). Also very low levels of fumarate were detected after 5 h of growth.

Analysing the results presented in Figure 4.32 it is possible to investigate *S. aureus*' energetic metabolism when acetate is the only carbon source present in the culture growth medium.

In the described *S. aureus* wild-type growth (filled bars), lactate was observed to be the first metabolite to be catabolized (Figure 4.32; green bars), despite the growth medium being supplemented with acetate. Based on the assigned metabolic pathways and since the uptake of lactate involves its conversion into pyruvate and leads to the production of NADH, the rapid consumption of lactate from the growth medium could be interpreted as a way to generate NADH, which is probably further oxidized by the respiratory chain. Figure 4.32 shows that both alanine and glycine were also rapidly catabolized, reflecting their direct catabolism in the production of pyruvate. Acetate concentration increased in the growth medium (although not significantly) while lactate and amino acids were imported. These results are again in agreement with recent published data[36], previously described above, recognizing the importance of amino acids involved in the generation of pyruvate, such as alanine and glycine, and hypothesising their use to produce ATP, through the conversion of pyruvate into acetate, via Acetyl-CoA.

Aspartate was also completely catabolized by *S. aureus* wild-type strain, after ~ 8h of growth. This consumption also agrees with the literature, that refers the catabolism of aspartate as a significant amino acid used to synthesize oxaloacetate, which is described as being important for initiating the growth in CDM[36].

As previously observed in CDM with glucose (Figures 4.31), in CDM with acetate, histidine was also completely catabolized by *S. aureus* wild-type strain, after ~ 11 h of growth (Figure 4.32).

The ^{1}H-NMR results relative to *S. aureus* mqoI::Tn strains revealed several differences when compared to those of *S. aureus* wild-type strain, in CDM supplemented with acetate (Figure 4.32). Constant increased acetate concentrations observed in the growth medium for *S. aureus* mqoI::Tn growth, led us to conclude that these strains were not able to catabolize acetate. However, Figure 4.32 indicates that *S. aureus* mqoI::Tn strains were able to uptake lactate from the culture growth medium. The inability to catabolize acetate had already been observed in a growth medium containing glucose (Figures 4.30 and 4.31) and is presumably associated with the compromised TCA cycle, in the absence of MQO I, which does not interfere with the catabolism of lactate. As previously suggested, the uptake of lactate could be advantageous to these cells, based on the production of NADH, and the consequently generated pyruvate could be probably converted into acetate via Acetyl-CoA, to produce ATP. Alanine and glycine were both completely catabolized by *S. aureus* strains lacking MQO I protein, after approximately 10 h of growth. Taking into account the incomplete TCA cycle and the assigned metabolic pathways, the catabolism of those amino acids would be advantageous because it leads to the production of pyruvate, and could allow the production of ATP by Acetyl-CoA.

Catabolism of aspartate was initiated around 8 h of growth. According to the literature, the catabolism of aspartate is reflected by the direct production of oxaloacetate. Figure 4.32 shows that the consumption of aspartate is coincident with the detection of oxaloacetic acid in the growth medium, ~ 8 h. The compromised TCA cycle, in the absence of MQO I enzyme, may lead to the accumulation of oxaloacetate, justifying the appearance of oxaloacetic acid in the growth medium. From the analysed metabolites, no other amino acids were catabolized by *S. aureus* strains lacking MQO I in these conditions.

A significant effect reflecting the absence of MQO I was previously observed in the growths in CDM supplemented with acetate, where *S. aureus* mqoI::Tn cells grew less when compared with the wild-type strain (Figure 4.24). The non-catabolism of acetate is probably responsible for the constant pH profile observed in our ^{1}H-NMR results, contrarily to the pH rise observed in *S. aureus* wild-type growth (Figure 4.24). Our NMR data demonstrate that *S. aureus* cells lacking MQO I are not able to catabolize acetate, despite having the other assigned MQO (MQO II) present. Our results show that MQO II does not compensate for the absence of MQO I in *S. aureus* mqoI::Tn growth. Thus, these observations revealed the inability of MQO II to perform the same reaction as MQO I, the oxidation of malate to oxaloacetate, in agreement with our biochemical data (section 4.2).

Intrigued by these ^{1}H-NMR results, and aiming to characterize *S. aureus* growth under different carbon sources, growths were also performed in a medium containing lactate, as sole carbon source, and samples were collected during these growths, in order to be analysed through NMR-based metabolomics.

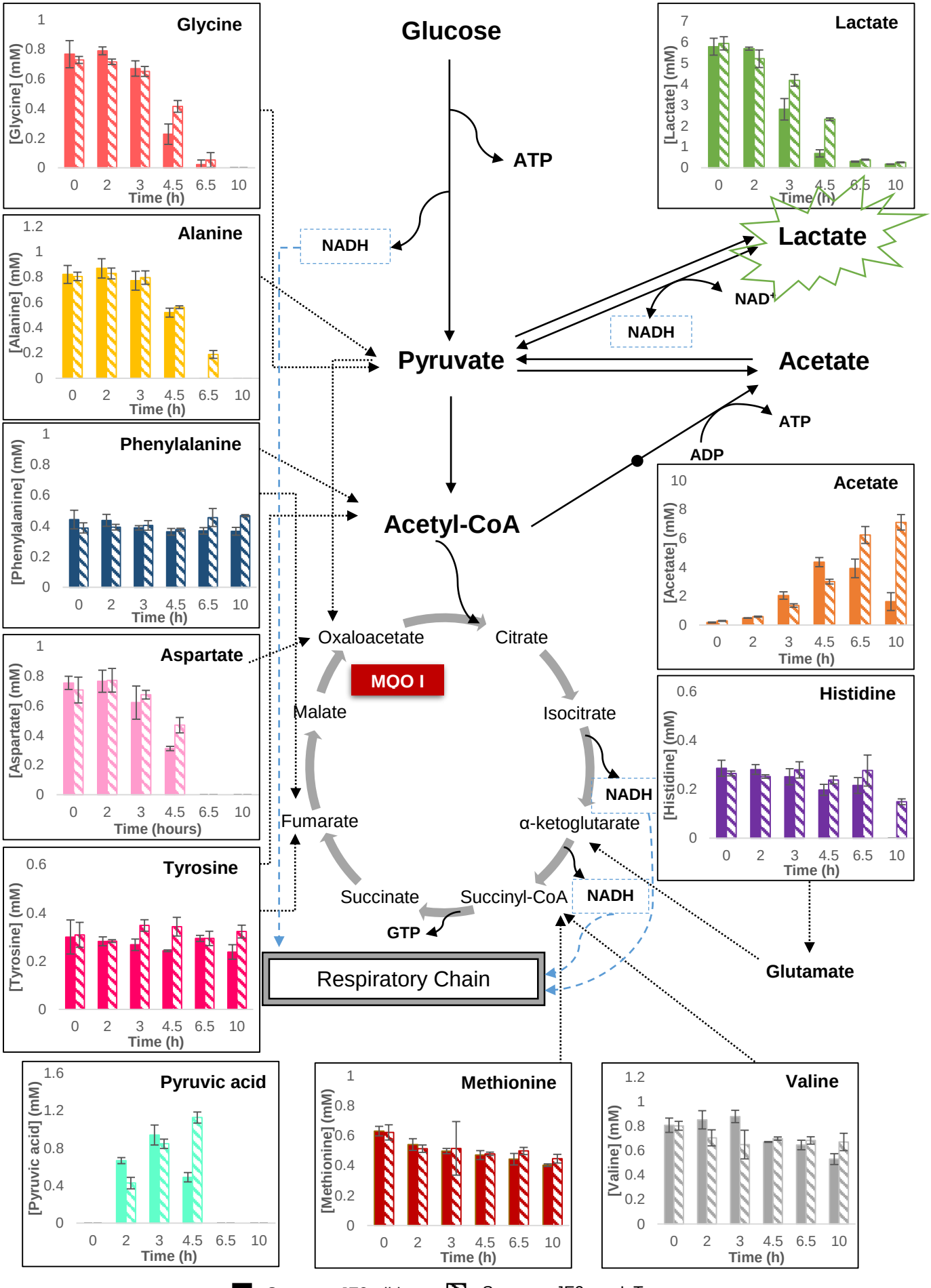
Glycine
[Glycine] (mM)
Time (h)
Alanine
[Alanine] (mM)
Time (h)
Phenylalanine
[Phenylalanine] (mM)
Time (h)
Aspartate
[Aspartate] (mM)
Time (hours)
Tyrosine
[Tyrosine] (mM)
Time (h)
Pyruvic acid
[Pyruvic acid] (mM)
Time (h)
Glucose
ATP
NADH
Pyruvate
Lactate
NAD+
NADH
Acetate
ATP
ADP
Acetyl-CoA
Oxaloacetate
Citrate
MQO I
Malate
Isocitrate
NADH
Fumarate
α-ketoglutarate
Succinate
Succinyl-CoA
NADH
GTP
Respiratory Chain
Glutamate
Lactate
[Lactate] (mM)
Time (h)
Acetate
[Acetate] (mM)
Time (h)
Histidine
[Histidine] (mM)
Time (h)
Methionine
[Methionine] (mM)
Time (h)
Valine
[Valine] (mM)
Time (h)
S. aureus JE2 wild-type
S. aureus JE2 mqol::Tn

Figure 4. 33 - Metabolomic analyses of *S. aureus* JE2 wild-type (filled bars) and mqoI::Tn (dashed bars) growths under aerobic conditions, monitored by ^{1}H-NMR. In the red box is represented MQO I. *S. aureus* strains grew aerobically in CDM supplemented with 5 mM lactate, at 37 ºC. Samples were collected every 1.5 h of growth, centrifuged and the supernatant was stored. Extracellular metabolite concentrations were measured (milimoles). The results are representative of three independent experiments. The respective growth curves are shown in Figure 7.7 in Supplemental Material.

Figure 4.33 presents the variation of extracellular metabolites along *S. aureus* aerobic growths in CDM supplemented with lactate, as the sole carbon source.

In these conditions, *S. aureus* wild-type is observed to totally catabolize the lactate present in the culture medium after approximately 6.5 h of growth, observed by a decrease in lactate concentration (Figure 4.33; green filled bars). Our data also demonstrate that both alanine (yellow filled bars), glycine (salmon colour filled bars) and aspartate (soft pink filled bars) were totally catabolized by *S. aureus* wild-type strain, after ~ 6.5 h of growth. Acetate concentration increased in the growth medium since the beginning of the growth, and reached maximum concentration of 4 mM, around 4.5 h of growth (orange filled bars). This concentration rise was subsequently followed by a decrease, which started at ~ 6.5 h of growth. Histidine was completely catabolized by the wild-type strain, after ~ 10 h of growth (purple filled bars). Valine concentration decreased, but not completely (grey filled bars). Phenylalanine (dark blue filled bars), tyrosine (pink filled bars) and methionine (burgundy filled bars) concentrations remained constant in the growth medium. Pyruvic acid was detected in the ^{1}H-NMR spectra after ~ 2 h of growth, and presented a maximum concentration around 1 mM after ~ 3 h. Pyruvic acid was subsequently imported from the growth medium, after ~ 6 h of growth (light blue filled bars).

The *S. aureus* mutant strain completely catabolized all the lactate present in the medium, as shown in Figure 4.33 (green dashed bars), by ~ 6.5 h of growth. Figure 4.33 shows that in *S. aureus* mqoI::Tn growth, acetate concentration constantly increased during the growth, presenting a maximum concentration of ~ 8 mM, around 10 h of growth (orange dashed bars). Our data also show that alanine (yellow dashed bars), glycine (salmon colour dashed bars) and aspartate (soft pink dashed bars) were totally consumed by *S. aureus* strains lacking MQO I, and that histidine (purple dashed bars) was also catabolized, but not completely until 10 h of growth. Our results demonstrate that phenylalanine (dark blue dashed bars), tyrosine (pink dashed bars), methionine (burgundy dashed bars) and valine (grey dashed bars) did not significantly vary their concentrations in the culture growth medium of these strains. Pyruvic acid was also detected after 2 h of growth (light blue dashed bars). This concentration was maximum at ~ 4.5 h of growth. Subsequently, pyruvic acid concentration totally decreased suggesting its uptake.

The ^{1}H-NMR results presented in Figure 4.33 allow us to acquire a new perspective of the studied *S. aureus* strains growth, this time in a medium containing lactate as sole carbon source.

Our data show that in CDM both *S. aureus* JE2 strains (wild-type and mqoI::Tn) completely catabolized lactate, although at different times of the growth. For the first time, pyruvic

acid was detected in the ^{1}H-NMR spectra of *S. aureus* strains, right after 2 h of growth and subsequently disappeared after ~ 6.5 h. As observed in Figure 4.33, pyruvic acid concentrations increased as lactate concentrations decreased. Based on the assigned metabolic pathways in the literature and looking at the metabolic scheme presented in Figure 4.33, the uptake of lactate from the culture growth medium is known to be converted into pyruvate and subsequently producing NADH[2,36]. The considerable concentration of lactate, probably leads to a significant amount of generated pyruvate, which accumulates in the cells and thus can be excreted to the growth medium. In the cells, generated pyruvate could enter the TCA cycle via citrate synthase, or could be converted into acetate via Acetyl-CoA, to produce ATP. Thus, we suggest that since pyruvate concentrations decreased inside the cell, *S. aureus* uptakes the previously excreted pyruvic acid from the growth medium. This could be one of the possible reasons to justify the detected pyruvic acid concentrations observed in both *S. aureus* growths under these conditions.

As previously observed in CDM supplemented with acetate, some amino acids start being consumed before acetate catabolism, which was only observed around 10 h of growth for *S. aureus* wild-type strain (orange filled bars). Figure 4.33 shows that alanine and glycine were completely catabolized after ~ 6.5 h of growth, for *S. aureus* wild-type strain. Recent publications reported that when *S. aureus* JE2 cells grow in the presence of amino acids that generate pyruvate, namely serine, threonine, alanine and glycine, these are primarily catabolized to acetate to fuel ATP synthesis, and that acetate only enters the TCA cycle after the depletion serine, threonine and alanine[36]. Our results show that acetate is only catabolized after alanine and glycine depletion, which in agreement with the literature.

However, Figure 4.33 shows that in *S. aureus* mqoI::Tn growth, acetate concentration did not decrease in the growth medium, contrarily to the decreased acetate concentration observed for the wild-type strain (orange bars). As expected, the catabolism of acetate did not occur in *S. aureus* strains due to the lack of MQO I, justifying the lowest growth of these strains when compared with the wild-type, and a not so pronounced rise in the pH profile (Figure 4.25). Once more, the inability of MQO II to compensate for the absence of MQO I in *S. aureus* mqoI::Tn growth is shown. Taking into account these observations and published data suggesting MQO II as a putative lactate:quinone oxidoreductase[34,35], and also regarding our biochemical characterization results of this enzyme, it is possible to conclude that MQO II catalyses a different reaction from MQO I.

5. Conclusion

S. aureus is an opportunistic pathogen and has become a worldwide problem in clinical medicine due to the increased incidence of its drug resistance. For this reason, it is fundamental to explore and understand not only the mechanism behind this strong resistance, but also the basic conditions that allow *S. aureus* to live and survive. We aimed to contribute to this knowledge by exploring respiratory enzymes involved in the catabolism of *S. aureus*, specifically malate:quinone oxidoreductases.

We investigated the two proteins, annotated as malate:quinone oxidoreductases, MQO I and MQO II, from this pathogen. Protein biochemical characterization and a thorough cellular investigation were performed. After several purification trials and intense search for the best conditions, the two proteins were expressed and purified for the first time. Purified MQO I was identified through mass spectrometry analysis, and a preliminarily biochemical characterization carried out. For MQO II, the amount of protein obtained allowed spectroscopic characterization, protein stability tests and enzymatic analyses including substrate affinity and pH profile. Both proteins presented the characteristic flavin UV-Visible spectrum. MQO II was shown to be redox active. Enzymatic studies showed that MQO II exhibits affinity for L-lactate instead of malate, and that its activity is maximal at pH 7.0. Thermal denaturation experiments indicated that this flavoprotein is stable up to approximately 47 ºC.

Our approach was extended to the cellular level in order to understand the impact of the role of MQO I in the metabolism of *S. aureus*. These studies involved cell growth of a wild-type strain and also of one mutant strain, presenting a transposon in the gene coding for MQO I.

A total of seventy-two *S. aureus* growths were performed and three hundred and fifteen samples were collected along the growths, from which two hundred forty-three were analysed through NMR-based metabolomics. For the first time, *S. aureus* growth was characterized under different carbon sources, glucose, acetate and lactate, in a chemically defined medium and also under nutrient rich conditions (TSB). The growths of the two strains were monitored by optical density and pH, and the respective metabolites were analysed by ^{1}H-NMR. This allowed us to investigate the energetic metabolism of *S. aureus* and also to explore the role of MQO I in the different metabolic pathways.

When grown in TSB medium *S. aureus* first catabolized all glucose present in the growth medium, excreting lactate and acetate, which were later imported back to the cell after glucose depletion, elucidating the de-repression of the TCA cycle. Our results are in agreement with the carbon catabolite repressor mechanism described in the literature. In CDM supplemented with glucose, *S. aureus* growths presented the same behaviour, but in addition it was possible to fully assess amino acid catabolism. Our results obtained from the growth using different carbon sources showed that *S. aureus* preferably catabolizes glucose, then lactate and some amino acids, such as alanine and glycine (whose catabolism is involved in the generation of pyruvate) before using acetate. Our observations are in agreement with previous reports that announced

the initial catabolism of amino acids, directly involved in the generation of pyruvate, to further fuel ATP synthesis, concluding that this pathogen catabolizes amino acids to obtain energy.

S. aureus mqoI::Tn growths showed the importance of MQO I in this microorganism. The inability of this strain to catabolize acetate was observed, demonstrating that a fully functioning TCA cycle is necessary for acetate catabolism. The inability of the protein MQO II to compensate for the absence of MQO I in *S. aureus* mqoI::Tn growths was observed. Our experiments showed that these proteins do not catalyse the same reaction.

We conclude that MQO II is not a malate:quinone oxidoreductase, as already suggested in the literature. This observation is confirmed through enzymatic assays, substrate affinity studies and is also reinforced through extracellular metabolites of *S. aureus* growths of strains lacking MQO I (under different growth conditions), quantified by NMR-based metabolomics.

Our data show the importance of MQO I in the energetic metabolism of this microorganism. *S. aureus* growths were affected and compromised, in the absence of MQO I, making this enzyme an attractive candidate for targeted therapeutics.

The work here presented on the study of malate:quinone oxidoreductases from *S. aureus*, opens new perspectives for future studies of these proteins. A better optimization of the purification processes is still needed, to develop a thorough biochemical characterization of both MQO I and MQO II. Both molecular and cellular approaches are fundamental to proceed with the study of these proteins and to contribute to the knowledge of *S. aureus*' respiratory enzymes. *S. aureus* growths can be tested under different growth conditions, limiting, for example, the amino acids provided in the growth medium. Exploring not only the role of these proteins, but also the spatial/temporal localization and regulation of MQO I and MQO II in the cell membrane, should be an interesting future work to find the answers to understand this strong and artistic mechanism behind the energetic metabolism of *S. aureus*.

6. References

1. Mitchell P. Coupling of Phosphorylation to Electron and Hydrogen Transfer by a Chemi-osmotic Type of Mechanism. *Nature*. 1961;191:144-148.

2. Nelson D, Cox M. *Lehninger Principles of Biochemistry*. 4th ed.; 2005.

3. Nicholls DG, Ferguson SJ. *Bioenergetics 4*. 4th ed.; 2013.

4. Marreiros BC, Calisto F, Castro PJ, et al. Exploring membrane respiratory chains. *Biochim Biophys Acta - Bioenerg*. 2016;1857:1039-1067.

5. Schlegel HG. *General Microbiology*. 7th ed.; 1986.

6. Madigan M. *Brock Biology of Microorganisms*. 14th ed.; 2014.

7. Boiteux A, Hess B. Design of Glycolysis. *Philos Trans R Soc B Biol Sci*. 1981;293:5-22.

8. Zannoni D. *Respiration in Archaea and Bacteria: Diversity of Prokaryotic Respiratory Systems*. Vol 16.; 2005.

9. Sazanov LA. Respiratory complex I: Mechanistic and structural insights provided by the crystal structure of the hydrophilic domain. *Biochemistry*. 2007;46:2275-2288.

10. Sazanov LA. The mechanism of coupling between electron transfer and proton translocation in respiratory complex I. *J Bioenerg Biomembr*. 2014;46:247-253.

11. Cecchini G. Function and Structure of Complex II of the Respiratory Chain. *Annu Rev Biochem*. 2003;72:77-109.

12. Iwata S. Complete Structure of the 11-Subunit Bovine Mitochondrial Cytochrome b*c1* Complex. *Science*. 1998;281:64-71.

13. Wikström M. Identification of the electron transfers in cytochrome oxidase that are coupled to proton-pumping. *Nature*. 1989;338:776-778.

14. Van der Rest ME, Frank C, Molenaar D. Functions of the membrane-associated and cytoplasmic malate dehydrogenases in the citric acid cycle of *Escherichia coli*. *J Bacteriol*. 2000;182:6892-6899.

15. Cohn D V. The enzymatic formation of oxalacetic acid by nonpyridine nucleotide. *J Biol Chem*. 1958;233:299-304.

16. Kabashima Y, Sone N, Kusumoto T, Sakamoto J. Purification and characterization of malate:quinone oxidoreductase from thermophilic *Bacillus sp.* PS3. *J Bioenerg Biomembr*. 2013;45:131-136.

17. Kather B, Stingl K, Rest ME Van Der, Rest MEV a NDER. Another Unusual Type of Citric Acid Cycle Enzyme in *Helicobacter pylori*: the Malate:Quinone Oxidoreductase. *J Bacteriol*. 2000;182:3204-3209.

18. Genda T, Nakamatsu T, Ozak H. Purification and characterization of malate dehydrogenase from *Corynebacterium glutamicum*. *J Biosci Bioeng*. 2003;95:562-566.

19. Molenaar D, van der Rest ME, Petrovic S. Biochemical and genetic characterization of the membrane-associated malate dehydrogenase (acceptor) from *Corynebacterium glutamicum*. *Eur J Biochem*. 1998;254:395-403.

20. Aliverti A, Curti B, Vanoni M a. Identifying and quantitating FAD and FMN in simple and in iron-sulfur-containing flavoproteins. *Methods Mol Biol*. 1999;131:9-23.

21. Watkins RR, David MZ, Salata RA. Current concepts on the virulence mechanisms of meticillin-resistant *Staphylococcus aureus*. *J Med Microbiol*. 2012;61:1179-1193.

22. Tavares A, Miragaia M, Rolo J, Coelho C, De Lencastre H. High prevalence of hospital-associated methicillin-resistant *Staphylococcus aureus* in the community in Portugal: Evidence for the blurring of community-hospital boundaries. *Eur J Clin Microbiol Infect Dis*. 2013;32:1269-1283.

23. Mcnicoll L, Marsella M. The Growing Problem of Methicillin-resistant *Staphylococcus aureus* : Will Hospitals Prevail ? *Med Health*. 2010:267-270.

24. Klevens R, Morrison M, Nadle J. Invasive methicillin-resistant *Staphylococcus aureus* infections in the United States. *Jama*. 2007;298:1763-1771.

25. Liu GY. Molecular Pathogenesis of *Staphylococcus aureus* Infection. *Pediatr Res*. 2009;65:71-77.

26. Adler A, Temper V, Block CS, Abramson N, Moses AE. Panton-Valentine leukocidin-producing *Staphylococcus aureus*. *Emerg Infect Dis*. 2006;12:1789-1790.

27. Fuchs S, Pané-Farré J, Kohler C, Hecker M, Engelmann S. Anaerobic gene expression in *Staphylococcus aureus*. *J Bacteriol*. 2007;189:4275-4289.

28. Ferreira MT, Manso AS, Gaspar P, Pinho MG, Neves AR. Effect of Oxygen on Glucose Metabolism: Utilization of Lactate in *Staphylococcus aureus* as Revealed by In Vivo NMR Studies. *PLoS One*. 2013;8(3).

29. Dassy B, Fournier JM. Respiratory activity is essential for post-exponential-phase production of type 5 capsular polysaccharide by *Staphylococcus aureus*. *Infect Immun*. 1996;64:2408-2414.

30. Somerville GA, Chaussee MS, Morgan CI, et al. *Staphylococcus aureus* Aconitase Inactivation Unexpectedly Inhibits Post-Exponential-Phase Growth and Enhances Stationary-Phase Survival. *Infect Immun*. 2002;70:6373-6382.

31. Diep BA, Gill SR, Chang RF, et al. Complete genome sequence of USA300, an epidemic clone of community-acquired meticillin-resistant *Staphylococcus aureus*. *Lancet*. 2006;367:731-739.

32. Becker K, Heilmann C, Peters G. Coagulase-Negative Staphylococci. *CMR*. 2014;27:870-926.

33. Mayer S, Steffen W, Steuber J, Gôtz F. The *Staphylococcus aureus* nuoL-like protein MpsA contributes to the generation of membrane potential. *J Bacteriol*. 2015;197:794-806.

34. Fuller JR, Vitko NP, Perkowski EF, et al. Identification of a Lactate:Quinone Oxidoreductase in *Staphylococcus aureus* that is Essential for Virulence. *Front Cell Infect Microbiol*. 2011;1:1-15.

35. Spahich NA, Vitko NP, Thurlow LR, Temple B, Richardson AR. *Staphylococcus aureus* lactate- and malate-quinone oxidoreductases contribute to nitric oxide resistance and virulence. *Mol Microbiol*. 2016;100:759-773.

36. Halsey CR, Lei S, Wax JK, et al. Amino Acid Catabolism in *Staphylococcus aureus* and the Function of Carbon Catabolite Repression. *MBio*. 2017;8.

37. Froger A, Hall JE. Transformation of plasmid DNA into *E. coli* using the heat shock method. *J Vis Exp*. 2007:253.

38. Thermo scientific. *BCA Protein Assay Kit*. 747(2000).

39. Albumin BS, Background SDS, Assay BP, Assay BP, Reagent B. *Biuret Protein Assay*.(2010).

40. Kruber O. Uber das 2.3-Dimethyl-naphthalin im Steinkohlenteer. 1929.

41. Fey PD, Endres JL, Yajjala K, et al. A Genetic Resource for Rapid and Comprehensive Phenotype Screening of Nonessential *Staphylococcus aureus* Genes. *MBio*. 2013;4:1-8.

42. Bae T, Banger AK, Wallace A, et al. *Staphylococcus aureus* virulence genes identified by bursa aurealis mutagenesis and nematode killing. *Pnas*. 2004;101.

43. Vitko N, Richardson A. Laboratory Maintenance of Methicillin-Resistant *Staphylococcus aureus* (MRSA). *Curr Protoc Microbiol*. 2013:1-21.

44. Gopal GJ, Kumar A. Strategies for the Production of Recombinant Protein in *Escherichia coli*. *Protein J*. 2013;32:419-425.

45. Keppy NK, Allen MW, Ph D, Scientific TF. *The Biuret Method for the Determination of Total Protein Using an Evolution Array 8-Position Cell Changer*., 8-9 (2000).

46. Boyer R. Principles and reactions of protein extraction, purification, and characterization: Ahmed, Hafiz. *Biochem Mol Biol Educ*. 2006;33:145-146.

47. Heikal A, Nakatani Y, Dunn E, et al. Structure of the bacterial type II NADH dehydrogenase: A monotopic membrane protein with an essential role in energy generation. *Mol Microbiol*. 2014;91:950-964.

48. Vanderkooi J, Erecinska M. Cytochrome c Interaction with Membranes Absorption and Emission Spectra and Binding Characteristics of Iron-Free Cytochrome *c*. *Biochemistry*. 1975;207:199-207.

49. Matsuno T, Mie Y, Yoshimune K, Yumoto I. Physiological role and redox properties of a small cytochrome c5, cytochrome c-552, from alkaliphile, *Pseudomonas alcaliphila* AL15-21. *J Biosci Bioeng*. 2009;108:465-470.

50. Kolaj-robin O, Kane SRO, Nitschke W, Léger C, Baymann F. Biochemical and biophysical characterization of succinate:quinone reductase from *Thermus thermophilus*. *Biochim Biophys Acta - Bioenerg*. 2011;1807:68-79.

51. Rosano GL, Ceccarelli EA. Recombinant protein expression in *Escherichia coli*: Advances and challenges. *Front Microbiol*. 2014;5:1-17.

52. Sena F V., Batista AP, Catarino T, et al. Type-II NADH:quinone oxidoreductase from *Staphylococcus aureus* has two distinct binding sites and is rate limited by quinone reduction. *Mol Microbiol*. 2015;98:272-288.

53. Maklashina E, Cecchini G. The quinone-binding and catalytic site of complex II. *Biochim Biophys Acta - Bioenerg*. 2010;1797:1877-1882.

54. Chakraborty S, Sakka M, Kimura T, Sakka K. Characterization of a Dihydrolipoyl Dehydrogenase Having Diaphorase Activity of *Clostridium kluyveri*. *Biosci Biotechnol Biochem*. 2008;72:982-988.

55. Fox JL. Sodium dithionite reduction of flavin. *FEBS Lett*. 1974;39:53-55.

56. Görke B, Stülke J. Carbon catabolite repression in bacteria: many ways to make the most out of nutrients. *Nat Rev Microbiol*. 2008;6:613-624.

57. Deutscher J. The mechanisms of carbon catabolite repression in bacteria. *Curr Opin Microbiol*. 2008;11:87-93.

58. Seidl K, Müller S, François P, et al. Effect of a glucose impulse on the CcpA regulon in *Staphylococcus aureus*. *BMC Microbiol*. 2009;9:95.

59. Fujita Y. Carbon Catabolite Control of the Metabolic Network in *Bacillus subtilis*. *Biosci Biotechnol Biochem*. 2009;73:245-259.

60. Castaño-Cerezo S, Pastor JM, Renilla S, Bernal V, Iborra JL, Cánovas M. An insight into the role of phosphotransacetylase (pta) and the acetate/acetyl-CoA node in *Escherichia coli*. *Microb Cell Fact*. 2009;8:54.

61. Chong H, Yeow J, Wang I, Song H, Jiang R. Improving Acetate Tolerance of *Escherichia coli* by Rewiring Its Global Regulator cAMP Receptor Protein (CRP). *PLoS One*. 2013;8:1-10.

62. Vitko NP, Grosser MR, Khatri D, Lance TR, Richardson AR. Expanded glucose import capability affords *Staphylococcus aureus* optimized glycolytic flux during infection. *MBio*. 2016;7:1-11.

63. Somerville GA, Saïd-salim B, Wickman JM, Raffel SJ, Kreiswirth BN, Musser JM. Correlation of Acetate Catabolism and Growth Yield in *Staphylococcus aureus*: Implications for Host-Pathogen Interactions. *Infect Immun*. 2003;71.

64. Lemma E, Unden G, Kröger A. Menaquinone is an obligatory component of the chain catalyzing succinate respiration in *Bacillus subtilis*. *Arch Microbiol*. 1990;155:62-67.

7. Supplemental Material

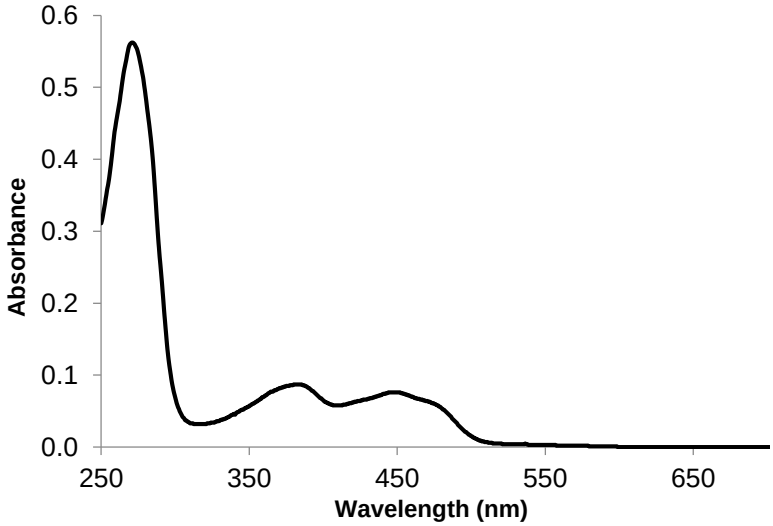

Figure 7. 1 - Flavin UV-Visible absorption spectrum.

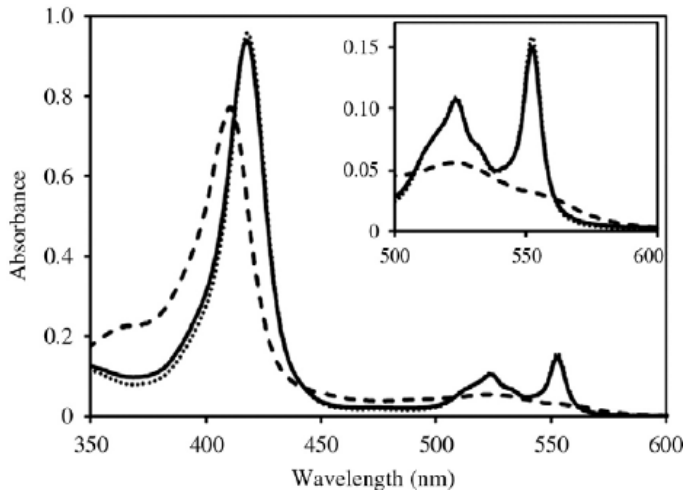

Figure 7. 2 – Absorption spectra of cytochrome *c* in its oxidized (dashed line) and reduced (solid line) form. Adapted from *Matsuno et al, 2009*[49].

Table 7. 1 - Composition of TSB medium (pH 7.3 ± 0.2) (Difco) used for *Staphylococcus aureus* growths. The medium was prepared in bi-distilled water (Millipore E-POD) sterile.

Solution	Item	Concentration	Sterilize
TSB medium	Tryptone (Pancreatic Digest of Casein)	17 g L^{-1}	Autoclave
	Dipotassium Hydrogen Phosphate (K_2HPO_4)	2.5 g L^{-1}	
	Glucose (Dextrose)	2.5 g L^{-1}	
	Sodium Chloride (NaCl)	5 g L^{-1}	
	Soytone (Peptic Digest of Soybean Meal)	3 g L^{-1}	

Table 7. 2 – Composition of CDM for *Staphylococcus aureus* growths. Salt solution, vitamin solution and trace elements solution were performed, the amino acids and bases were made separately to maximize the longevity of storage. All the solutions were stored at 4 ºC. Per each 100 mL of CDM medium prepared, were added 10 mL of the salt solution, 1 mL of each amino acid, 1 mL of each base, 0.1 mL of the vitamin solution and 0.1 mL of the trace elements solution. The medium was prepared in bi-distilled water (Millipore E-POD) sterile and the pH adjusted to 7.4 using sterile 10 M NaOH solution.

Solution	Item	Concentration	Sterilize
Salt Solution	K_2HPO_4	70 g L^{-1}	Autoclave
	KH_2PO_4	20 g L^{-1}	
	$(NH_4)_2SO_4$	10 g L^{-1}	
	$MgSO_4 \cdot 7H_2O$	0.1 g L^{-1}	
Amino Acids	Phenylalanine	0.004 g mL^{-1}	Filter Sterilize
	Isoleucine	0.003 g mL^{-1}	Filter Sterilize
	Tyrosine	0.005 g mL^{-1}	Filter Sterilize
	Cystine	0.002 g mL^{-1}	Filter Sterilize
	Glutamine	0.01 g mL^{-1}	Filter Sterilize
	Lysine	0.001 g mL^{-1}	Filter Sterilize
	Methionine	0.007 g mL^{-1}	Filter Sterilize
	Histidine	0.003 g mL^{-1}	Filter Sterilize
	Tryptophan	0.001 g mL^{-1}	Filter Sterilize
	Leucine	0.009 g mL^{-1}	Filter Sterilize
	Aspartic-acid	0.009 g mL^{-1}	Filter Sterilize
	Arginine	0.007 g mL^{-1}	Filter Sterilize
	Serine	0.003 g mL^{-1}	Filter Sterilize
	Alanine	0.006 g mL^{-1}	Filter Sterilize
	Threonine	0.003 g mL^{-1}	Filter Sterilize
	Glycine	0.005 g mL^{-1}	Filter Sterilize
	Valine	0.008 g mL^{-1}	Filter Sterilize
	Proline	0.001 g mL^{-1}	Filter Sterilize
Bases	Adenine	0.0005 g mL^{-1}	Filter Sterilize
	Cytosine	0.0005 g mL^{-1}	Filter Sterilize
	Guanine	0.0005 g mL^{-1}	Filter Sterilize
	Thymine	0.002 g mL^{-1}	Filter Sterilize
	Uracil	0.0005 g mL^{-1}	Filter Sterilize
Vitamin Solution	Thiamine	0.001 g mL^{-1}	Filter Sterilize
	Niacin	0.0012 g mL^{-1}	
	Biotin	5E-06 g mL^{-1}	
	Calcium Pantothenate	2.5E-04 g mL^{-1}	
Trace Elements	$FeCl_3$	0.008 g mL^{-1}	Filter Sterilize
	ZnCl	6.95E-05 g mL^{-1}	
	$MnCl \cdot 4H_2O$	9.9E-05 g mL^{-1}	
	Boric Acid	6E-06 g mL^{-1}	
	$CoCl_2 \cdot 6H_2O$	3.97E-04 g mL^{-1}	
	$CuCl_2 \cdot 2H2O$	2.56E-06 g mL^{-1}	
	$NiCl_2 \cdot 6H_2O$	2.38E-05 g mL^{-1}	
	$Na_2MoO_4 . \cdot 2H_2O$	3.58E-05 g mL^{-1}	

Table 7. 3 – Compounds analysed by ^{1}H-NMR in the respective analysed peaks (approximated chemical shifts) and the number of protons responsible for each signal in the defined ppm. Assignment performed based on the *Chenomx Nmr Suite software* and on the Biological Magnetic Resonance Data Bank.

Compound	~ Chemical Shift (ppm)	Number of protons
Acetate	1.9	3
Adenine	8.2	1
Alanine	1.47	3
Aspartate	2.78	1
Fumarate	6.51	2
Glycine	3.55	2
α - Glucose	5.23	1
β - Glucose	4.64	
Histidine	7.9	1
Lactate	1.31	3
Methionine	2.12	3
Oxaloacetic acid	2.39	2
Phenylalanine	7.3	1
Pyruvic acid	2.36	3
Tyrosine	7.2	2
Valine	3.6	1

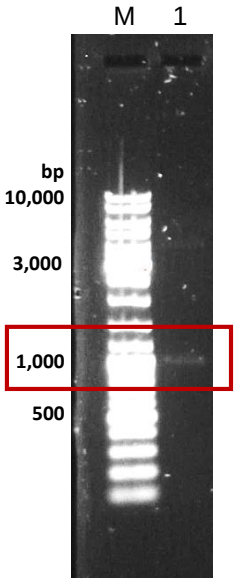

Figure 7. 3 - 1 % Agarose gel of the confirmation of mutation mqoI::Tn. Lane 1 - PCR product (1,106 bp). GeneRuler DNA Ladder Mix (Fermentas) was used (M).

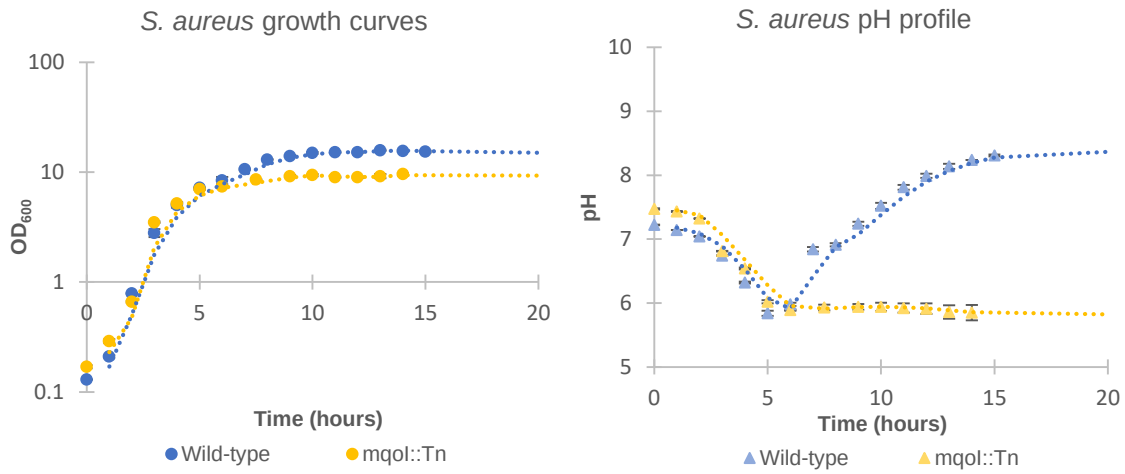

Figure 7. 4 – Logarithmic representation of *S. aureus* JE2 growth (wild-type and mqoI::Tn strains) in TSB medium (initial OD 0.15, in aerobic conditions). The absorbance at 600 nm and the pH values were measured and samples were collected every 2 h of growth. The results presented are representative of three independent experiments (respective error bars).

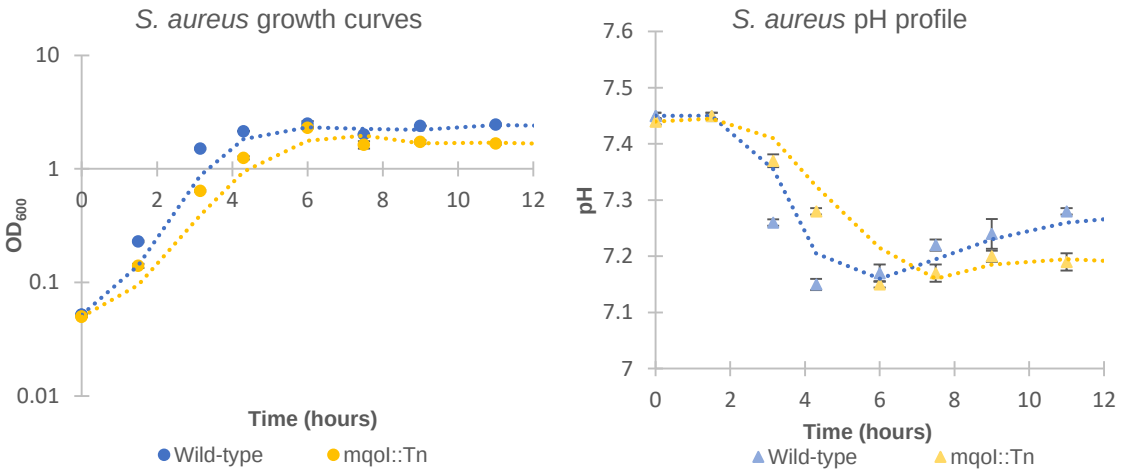

Figure 7. 5 – Logarithmic representation of *S. aureus* JE2 growth (wild-type and mqoI::Tn strains) in CDM supplemented with 5 mM glucose (initial OD 0.05, in aerobic conditions). The absorbance at 600 nm and the pH values were measured and samples were collected every 1.5 h of growth. The results presented are representative of three independent experiments (respective error bars).

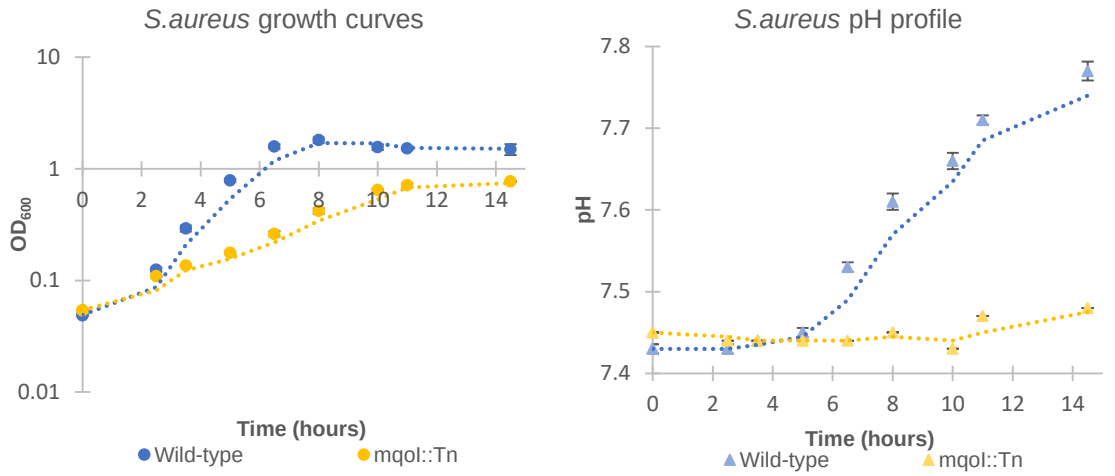

Figure 7. 6 – Logarithmic representation of *S. aureus* JE2 growth (wild-type and mqoI::Tn strains) in CDM supplemented with 5 mM acetate (initial OD 0.05, in aerobic conditions). The absorbance at 600 nm and the pH values were measured and samples were collected every 1.5 h of growth (excepting the first point of the growth). The results presented are representative of three independent experiments (respective error bars).

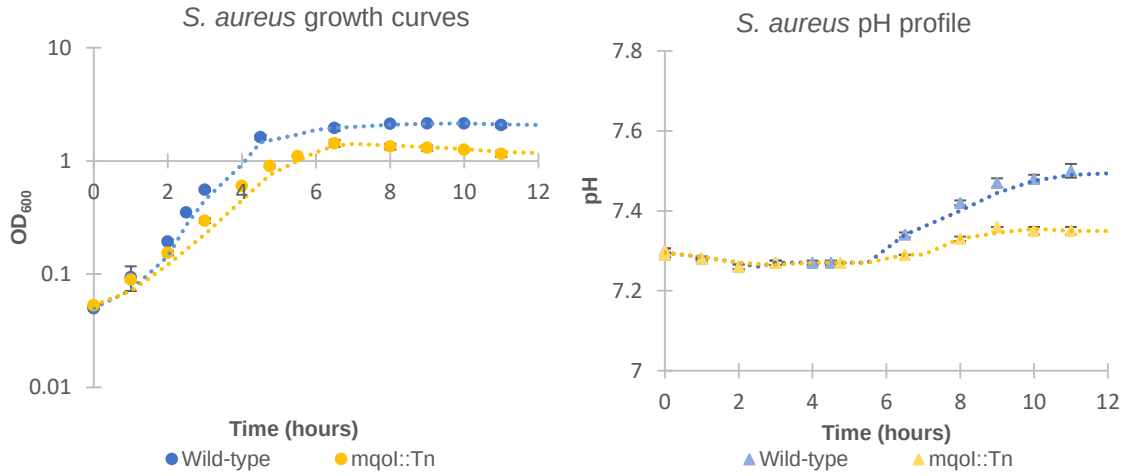

Figure 7. 7 – Logarithmic representation of *S. aureus* JE2 growth (wild-type and mqoI::Tn strains) in CDM supplemented with 5 mM lactate (initial OD 0.05, in aerobic conditions). The absorbance at 600 nm and the pH values were measured and samples were collected every 1.5 h of growth. The results presented are representative of three independent experiments (respective error bars).

Report number 1

Mass Spectrometry Unit

Assay Report: UniMS184/16

Protein sequence coverage:

Sample AS_1

MATRIX SCIENCE MASCOT SEARCH RESULTS

PROTEIN VIEW

Match to: **sp|Q6G6V5|MQO1_STAAS** Score: **754** Expect: **1.3e-070**
Probable malate:quinone oxidoreductase 1 OS=Staphylococcus aureus (strain MSSA476) GN=mqo1 PE=3 SV=2

Nominal mass (M_r): **54751**; Calculated pI value: **6.26**

Variable modifications: Carbamidomethyl (C),Deamidated (NQ),Gln->pyro-Glu
(N-term Q),Oxidation (M)
Cleavage by Trypsin: cuts C-term side of KR unless next residue is P
Sequence Coverage: **54%**

Matched peptides shown in **Bold Red**

```
    1 MTTQHSKTDV ILIGGGIMSA TLGTLLKELS PEKNIKVFEK LAQPGEESSN
   51 VWNNAGTGHS ALCELNYTKE GKDGTVDCSK AIKINEQYQI SKQFWAYLVK
  101 TGQLDNPDRF IQAVPHMSFV IGEDNVAFIK SRVATLKKSV LFEKMKLSQD
  151 EEEMKSWVPL MIEGRKSDEP IALTYDETGT DVNFGALTAK LFENLEQRGV
  201 GIQYKQNVLD IKKQKSGAWL VKVKDLETNE TTTYESDFVF IGAGGASLPL
  251 LQKTGIKQSK HIGGFPVSGL FLRCTNQEVI DRHHAKVYGK AAVGAPPMSV
  301 PHLDTRFVDG KRSLLFGPFA GFSPKFLKTG SHMDLIKSVK PNNIVTMLSA
  351 GIKEMSLTKY LVSQLMLSND ERMDDLRVFF PNAKNEDWEV ITAGQRVQVI
  401 KDTEDSKGNL QFGTEVITSD DGTLAALLGA SPGASTAVDI MFDVLQRCYR
  451 DEFKGWEPKI KEMVPSFGYR LTDHEDLYHK INEEVTKYLQ VK
```

Report number 2

Mass Spectrometry Unit

Assay Report: UniMS114/17

Protein sequence coverage:

Sample MQ02

MATRIX SCIENCE MASCOT SEARCH RESULTS

PROTEIN VIEW

Match to: **DLDH_ECOL6** Score: **887** Expect: **1.1e-083**
Dihydrolipoyl dehydrogenase OS=Escherichia coli O6:H1 (strain CFT073 / ATCC 700928 / UPEC) GN=lpdA PE=3 SV=2

Nominal mass (M_r): **50657**; Calculated pI value: **5.79**

Variable modifications: Carbamidomethyl (C),Deamidated (NQ),Gln->pyro-Glu
(N-term Q),Oxidation (M)
Cleavage by Trypsin: cuts C-term side of KR unless next residue is P
Sequence Coverage: **54%**

Matched peptides shown in **Bold Red**

```
    1 MSTEIKTQVV VLGAGPAGYS AAFRCADLGL ETVIVERYNT LGGVCLNVGC
   51 IPSKALLHVA KVIEEAKALA EHGIVFGEPK TDIDKIRTWK EKVINQLTGG
  101 LAGMAKGRKV KVVNGLGKFT GANTLEVEGE NGKTVINFDN AIIAAGSRPI
  151 QLPFIPHEDP RIWDSTDALE LKEVPERLLV MGGGIIGLEM GTVYHALGSQ
  201 IDVVEMFDQV IPAADKDIVK VFTKRISKKF NLMLETKVTA VEAKEDGIYV
  251 TMEGKKAPAE PQRYDAVLVA IGRVPNGKNL DAGKAGVEVD DRGFIRVDKQ
  301 LRTNVPHIFA IGDIVGQPML AHKGVHEGHV AAEVIAGKKH YFDPKVIPSI
  351 AYTEPEVAWV GLTEKEAKEK GISYETATFP WAASGRAIAS DCADGMTKLI
  401 FDKESHRVIG GAIVGTNGGE LLGEIGLAIE MGCDAEDIAL TIHAHPTLHE
  451 SVGLAAEVFE GSITDLPNPK AKKK
```